論文 / 著書情報
Article / Book Information

題目(和文)	液晶性ポリイミドを用いた高熱伝導性絶縁材料の開発
Title(English)	Development of high thermally conductive insulating materials based on liquid crystalline polyimides
著者(和文)	荘司優
Author(English)	Yu Shoji
出典(和文)	学位:博士(工学), 学位授与機関:東京工業大学, 報告番号:甲第9067号, 授与年月日:2013年3月26日, 学位の種別:課程博士, 審査員:上田 充
Citation(English)	Degree:Doctor (Engineering), Conferring organization: Tokyo Institute of Technology, Report number:甲第9067号, Conferred date:2013/3/26, Degree Type:Course doctor, Examiner:
学位種別(和文)	博士論文
Type(English)	Doctoral Thesis

Ph.D. Dissertation

Development of High Thermally Conductive Insulating Materials Based on Liquid Crystalline Polyimides

液晶性ポリイミドを用いた高熱伝導性絶縁材料の開発

2012

Yu Shoji

10D07080

Department of Organic and Polymeric Materials,

Graduate School of Science and Engineering,

Tokyo Institute of Technology

Contents

Chapter 1

General Introduction

1-1. Thermal Conductivity of Materials

During a past few decades, the development of electronics is currently accelerated toward integration, miniaturizarion, and functionalization, where both semiconductors and insulating materials in integrated circuits have been packaged as dense as possible. These used to be crammed in a two-dimensional surface, whereas three-dimensional stacking technologies have been developed in decades, such as multi-chip package (MCP) (Figure 1-1).[1] However, if the insulating materials possess low thermal conductivity, a substantial amount of generated heat would be accumulated inside the devices, which gives rise to electric connection failure and reduces the life time of these devices. Indeed, the insulating materials mainly composed of organic resins have quite low thermal conductivities, usually from 1 to 3 orders lower than those of ceramics and metals (Figure 1-2),[2] which substantially prevent the heat from diffusing. Therefore, the high thermally conductive insulating materials have recently been attractive materials for releasing the generated heat effectively from those densely-packaged electronics devices to realize the further integrated circuits.

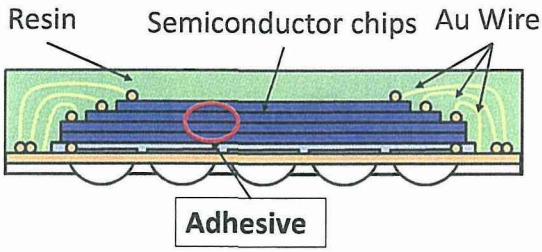

Figure 1-1. Schematic device structure of MCPs.

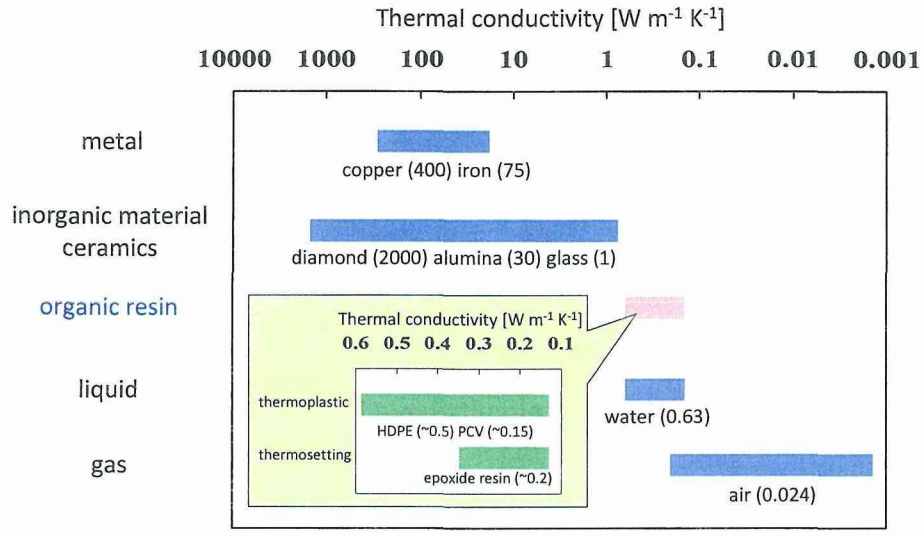

Figure 1-2. Thermal conductivity of materials.

1-2. Media of Thermal Conductivity for Materials

The heat transporting media depends on materials; free electrons for metals whereas lattice vibrations, defined as "phonon",[3] for ceramics and organic materials. In the case of metals, free electrons can effectively conduct the electricity and heat because it is easy for free electrons to move inside metal matrices. On the other hand, the phonon conduction strongly depends on the lattice arrangement or the orientation direction of materials. Therefore, thermal conductivity of ceramics shows 2 or 3 orders higher values than those of organic resins because ceramics form the well-ordered lattice, and the phonon can effectively conduct in ceramics, which leads to high thermal

conductivity. In contrast, the phonon in organic materials does not conduct effectively but scatters because they generally have the amorphous nature. As a result, organic resins show the quite low thermal conductivity compared with other materials such as metals and ceramics.

1-3. Improvement of Thermal Conductivity for Organic Resins

1-3-1. Composite Resins with High Thermally Conductive Inorganic Fillers

There are several ways to improve the low thermal conductivity of organic resins. One approach to improve the thermal conductivity of an organic resin is to add an inorganic filler material such as high thermally conductive carbon fillers (120–5000 W m^{-1} K^{-1}), which are carbon black,[4] carbon fiber,[4] carbon nanotube,[5] and carbon nanosheet (Table 1-1).[6]

Moisala *et al.*[5a] reported the enhanced thermal and electrical conductivity of epoxy composites containing the small amount (0.005–0.5 wt%) of single-walled (SWNTs) or multi-walled (MWNTs) carbon nanotubes, where the case of MWNT composites possessed the modestly increased thermal conductivity as a function of the filler content. Therefore, carbon nanotubes are ones of the most effective fillers to improve the thermal conductivity of matrix resin because of their high thermal conductivity (3000 W m^{-1} K^{-1}).

Table 1-1. Thermal conductivity of the carbon-based composite materials.

Matrix resin	Filler (wt% or vol%)	Thermal conductivity of composites [W m^{-1} K^{-1}]	References
Vectra A950RX[a]	Carbon black (12 vol%)	0.40	Ref. 4a
	Graphite (48 vol%)	1.5	
	Carbon fiber (50 vol%)	1.0	
Epoxy resin	MWCNT[b] (0.5 wt%)	0.29	Ref. 5a
Epoxy resin	Carbon nanosheet (33 vol%)	80	Ref. 6a
Epoxy resin	GNP[c] (15 wt%)	21	Ref. 6b
Nylon 66	GNP[c] (20 vol%)	3.7	Ref. 6d
HDPE[d]	GNP[c] (20 vol%)	1.1	
Nylon 6	GNP[c] (20 vol%)	4.1	

[a] Ticona Vectra Liquid Crystal Polymer (LCP) Product Information; Ticona: Summit, NJ, 2000. [b] Multi-walled carbon nanotube. [c] Graphite nanoplatelet. [d] High density polyethylene.

Recently, there is an increasing attention being paid to the use of exfoliated graphite such as carbon nanosheet or graphene to produce thermally conductive nanocomposites, since the thermal conductivity of graphene was estimated to be as high as 5300 W m^{-1} K^{-1}.[6] Veca *et al.*[6a] successfully produced the polymeric nanocomposites exhibiting ultrahigh thermal conductivities by filling the treated carbon nanosheet into matrix epoxy resins. The nanocomposite thin films with a 35 vol% carbon nanosheet had 2 orders higher thermal conductivity than those of pristine matrix resins. At comparable

loading level, the carbon nanosheets were demonstrated as more effective fillers than carbon nanotubes to produce the high thermally conductive nanocomposites.

The introduction of high thermally conductive carbon fillers could realize the improvement of the thermal conductivity of organic resins. However, carbon materials unavoidably make the target composites electrically conductive as well as thermally conductive. Therefore, the insulating ceramic fillers are the appropriate candidates to improve the thermal conductivity of organic resins. There are many composite systems investigated including different kinds of organic resins and ceramic fillers such as SiO_2,[7] S_3N_4,[8] Al_2O_3,[9] AlN,[10] BN,[11] and so on. These reports considered the effect of matrix resin type, filler category, volume fraction, shape, size distribution, and surface treatment of filler (Table 1-2).

For instance, Kume *et al.*[10] reported polymer/ceramics composites with high thermally conductive AlN granules which showed 266±26 W m^{-1} K^{-1}. Ceramic fillers consisting of the 49 vol% AlN granules (granule size: 79 μm) and 21 vol% hexagonal BN (h-BN) powder (particle size: 1 μm) showed the significant enhancement of the thermal conductivity up to 9.3 W m^{-1} K^{-1} for polymer/ceramics composites based on a polyimide resin due to the formation of high thermal conduction pathways. This thermal conductivity was about 50 times higher than that of pristine polyimide resin. It was also demonstrated that the composite system with high thermally conductive ceramics was the effective method to improve the thermal conductivity of organic resins.

Table 1-2. Thermal conductivity of the ceramic-based composite materials.

Matrix resin	Filler (wt% or vol%)	Thermal conductivity of composites [W m^{-1} K^{-1}]	References
Epoxy resin	AlN (50 vol%)	1.96	Ref. 7
Epoxy resin	Si_3N_4 (60 vol%)	2.51	Ref. 8
Polyurethane	Al_2O_3 (40 vol%)	0.85	Ref. 9
Polyimide	AlN/h-BN[a] (49/29 vol%)	9.3	Ref. 10
Polyimide	h-BN[a] (60 vol%)	7	Ref. 11a
Polyimide	BN (30 wt%)	1.2	Ref. 11b
PMMA[b]	BNNT[c] (24 wt%)	3.16	Ref. 11d
PS[d]	BNNT[c] (35 wt%)	3.61	
PVB[e]	BNNT[c] (18 wt%)	1.81	
PEVA[f]	BNNT[c] (37 wt%)	2.50	
PVA[g]	BN nanosheet (50 vol%)	13[h]	Ref. 11e
Epoxy resin	BN nanosheet (50 vol%)	38[h]	

[a] Hexagonal boron nitride. [b] Poly(methyl methacrylate). [c] Boron nitride nanotube. [d] Polystylene. [e] Poly(vinyl butyal). [f] Poly(ethylene vinyl alcohol). [g] Poly(vinyl alcohol). [h] Calculated values from the equation, $\lambda=\alpha\rho C_p$. λ: Thermal conductivity [W m^{-1} K^{-1}], α: thermal diffusivity [mm^2 s^{-1}], ρ: density [g cm^{-3}], and C_p: specific heat [J g^{-1} K^{-1}].

1-3-2. Control in Orientation of Matrix Resins

The insulating materials with high thermal conductivity have been achieved by composite systems with high thermally conductive ceramic fillers at over 50 vol% loading. However, a large amount of fillers leads to low processability of the composite materials, increasing the melt or solution viscosity. In addition, the adhesion ability between composite materials and substrates becomes poor, and high roughness of the materials surface is induced with increased weight ratio of fillers. Therefore, the amount of fillers should be decreased as less as possible to maintain such processing properties, without sacrificing thermal conductivity. To predict thermal conductivity of the composites, there are many established models for composite systems.[12] The Bruggeman theoretical model[12b] is based upon potential theory to obtain an exact solution for the conductivity of a system with spherical non-interacting particles in a continuous matrix, including different assumptions about the permeability and field strength of the system. It is given as

$$1 - v = \frac{\lambda_{\text{mix}} - \lambda_{\text{filler}}}{\lambda_{\text{resin}} - \lambda_{\text{filler}}} \left(\frac{\lambda_{\text{resin}}}{\lambda_{\text{mix}}}\right)^{\frac{1}{3}},$$

where v is the volume fraction of the filler, λ_{resin} is the thermal conductivity of a matrix resin, λ_{filler} is the thermal conductivity of a filler, λ_{mix} is the thermal conductivity of a composite. According to the Bruggeman theoretical model, filling more than 70 vol% fillers with thermal conductivity of 30 W m^{-1} K^{-1} in polymer matrices with one of 0.2 W m^{-1} K^{-1} produces the composite with thermal conductivity of ca. 5 W m^{-1} K^{-1}, while the thermal conductivity of the composite prepared from less than 50 vol% fillers (30 W m^{-1} K^{-1}) with polymer matrices (1 W m^{-1} K^{-1}) would also be ca. 5 W m^{-1} K^{-1} (Figure 1-3). Therefore, the development of high thermally conductive polymers is crucial to achieve

high thermally conductive composites containing a small amount of fillers. However, the thermal conductivity of organic polymers is generally low. To increase thermal conductivity of polymers, highly oriented polymers, that is, liquid crystalline (LC) polymers are promising candidates because the well-aligned LC polymers effectively conduct "phonon" which is the medium of thermal conduction for organic polymers.[13]

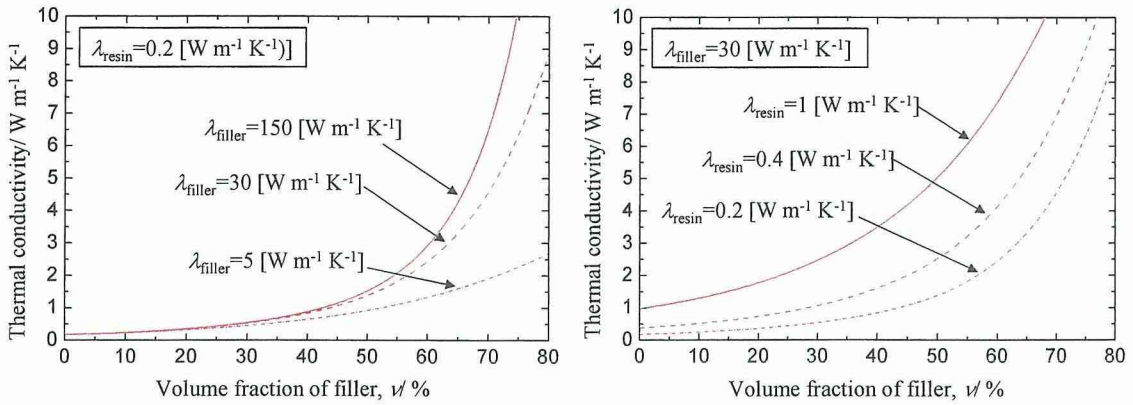

Figure 1-3. Bruggeman theoretical model for the thermal conductivity in the composite systems.

Takezawa *et al.*[13] reported the high ordered LC epoxy resins with high thermal conductivity up to 0.96 W m^{-1} K^{-1}, which shows 5 times higher than those of conventional epoxy resins by the self-organized structures (Figure 1-4). The microscopic alignments of smectic-like polymer chains are thus important to enhance their thermal conductivity compared to homogeneous and amorphous resins (Figure 1-5).

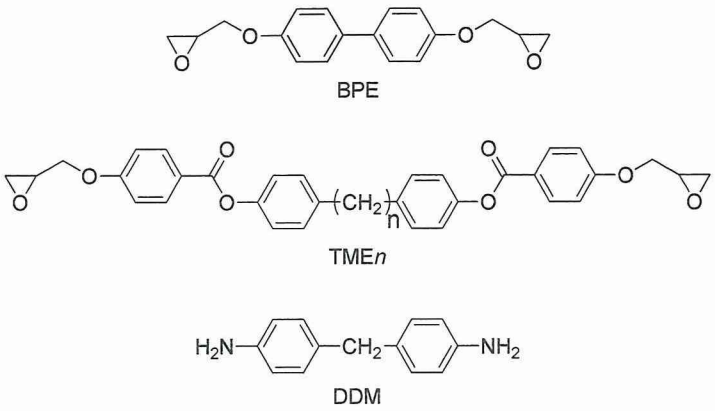

TME4/DDM: 0.96 [W m^{-1} K^{-1}]

Figure 1-4. Structures of diepoxy monomers, BPE and TME*n* (*n*=4, 6, 8), and a diamine curing agent, DDM.[13]

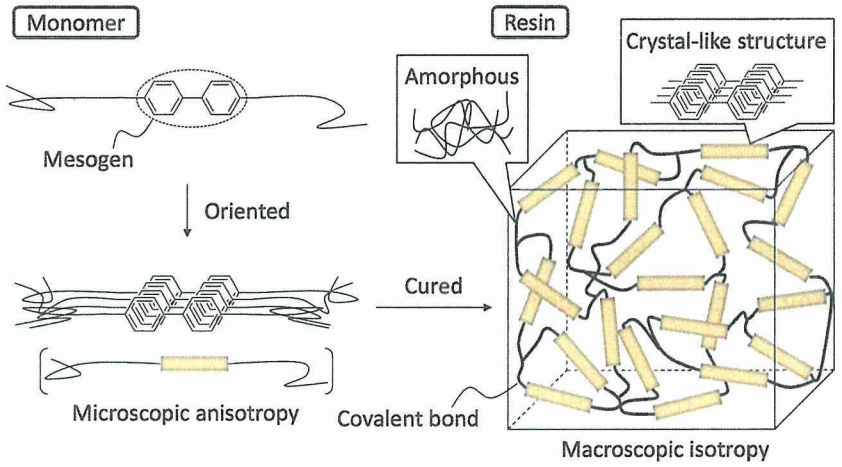

Figure 1-5. Schematic representation of the strategy to afford macroscopic isotropic resin with high thermal conductivity.[13]

Meanwhile, controlling the macroscopic orientation by the external fields is the effective method to enhance the thermal conductivity along the same direction in the applied field because the alignment of LC polymers can be easily controlled in common ways, such as stretching, rubbing, magnetic field, and so on,[14] and the thermal condcutivities of the anisotropic resins were enhanced along the oriented direction.

Harada *et al.*[14g] reported the highly ordered LC epoxy resin (DGETAM/DDE) cured under a magnetic field, where the thermal conductivity in the direction along the applied field had a significantly high value (0.89 W m^{-1} K^{-1}) as compared with that (0.32 W m^{-1} K^{-1}) in the cross direction (Figure 1-6). Moreover, the thermal conductivity increased with an increase in the magnitude of the magnetic field and shoed the highest value at 10 T, due to the highly ordered network structure of the epoxy resin.

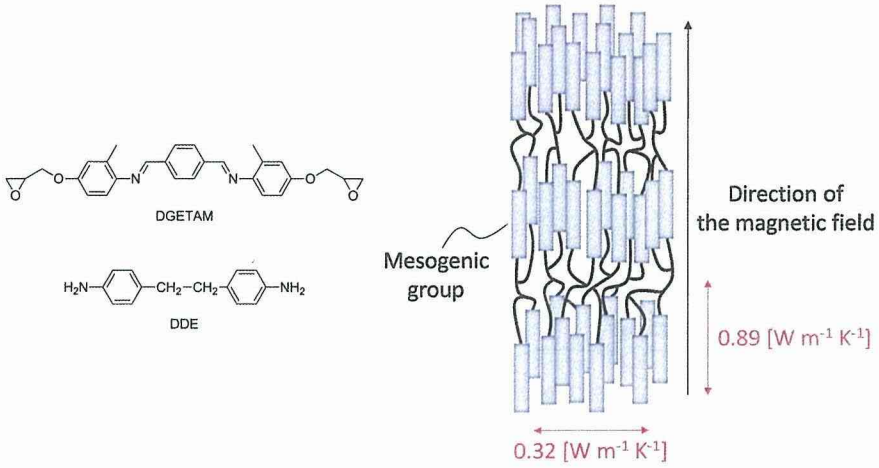

Figure 1-6. Model of the cured resin from diepoxy monomers, DGETAM, and a diamine curing agent, DDE, under the magnetic field.[14g]

Moreover, not only epoxy resins but also the anisotropic resins with 3D polymerizable moieties possess the high thermal conductivity. Kato *et al.*[14j] reported the photo-crosslinkable acrylic LCs with the different ratio of polymerizable moieties, and the relationship between the thermal conductivity and the LC network styles, where uniazially aligned films were prepared from the mixtures of the mono-functional polymerizable LC and di-functional one by photo polymerization after aligning the molecular directions based on the rubbing method (Figure 1-7). As a result, homogeneously aligned acrylic films were successfully obtained, and they showed the improved thermal conductivity along the rubbing direction from 0.45 to 0.68 W m^{-1} K^{-1}

with the increase of the bi-functional polymerizable LC content.

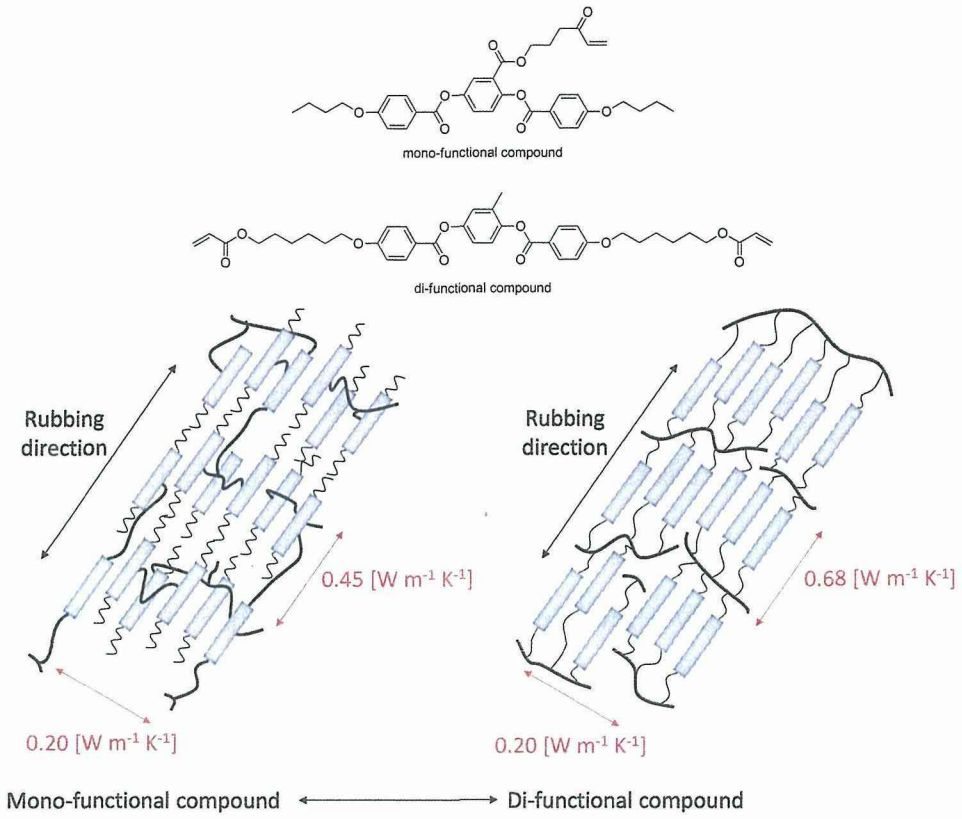

Figure 1-7. Illustrations of molecular alignment in homogeneous alignment films.[14j]

Thus, it was demonstrated that controlling the high-order structures of the LC polymers was the effective method to improve the thermal conductivity of the organic resins.

1-4. Liquid Crystalline Polyimides

The LC polymers are expected as the high thermally conductive materials in the chain-aligned direction, where the continuous alignment of the polymer main chain corresponds to the direction of the phonon conduction. For the application to the electric devices, the next-generation polymeric insulators with the high thermal conductivity

require the solution processability in the practical screen printing applications and the low phase transition temperatures to decrease the processing temperature. Aromatic polyimides are the promising materials for the applications to the aerospace and electronic devices due to their excellent physical and chemical properties, that is, they have outstanding thermal and chemical stabilities, mechanical properties, electrical properties, and radiation resistance.[15] Thus, the LC polyimides should be one of the candidates as the thermally conductive materials and more applicable than the epoxy resins because the precursors of polyimides, which are poly(amic acid)s (PAAs), have the advantages of solution processability, although most polyimides are generally insoluble. However, only a few kinds of LC polyimides have so far reported (Figure 1-8).[16–18]

Asanuma *et al.*[16a] reported the wholly aromatic thermotropic LC polyimide prepared by the polymerization of 1,2,4,5-benzenetetracarboxylic dianhydride (PMDA) and 1,3-bis[4-(4'-aminophoxy)cumyl]benzene (BABC). This polyimide shows the LC phase at 276–320 °C, in which the hard pyromellitic diimide unit and the flexible *m*-diisopropylbenzene unit are important for producing the thermotropic LC polyimide.

In contrast with the wholly aromatic LC polyimide, the segmented polyimides with the aliphatic flexible spacers such as methylene and oxyethylene units possess the thermotropic LC nature.[17,18] Yokokura *et al.*[17a] reported the nematic LC polyimides from 3,3',4,4'-biphenyltetracarboxylic dianhydride (BPDA) and aliphatic diamines with different chain lengths, and their anomalous odd-even effect in tilt bias angles was investigated. In the related work, Watanabe *et al.*[17c] reported the series of main-chain type LC polyimides derived from aliphatic diamines with 4,4"-terphenyltetracarboxylic acid, and the ability for liquid crystal formation in main-chain polyimides was discussed.

The mesophase forms only from polyimides based on terphenyl moiety but based on benzene or biphenyl one, although all mesogenic moieties can be considered stiff and long enough to form a mesophase. The difficulty in the LC formation was explained by the high stability of the crystal, which may be attributable to imide ring interaction.

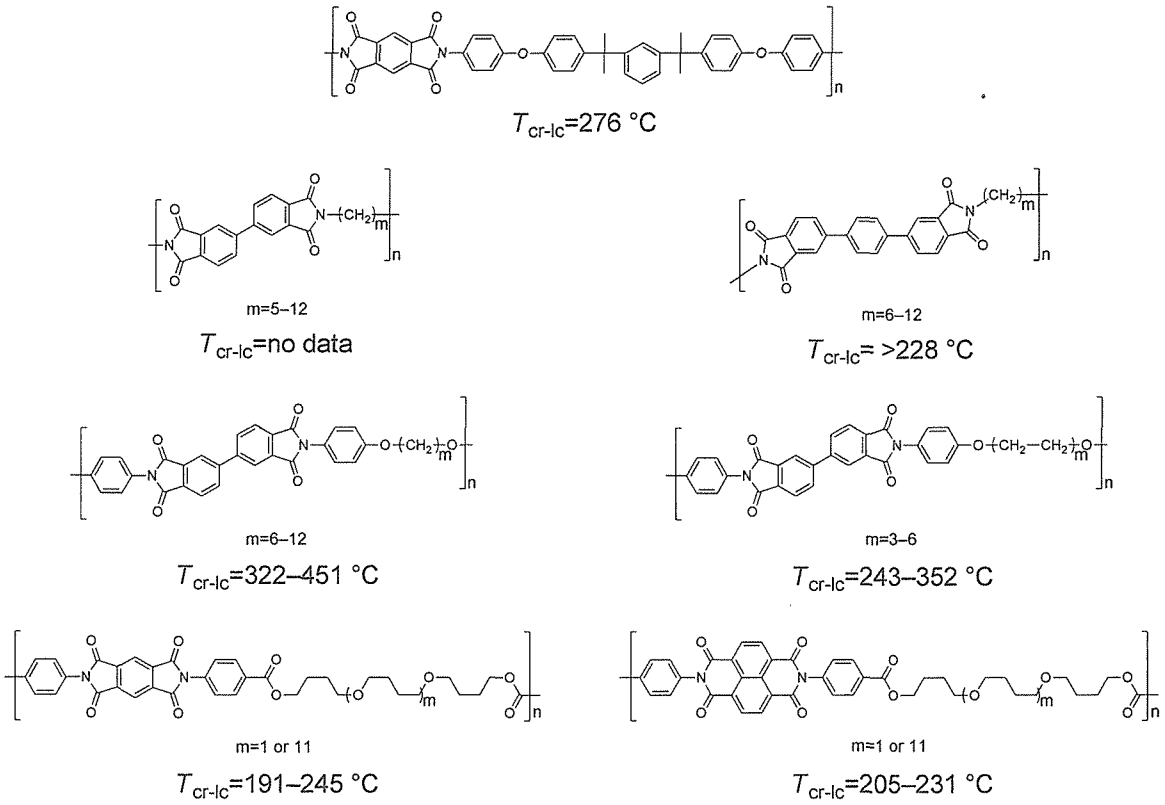

Figure 1-8. Chemical structures of LC polyimides. $T_{cr\text{-}lc}$: crystalline-LC transition temperature on the heating process.[16–18]

In 2008, Eastmond *et al.*[18b] reported the LC polyimides with flexible poly(oxyethylene) blocks and their LC behavior, in which the polymers with five or six oxyethylene units exhibited LC phases stable over temperature ranges of 50 °C or more. These sorts of polyimides derived from tetracarboxylic dianhydrides with aromatic diamines meet the requirement of the solution processability for the practical screen printing applications compared to those with aliphatic diamines, producing the

precursor PAAs. In addition, they showed the relatively lower crystal-LC transition temperature of 243 °C than the wholly aromatic LC polyimide (>276 °C). Therefore, LC polyimides derived from aromatic diamines with flexible spacers are effective candidates for high thermally conductive polymers with good processabilities.

1-5. Purposes of This Work

The introduction of flexible spacer units such as oxyethylene units in the main chain of LC polyimides is effective to develop the materials for the screen printing applications which potentially have the high thermal conductivity. However, further decrease of fabrication temperatures are required to avoid oxidation of copper wires inside integrated circuits in virtual electronics applications. It should be mentioned that there has been no example of the LC fabrication temperature less than 191 °C among polyimide-based thermotropic LC materials derived from tetracarboxylic anhydrides and aromatic diamines with flexible spacer units that meet the requirement of the solution processability. The purpose of this work is to develop high thermally conductive materials based on the LC polyimides which can be used as insulating layers via the screen printing applications.

As siloxane units are well known to be highly flexible compared with alkylene and oxyethylene ones, the introduction of siloxane linkages to a polyimide main chain should decrease LC transition temperatures. The novel thermotropic LC polyimides containing the siloxane linkages were developed, and their LC orientation was controlled to enhance the thermal diffusivity. The high thermally conductive h-BN composites based on LC polyimides were also developed.

In this dissertation, the development of high thermally conductive insulating

materials based on LC polyimides is described in the following six chapters.

The general introduction regarding the background of this study is described in chapter 1.

In chapter 2, the novel siloxane-containing LC polyimides and their LC behavior are described in detail.

In chapter 3, the effect of substituents on mesogenic units of novel siloxane-containing LC polyimides to decrease LC transition temperatures is investigated, and their LC behavior is described in detail.

In chapter 4, the relationship between the morphology and thermal diffusivity of cross-linked liquid crystalline polyimides with siloxane spacer units are described.

In chapter 5, the thermal diffusivity and morphological study of hexagonal boron nitride composites based on cross-linked LC polyimides are described.

Finally, this study on high thermally conductive materials is concluded in chaper 6.

1-6. References and Notes

1. (a) Diebold, A. In *Metrogy Roadmap: A Supplement to the National Technology Roadmap for Semiconductors*; SEMATECH, 1995. (b) *The International Technology Roadmap for Semiconductors*, 2002 update.
2. Chung, D. D. L. *Applied Thermal Engineering* **2001**, *21*, 1593.
3. C. L. Choy, *Polymer* **1977**, *40*, 984.
4. (a) Keith, J. M.; King, J. A.; Lenhart, K. M.; Zimmy, B. *J. Appl. Polym. Sci.* **2007**, *105*, 3309. (b) Hauaser, R. A.; King, J. A.; Pagel, R. M.; Keith, J. M.; *J. Appl. Polym. Sci.* **2008**, *109*, 2145. (c) Hauaser, R. A.; Keith, J. M.; King, J. A.; Holdren, J. L. *J. Appl. Polym. Sci.* **2008**, *110*, 2914.
5. (a) Moisala, A.; Li, Q.; Kinloch, I. A.; Windle, A. H. *Compos. Sci. Technol.* **2006**, *66*, 1285. (b) Kim, P.; Shi, L.; Majumdar, A.; McEuen, P. L. *Phys. Rev. Lett.* **2001**, *87*, 215502.
6. (a) Veca, L. M.; Meziani, M. J., Wang, W.; Wang, X.; Lu, F.; Zhang, P.; Lin, Y.; Fee, R.; Connell, J. W.; Sun, Y.-P. *Adv. Mater.* **2009**, *21*, 2088. (b) Wu, H.; Drzal, L. T. *Carbon* **2012**, *50*, 1135. (c) Balandin, A. A.; Ghosh, S.; Bao, W.; Calizo, I.; Teweldebrhan, D.; Miao, F.; Lau, C. N. *Nano Lett.* **2008**, *8*, 902. (d) Fukushima, H.; Drazal, L. T., Rook, B. P.; Rich, M. J. *J. Therm. Anal. Cal.* **2006**, *85*, 235.
7. Wong, C. P.; Bollampally, R. S. *J. Appl. Polym. Sci.* **1999**, *74*, 3396.
8. Zeng, J.; Fu, R.; Shen, Y.; He, H.; Song, X. *J. Appl. Polym. Sci.* **2009**, *113*, 2117.
9. Lu, X.; Xu, G. *J. Appl. Polym. Sci.* **1997**, *65*, 2733.
10. Kume, S.; Yamada, I.; Watari, K.; Harada, I.; Mitsuishi, K. *J. Am. Ceram. Soc.* **2009**, *92*, S153.
11. (a) Sato, K.; Horibe, H.; Shirai, T.; Hotta, Y.; Nakano, H.; Nagai, H.; Mitsuishi, K.;

Watari, K. *J. Mater. Chem.* **2010**, *20*, 2749. (b) Li, T.-L.; Hsu, S. L.-C. *J. Phys. Chem. B* **2010**, *114*, 6825. (c) Kizilkaya, C.; Mülazim, Y.; Kahraman, V.; Kayaman, N. A.; Güngör, A. *J. Appl. Polym. Sci.* **2012**, *124*, 706. (d) Zhi, C.; Bando, Y.; Terao, T.; Tang, C.; Kuwahara, H.; Golberg, D. *Adv. Funct. Mater.* **2009**, *19*, 1857. (e) Song, W.-L.; Wang, P.; Cao, L.; Anderson, A.; Meziani, M. J.; Farr, A. J.; Sun, Y.-P. *Angew. Chem. Int. Ed.* **2012**, *51*, 6498.

12. (a) Keith, J. M.; King, J. A.; Lenhart, K. M.; Zimny, B. *J Appl. Polym. Sci.* **2007**, *105*, 3309. (b) Bruggeman, D. *Ann Phys* **1935**, *24*, 636.

13. Akatsuka, M.; Takezawa, Y. *J. Appl. Polym. Sci.* **2003**, *89*, 2646.

14. (a) Osada, K.; Niwano, H.; Tokita, M.; Kawauchi, S.; Watanabe, J. *Macromolecules* **2000**, *33*, 7420. (b) Tokita, M.; Osada, K.; Kawauchi, S.; Watanabe, J. *Polym. J.* **1998**, *30*, 687. (c) Tokita, M.; Tokunaga, K.; Funaoka, S.; Osada, K.; Watanabe, J. *Macromolecules* **2004**, *37*, 2527. (d) Osada, K.; Koike, M.; Tagawa, H.; Hunaoka, S.; Tokita, M.; Watanabe, J. *Macromolecules* **2005**, *38*, 7337. (e) Tokita, M.; Watanabe, J. *Polym. J.* **2006**, *38*, 611. (f) Patil, H. P.; Lentz, D. M.; Hedden, R. C. *Macromolecules* **2009**, *42*, 3525. (g) Harada, M.; Ochi, M.; Tobita, M.; Kimura, T.; Ishigaki, T.; Shimayama, N.; Aoki, H. *J. Polym. Sci. Part B: Polym. Phys.* **2003**, *41*, 1739. (h) Kato, T.; Nagahara, T.; Agari, Y.; Ochi, M. *J. Polym. Sci. Part B* **2005**, *43*, 3591. (i) Kato, T.; Nagahara, T.; Agari, Y.; Ochi, M. *J. Polym. Sci. Part B* **2006**, *44*, 1419. (j) Kato, T.; Nagahara, T.; Agari, Y.; Ochi, M. *J. Appl. Polym. Sci.* **2007**, *104*, 3453. (k) Defaux, M.; Vidal, L.; Möller, M.; Gearba, R. I.; DiMasi, E.; Ivanov, D. A. *Macromolecules* **2009**, *42*, 3500. (l) Yoshihara, S.; Ezaki, T.; Nakamura, M.; Watanabe, J.; Matsumoto, K. *Macromol. Chem. Phys.* **2012**, *213*, 2213.

15. (a) Bessonov, M. I.; Koton, M. M.; Kudryavstev, V. V.; Laius, L. A. In *Polyimides: Thermally Stable Polymers*; *Consultants Bureau*: New York, 1987. (b) Wilson, D.; Stenzenberger, H. D.; Hergenrother, P. *Polyimides*: Blackie: New York, 1990.

16. (a) Asanuma, T.; Oikawa, H.; Ookawa, Y.; Yamasita, W.; Matsuo, M.; Yamaguchi, A. *J. Polym. Sci.: Part A* **1994**, *32*, 2111. (b) Pramoda, K. P.; Liu, S.; Chung, T.-S. Macromol. Mater. Eng. **2002**, *287*, 931. (c) Ho, C.-Y.; Lee, J.-Y. *J. Appl. Polym. Sci.* **2006**, *100*, 1688.

17. (a) Yokokura, H.; Oh-e, M.; Kondo, K.; Oh-hara, S. *Mol. Cryst. Liq. Cryst.* **1993**, *225*, 253. (b) Shiotani, A.; Kohda, M. *J. Appl. Polym. Sci.* **1999**, *74*, 2404. (c) Inoue, T.; Kakimoto, M.; Imai, Y.; Watanabe, J. *Macromol. Chem. Phys.* **1997**, *198*, 519. (d) Kaneko, T. I.; Imamura, K.; Watanabe, J. *Macromolecules* **1997**, *30*, 4244. (e) Huang, H. W.; Kaneko, T. I.; Horie, K.; Watanabe, J. *Polymer* **1999**, *40*, 3821.

18. (a) de Visser, A. C.; Gregonis, D. E.; Driessen, A. A. *Makromol. Chem.* **1978**, *179*, 1885. (b) Costa, G.; Eastmond, G. C.; Fairclough, J. P. A.; Paprotny, J.; Ryan, A. J.; Stagnaro, P. *Macromolecules* **2008**, *41*, 1034. (b) Schab-Balcerzak, E.; Wegrzyn, M.; Janeczek, H.; Jarzabek, B.; Rannou, P.; Iwan, A. *Liquids Crystals* **2010**, *37*, 1347.

Chapter 2

Thermotropic Liquid Crystalline Polyimides with Siloxane Linkages: Synthesis, Characterization, and Liquid Crystalline Behavior

Abstract.

Thermotropic liquid crystalline (LC) semialiphatic polyimides have been developed from diamines containing siloxane spacer units. These novel polyimides exhibited high thermal stability and a lower crystal-LC transition temperature compared to reported polyimides containing alkylene or oxyethylene spacer units. X-ray studies were performed for investigating the oriented smectic mesophases of each polyimide. In the polyimides derived from PMDA, a smectic A (SmA) phase was formed on gradual cooling from the isotropic liquid phase. On the other hand, the polyimides based on BPDA formed a smectic C (SmC) phase as well as a SmA phase.

2-1. Introduction

Liquid crystalline (LC) polymers are expected to increase thermal conductivity because the alignment of LC polymers effectively conducts "phonon" which is the media of thermal conductivity for organic polymers.[1] Furthermore, the direction of phonon conductivity corresponds to the alignment of polymer main chains, and such alignment can easily be controlled in common ways, for example, by stretching, rubbing, magnetic fields, self-alignment, etc.[1–5]

Aromatic polyimides are promising materials for the applications to aerospace and electronic devices due to their excellent physical and chemical properties, that is, they have outstanding thermal and chemical stabilities, mechanical properties, electrical properties, and radiation resistance.[6,7] Next-generation polymeric insulators with high thermal conductivity required relatively low phase transition temperatures for easy processing. Thus, LC polyimides possessing flexible spacer units are good candidates. A few LC polyimides with sequences of methylene or ethylene oxide units in the main chains have been reported, such as thermotropic LC polyimides with methylene units (8–12) from a tetracarboxylic dianhydride, 4,4"-terphenyltetracarboxylic dianhydride and aliphatic diamines,[8–10] and segmented LC polyimides prepared from 3,3',4,4'-tetracarboxybiphenyl dianhydride (BPDA) and α,ω-bis(4-aminophenoxy)oxyethylene units.[11] These polyimides showed liquid crystallinity and lower phase transition temperatures compared to the polyimides based on BPDA and diamines with methylene spacer units (>350 °C). For practical applications, a further decrease in fabrication temperatures is required to avoid oxidation of the copper wires inside integrated circuits. It is well-known that a siloxane unit is highly flexible, thus polyimides containing siloxane linkages are expected to show lower LC transition

temperatures.

In this chapter, the synthesis of novel LC polyimides derived from pyromellitic dianhydride (PMDA) or BPDA with diamines containing siloxane spacer units and their thermotropic LC behavior are described in detail. The key technique in this chapter is the extension of the length of the siloxane units and/or alkyl chains for decreasing the crystal-LC transition temperatures of LC polyimides. The relationship between molecular designs and LC behavior is especially forcused on.

2-2. Results and Discussion

2-2-1. Synthesis of Diamines and Polyimides

The diamine monomers containing siloxane linkages (**3a**–**3e**) were synthesized under the standard conditions for Williamson's ether synthesis, hydrosilylation, and reduction, as shown in Figure 2-1. The reaction of 4-nitrophenol or with 4-bromo-1-butene or 6-bromo-1-hexene yielded **1a** and **1b** in the presence of potassium carbonate in acetonitrile. The hydrosilylation of compound **1a** or **1b** with 1,1,3,3-tetramethyldisiloxane, 1,1,3,3,5,5-hexamethyltrisiloxane, 1,1,3,3,5,5,7,7-octamethyltetrasiloxane, or 1,1,3,3,5,5,7,7,9,9,11,11-dodecamethylhexasiloxane in the presence of Karstedt's catalyst gave compound **2**. Analytically pure compounds were obtained in good yields (65–97%) after purification, which were hydrogenated to prepare monomer diamines **3**.

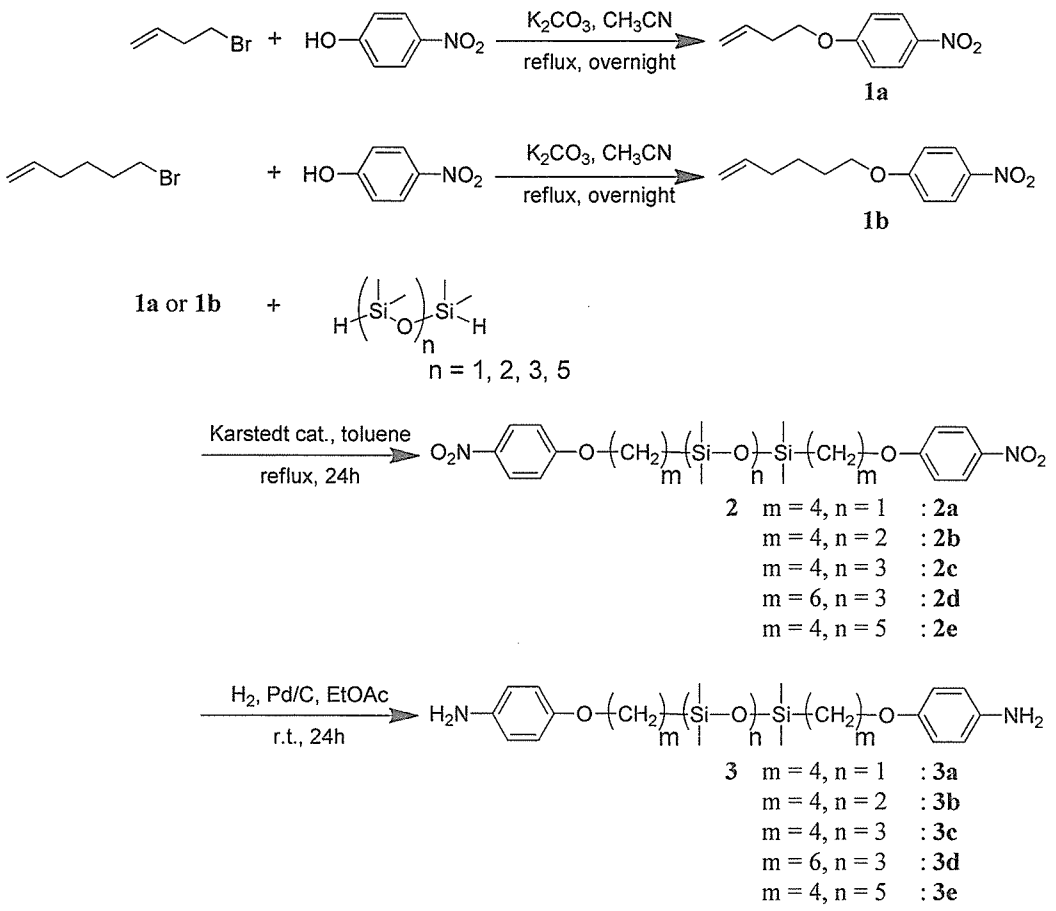

Figure 2-1. Synthetic routes of monomers and diamines **3**.

Figure 2-2 shows the ^{1}H and ^{13}C NMR spectra for diamine **3b** in $CDCl_3$. The signal positions in the ^{1}H NMR spectrum of **3b** are consistent with the proposed structures. The signals at 6.74 and 6.63 ppm can be assigned to the aromatic protons. Furthermore, the methyl protons adjacent to the silyl methyl groups appeared at 0.07 and 0.02 ppm. Similarly, the ^{13}C NMR spectrum shows the expected ten signals.

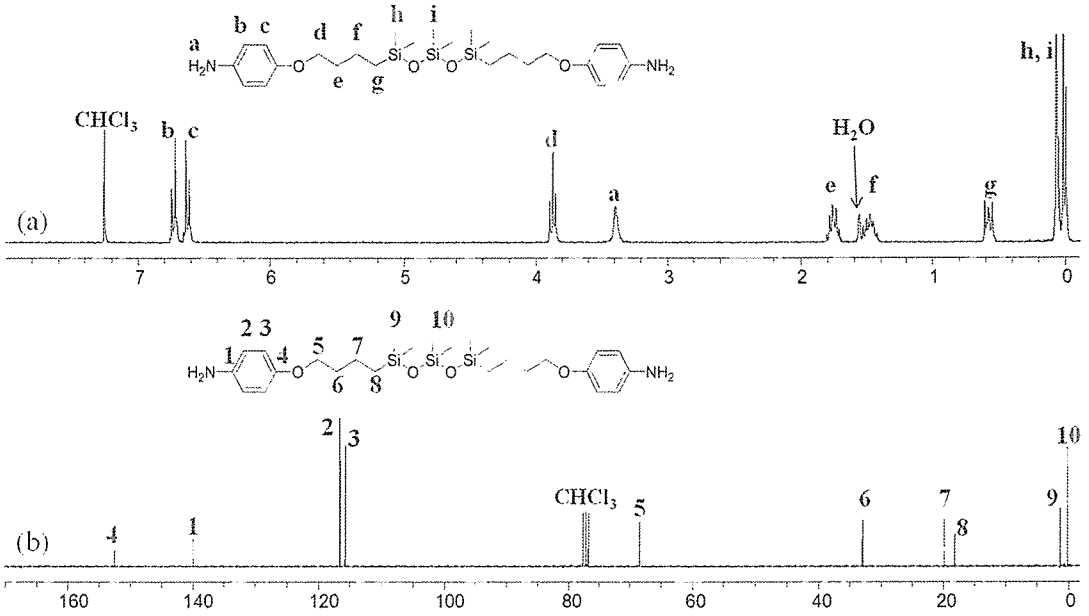

Figure 2-2. (a) ^{1}H and (b) ^{13}C NMR spectra of the diamine **3b**.

The LC polyimides **6** showing in Figure 2-3 were prepared by using a two-step polycondensation procedure. PMDA (**4a**) or BPDA (**4b**) reacted with each diamine **3** at room temperature in *N*-methylpyrrolidone (NMP) to produce poly(amic acid)s (PAAs) **5** with high inherent viscosities in the range of 0.65–1.73 dL/g (Table 2-1). Then, polyimide films were obtained by thermal imidization of the PAAs cast on glass substrates under nitrogen, followed by immersion in warm water. In the representative FT-IR spectrum of prepared polyimide **6h**, the peaks for the amic acid groups disappeared and the characteristic imide peaks at 1770 (C=O asymmetric stretching), 1712 (C=O symmetric stretching), and 1389 cm^{-1} (C–N stretching) appeared, indicating complete imidization. In addition, strong absorption bands were also observed at 2958 and 1257 cm^{-1}, corresponding to C–H stretching of the alkyl groups and Si–C stretching of the siloxane groups, respectively, which further confirms the structures of the polyimides.

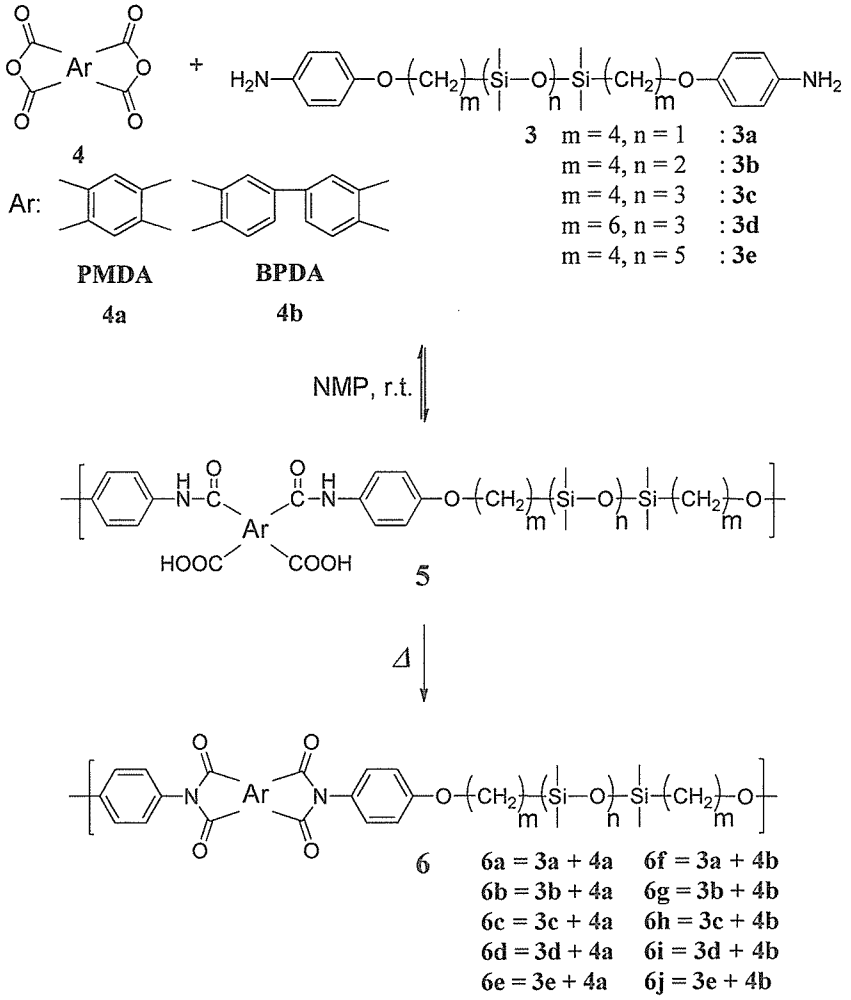

Figure 2-3. Synthetic routes of LC polyimides 6.

Table 2-1. Polymerization results and thermal stabilities.

polymer	Ar	m	n	η_{inh} [dL g^{-1}][a]	$T_{d1\%}$ [°C][b]	$T_{d5\%}$ [°C][b]
6a	**4a**	4	1	0.72	399	454
6b	**4a**	4	2	0.73	426	456
6c	**4a**	4	3	0.66	415	455
6d	**4a**	6	3	0.79	428	454
6e	**4a**	4	5	0.95	431	459
6f	**4b**	4	1	1.07	407	448
6g	**4b**	4	2	1.73	426	460
6h	**4b**	4	3	1.43	430	457
6i	**4b**	6	3	1.19	406	447
6j	**4b**	4	5	1.13	426	454

[a] Inherent viscosities were measured at 30 °C in NMP at a PAAs **5** concentration of 0.5 g dL^{-1}. [b] Decomposition temperature. $T_{d1\%}$: 1% weight loss temperature, $T_{d5\%}$: 5% weight loss temperature in the nitrogen atmosphere.

2-2-2. Thermal Properties

Analyses by TGA under nitrogen indicate that all polyimides **6** are thermally stable up to 400 °C (Table 2-1). The DSC curves of all polyimides **6b–6j** are shown in Figure 2-4. Except for polyimides **6d**, **6e**, and **6j**, all polyimides show more than two exothermic peaks upon cooling. Birefringence and fluidity were observed in the temperature range between these peaks by cross-polarizing microscopy. Therefore, the phase between the transition temperatures corresponds to a liquid crystalline phase. Compared with polyimides **6c** and **6h**, polyimide **6c** has higher crystalline-LC transition temperatures than polyimide **6h** because the aromatic and imide rings in the mesogenic units of polyimide **6c** are coplanar to one another, therefore the intermolecular interactions are stronger between each mesogenic unit than those of polyimide **6h**. As a result, polyimides **6a–c** and **6f–h** show lower crystalline-LC transition temperatures,

275 and 257 °C (**6b**), 237 and 214 °C (**6c**), 253 and 236 °C (**6f**), 250 and 236 °C (**6g**), and 222 and 203 °C (**6h**) on the heating and cooling processes, respectively, by increasing the siloxane units because of the increasing flexibility of the main chains (Table 2-2, Figure 2-5). Moreover, we investigated polyimides **6d** and **6i** with longer methylene spacer units, which are expected to decrease the transition temperatures. However, there is no noticeable change in the temperatures observed by DSC, which suggests that the methylene units are less flexible than siloxane due to the gauche or trans conformational limitations and are therefore ineffective in decreasing the crystal-LC transition temperature. Interestingly, in the case of polyimides **6b–d**, the temperature range of LC behavior narrows as the spacer units become longer and, finally, polyimide **6d**, which has the longest spacer unit among **6b–d**, does not exhibit liquid crystallinity at all. On the other hand, polyimides **6e** and **6j**, with the extended flexible siloxane linkages, have also been designed to decrease transition temperatures. The flexible spacer was expected to lead to a decrease in their transition temperatures. However, neither polyimide **6e** nor **6j** show liquid crystallinity, but instead polyimides **6e** and **6j** exhibit a crystaline and an amorphous nature, respectively, by DSC trace and polarized optical microscopy (POM).

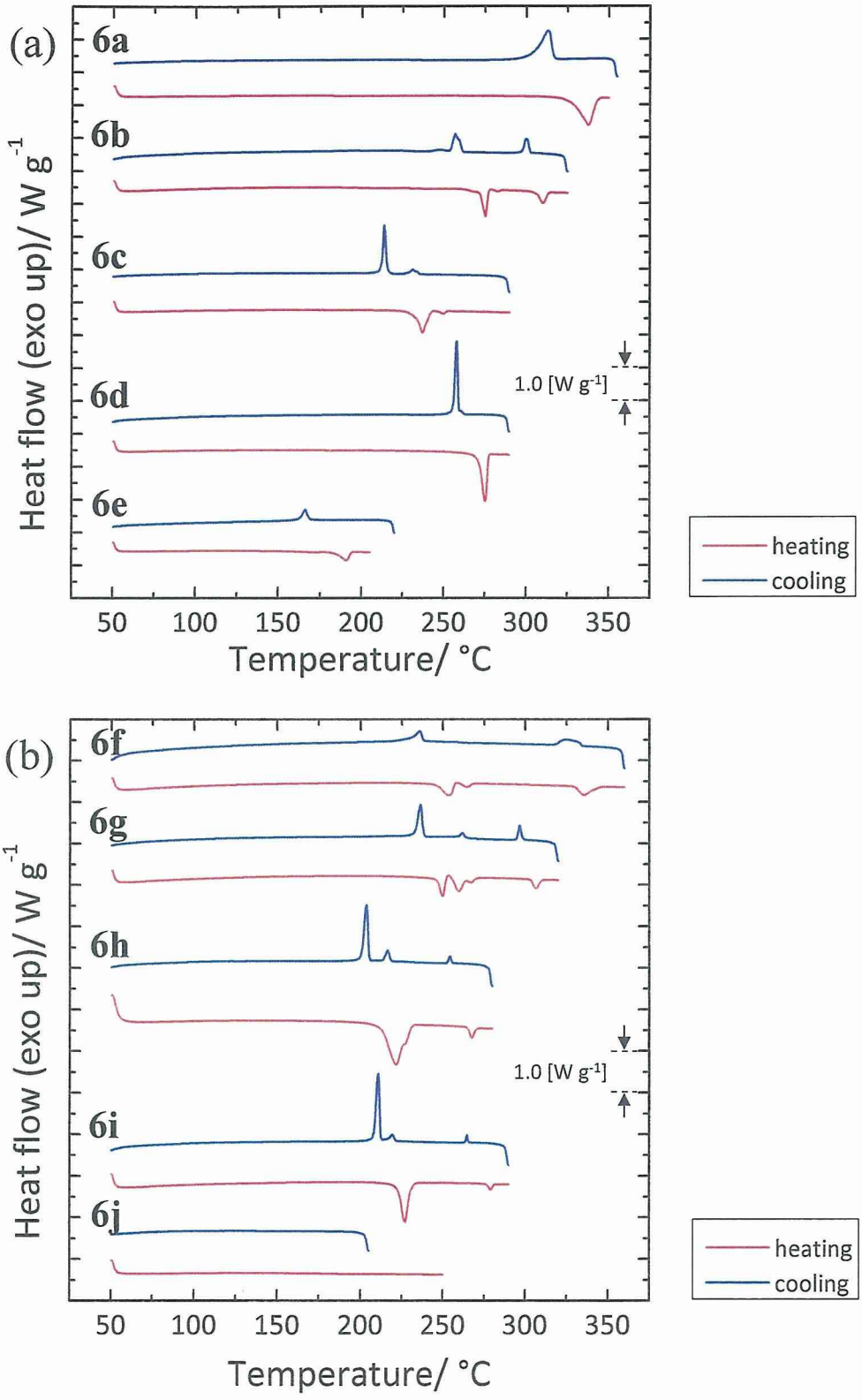

Figure 2-4. DSC heating and cooling curves of polyimides **6** derived from (a) PMDA and (b) BPDA by the measurement performed at a scanning rate of 10 °C min^{-1}.

Table 2-2. Thermal transition temperatures of polyimides **6.**

polymer	Ar	m	n	T_m [°C][a]	$T_{cr\text{-}lc}$ [°C][a]	$T_{lc\text{-}lc}$ [°C][a]	$T_{lc\text{-}i}$ [°C][a]	d_{LC1} [Å]	d_{LC2} [Å]
6a	**4a**	4	1	337	313	*b*	*b*		
6b	**4a**	4	2	275	257	*c*	300		30.8
6c	**4a**	4	3	237	214	*c*	231		32.7
6d	**4a**	6	3	275	*d*	*d*	*d*		
6e	**4a**	4	5	191	*e*	*e*	*e*		
6f	**4b**	4	1	253	236	*c*	325		36.2
6g	**4b**	4	2	250	236	262	297		36.1
6h	**4b**	4	3	222	203	216	254	34.7	35.9
6i	**4b**	6	3	227	211	219	265	32.6	39.1
6j	**4b**	4	5	*e*	*e*	*e*	*e*		

[a] Peak-top temperatures determined by DSC at a second heating and cooling process at the rate of 10 °C min^{-1}. T_m: melting points of polyimide **6** on the heating process. $T_{cr\text{-}lc}$: crystal-LC transition temperature, $T_{lc\text{-}lc}$: LC-LC transition temperature, $T_{lc\text{-}i}$: LC-isotropic transition temperature. [b] No data because of a too high transition temperature (>330 °C) by POM. [c] No detection of the LC-LC transition temperature. [d] There is no LC phase. $T_{cr\text{-}i}$=258 [°C] on a cooling process. [e] Crystalline polyimide **6e**. Amorphous polyimide **6j**; no detection of T_g. T_m: melting temperature and T_g: glass transition temperature.

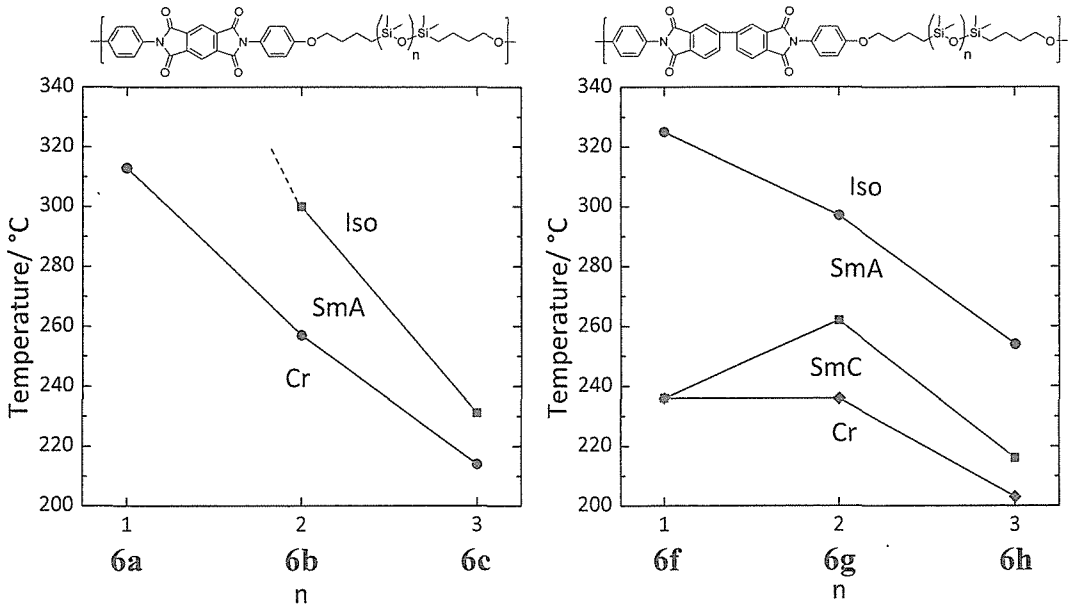

Figure 2-5. Plots of phase transition temperatures of polyimides **6** on the cooling process.

2-2-3. Thermotropic Liquid Crystalline Behavior

Figure 2-6 shows the optical microscopic texture observed for the mesophase of polyimide **6h**. The clear fan-shaped texture observed here is assigned to smectic LC phase. A similar texture was observed in the mesophases of poyimides **6b**, **6c**, **6f**, **6g**, and **6i**. In order to identify the smectic structure, wide-angle X-ray diffraction (WAXD) measurements were performed for fibers spun from the isotropic melt. The typical X-ray patterns are shown in Figure 2-7, as observed for **6g**, which forms two LC phases. For the higher-temperature LC phase, sharp inner reflections are observed on the equator, i.e., along the fiber axis, and broad outer reflections are observed on the meridian (see Figure 2-7a). These profiles clearly show the formation of the SmA phase.[12] On cooling to a lower-temperature LC phase, the inner reflections are evidently split while the outer broad pattern is not significantly altered (Figure 2-7b), showing the transformation from the SmA to the SmC phase. The tilt angle of the molecules of the layer are elucidated as 22° from the splitting angle, which roughly corresponds to 24° calculated from the layer spacing ratio of the SmA to the SmC phase. Polyimide **6h** also shows a similar SmA-SmC transformation, while **6b**, **6c**, **6f**, and **6i** form a single SmA phase before crystallization.

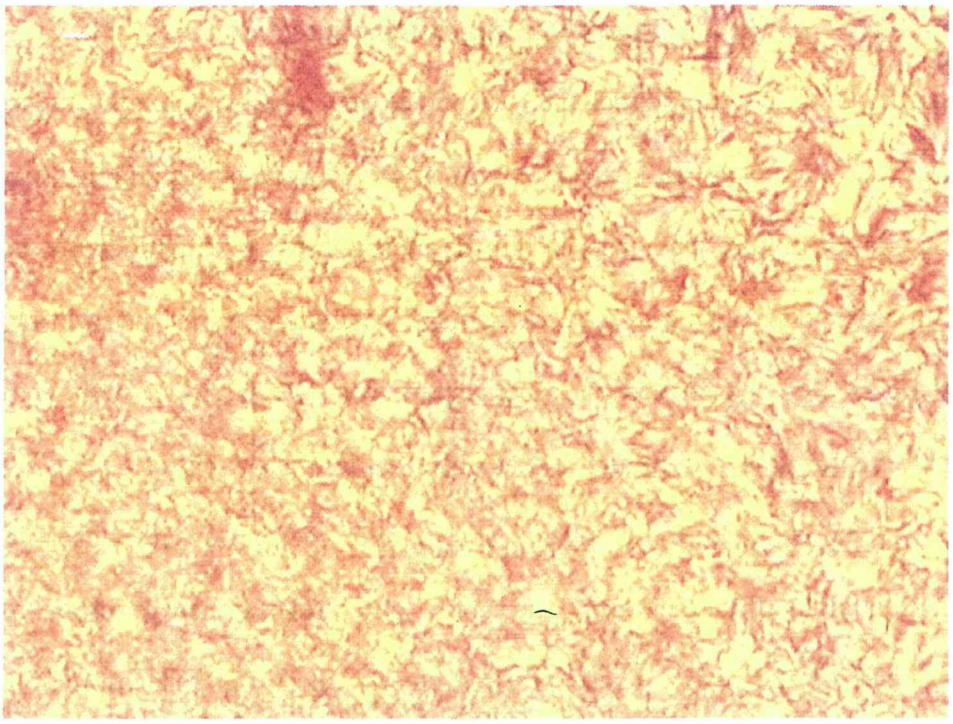

Figure 2-6. Polarized optical microscopic texture observed for SmA of polyimide **6h** at 245 °C.

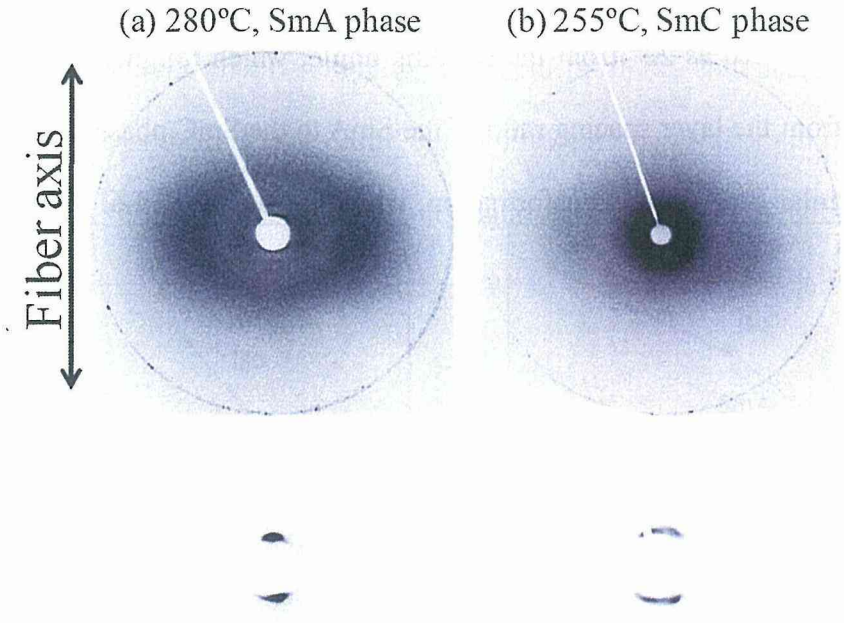

Figure 2-7. Wide angle X-ray diffraction patterns of (a) SmA and (b) SmC phases observed in the fiber samples of **6g**. To show the smectic layer reflection, the small angle region is enlarged in the lower photographs. Fiber axis is set in a vertical direction.

The present polyimides consist of three components, the aromatic, methylene and siloxane groups so the SmA structure can be illustrated as a microsegregation structure of three components (Figure 2-8). Referring to this structure, we compared the SmA layer spacings between homologous polyimides. Of interest is that the layer spacing of the SmA phase, i.e., the average length of the repeating unit, does not change significantly as the number of the siloxane units in the homologous series increases. For example, the layer spacings of SmA for **6f**, **6g**, and **6h** are 36.2, 36.1, and 35.9 Å, respectively, showing no expansion of layer spacing with an increase of two siloxane units (Table 2-2).[13] From a comparison of **6h** and **6i**, however, the SmA layer spacing increases from 35.9 to 39.1 Å; an increase of four methylene units causes a 3.2 Å increase in layer spacing. Thus, it can be concluded that the alkylene parts in the flexible spacer take a relatively extended shape, conforming similarly to the orientational order of the LC, as in the usual case of main-chain LC polymers,[12] while the siloxane parts are not extended at all. In other words, the cross sectional area of the siloxane microdomain should be increased to a significant extent, which spontaneously leads to the unusually large cross sectional areas of the alkylene and mesogenic microdomains. In fact, this trend can be found to express on the spacing of the broad reflection that corresponds to the averaged lateral distance of polymers. In Figure 2-9, 2□ intensity profiles on the equator obtained in the SmA phases of **6f**, **6g**, **6h**, and **6i** are shown. From these intensity profiles, one can find that the peak position of the outer broad reflections gradually shifts from 5.5 to 6.4 Å with an increase in siloxane units. These values are considerably larger than 4.8 Å observed in the analogous polyimide BPDA/6OE, consisting of a BPDA mesogen and polyoxyethylene spacer with 6 oxyethylene units.[14] Therefore, the reason why **6e** and **6j** did not show the LC properties

can be related to the large cross sectional area preventing their mesogenic units from the formation of the smectic layer. Furthermore, it is interested that the outer broad reflection profile seems to have two maximum peaks in the SmA phases in **6b** and **6c**. The corresponding spacings are 7.3 and 5.3 Å for **6c**. Such an appearance of two outer broad reflections has been observed in similar main-chain polymers including the siloxane spacer,[13] and suggests the biaxiality of SmA.[15] Thus, the present polymers including the siloxane unit show some abnormality in their smectic structure formation.

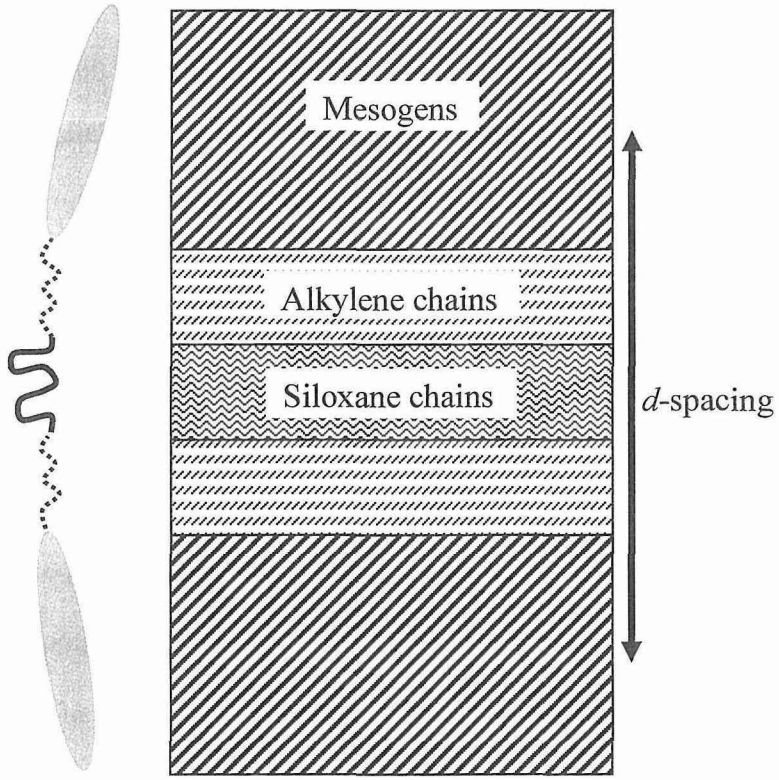

Figure 2-8. Schematic illustration of SmA layer structure in which aromatic, methylene, and siloxane groups are segregated to form sublayers.

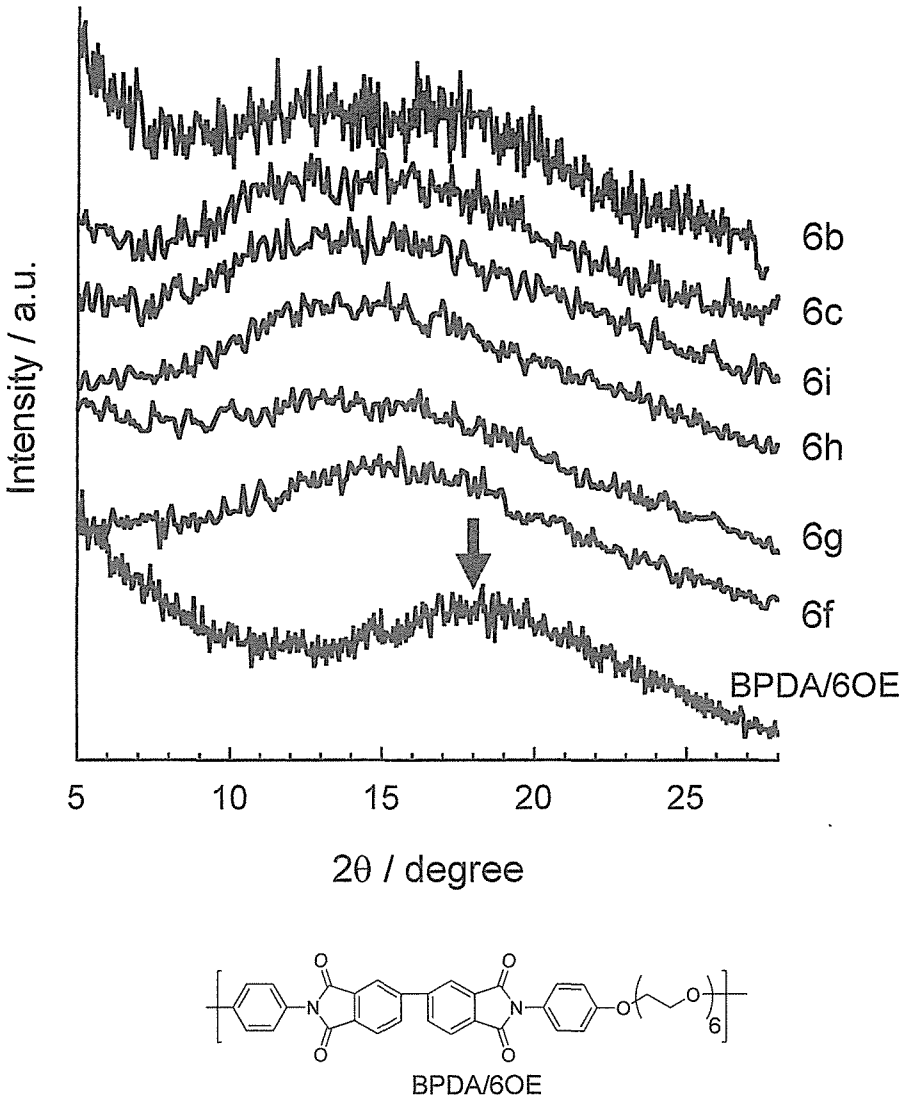

Figure 2-9. *2θ* intensity profiles of outer broad reflections for fiber SmA samples of **6b**, **6c**, **6h**, **6i**, **6g** and **6f**. As a reference, the profile observed for the SmA of BPDA/6OE without polysiloxane spacer (refer to the text) is shown. The arrow indicates the peak position of 4.5 $Å^{-1}$ normally observed in the LC phases of main-chain polymers.

In the course of this study, it was found that all transition temperatures of polyimides **6** became much lower simply by increasing the siloxane units. LC polymers with shorter flexible spacer units are desirable to achieve high thermal conductivity for IC applications. Therefore, the siloxane units indicated the superiority of the alkylene

chains for decreasing the transition temperatures and the obtained polyimides are candidates as high thermal conductive polymers.

2-3. Conclusions

A new series of LC semialiphatic polyimides containing siloxane spacer units were synthesized. They showed higher thermal stabilities ($T_{d5\%}$>450 °C) and lower crystal-LC transition temperatures, 275 and 257 °C (**6b**), 237 and 214 °C (**6c**), 253 and 236 °C (**6f**), 250 and 236 °C (**6g**), and 222 and 203 °C (**6h**) on the heating and cooling processes, respectively, compared to polyimides containing alkylene or oxyethylene spacer units. The transition temperature decreased by the increasing siloxane spacer units, as expected. On the other hand, the polyimides **6e** and **6j** with the extended siloxane linkages aiming at increasing the flexibility did not show liquid crystallinity, unfortunately. WAXD experiments confirmed the layered morphologies of LC polyimides with siloxane spacer units and their *d*-spacings. A SmA phase was formed in the polyimides derived from PMDA, while the polyimides based on BPDA formed a SmC phase as well as a SmA phase. Moreover, the layer spacings of SmA indicated that the alkylene chains in the flexible spacer take a relatively extended conformation, while the siloxane units are not extended at all. From 2θ intensity profiles, the peak position of the outer broad reflections gradually shifts from 5.5 to 6.4 Å with an increase of siloxane units. Further, there is the possibility that the biaxiality in the polyimides is derived from PMDA. These polyimides will be expected that the exhibition of the relatively high thermal conductivity combining with a small amount of thermal conducting fillers and may possibly be used as insulators in electronics fields.

2-4. Experimental Section

2-4-1. Measurements

FT-IR spectra were measured on a Horiba FT-720 spectrometer. ^{1}H and ^{13}C NMR spectra were recorded with a Bruker DPX300S spectrometer. Inherent viscosities were measured at 30 °C in NMP at a polymer concentration of 0.5 g dL^{-1}. The transition characteristics were surveyed with a polarizing microscope (OLYMPUS BX51), together with the use of a LINKAM LTS-350 hot-stage equipped with a temperature controller by setting a polyimide film between crossed polarizers. Thermal analysis was performed on a Seiko EXSTAR 6000 TG/DTA 6300 thermal analyzer at a heating rate of 10 °C/min for thermogravimetry (TG) and a Perkin-Elmer DSC7 calorimeter connected to a cooling system at a heating rate of 10 °C min^{-1} for differential scanning calorimetry (DSC). WAXD measurements were performed at ambient temperature by using a Rigaku-Denki RINT-2500 X-ray generator with monochromic CuKR radiation (40 kV, 50 mA) from graphite crystal of monochromator and flat-plate type of imaging plate.

2-4-2. Materials

PMDA and BPDA were purified by sublimation prior to use. NMP, acetonitrile and toluene were purified by distillation. 1,1,3,3,5,5,7,7,9,9,11,11-Dodecamethylhexasiloxane was synthesized according to the literature.[16] Other reagents and solvents were obtained commercially and used as received.

2-4-3. General Synthesis for Diamines

The diamine monomers containing siloxane linkages (**3a–3e**) were synthesized under the standard conditions for Williamson's ether synthesis, hydrosilylation, and reduction.

Synthesis of 4-(3-Butenyloxy)nitrobenzene (**1a**). The title compound, **1a**, was synthesized according to the literature.[17] To a solution of 4-nitrophenol (0.423 g, 3.04 mmol) and K_2CO_3 (1.11 g, 8.02 mmol) in CH_3CN (20 mL) was added 4-bromo-1-butene (0.827 g, 6.13 mmol), and the mixture was refluxed overnight. The solution was filtered through Celite and the filtrate was concentrated under reduced pressure. The residue was dissolved in CH_2Cl_2, washed with water, dried over $MgSO_4$, and the solvent was removed under reduced pressure to give a crude product, which was flash-chromatographed to give **1a** (yellow oil, 0.57 g, 97% yield). IR (NaCl), ν (cm^{-1}): 2943 (alkyl C–H), 1643 (C=C), 1593 (Ar C–C), 1508, 1335 (–NO_2). ^{1}H NMR (300 MHz, $CDCl_3$, δ, ppm, 25 °C): 8.20 (d, J=9.3 Hz, ArH, 2H), 6.95 (d, J=9.0 Hz, ArH, 2H), 5.96–5.82 (m, vinyl proton, 1H), 5.23–5.12 (m, vinyl proton, 2H), 4.11 (t, J=6.6 Hz, –CH_2–, 2H), 2.62–2.55 (m, –CH_2–, 2H). ^{13}C NMR (75 MHz, $CDCl_3$, δ, ppm, 25 °C): 164.1, 141.5, 133.7, 125.9, 117.7, 114.5, 68.1, 33.4.

Synthesis of 4-(5-Hexenyloxy)nitrobenzene (**1b**). The title compound, **1b**, was synthesized by the same procedure as **1a** performed with 2.79 g (20.0 mmol) of 4-nitrophenol, 4.15 g (30.1 mmol) of K_2CO_3, 4.01 g (24.6 mmol) of 6-bromo-1-hexene, and 40 mL of CH_3CN. The compound, **1b**, (4.11 g, 93% yield) was then isolated as a yellow oil after the vacuum. IR (NaCl), ν (cm^{-1}): 2943 (Alkyl C–H), 1639 (C=C), 1593

(Ar C–C), 1512, 1342 ($–NO_2$). ^1H NMR (300 MHz, $CDCl_3$, δ, ppm, 25 °C): 8.19 (d, J=9.3 Hz, ArH, 2H), 6.94 (d, J=9.3 Hz, ArH, 2H), 5.89–5.76 (m, vinyl proton, 1H), 5.08–4.97 (m, vinyl proton, 2H), 4.06 (t, J=6.5 Hz, $–CH_2–$, 2H), 2.14 (q, J=7.1 Hz, $–CH_2–$, 2H), 1.89–1.80 (m, $–CH_2–$, 2H), 1.63–1.49 (m, $–CH_2–$, 2H). ^{13}C NMR (75 MHz, $CDCl_3$, δ, ppm, 25 °C): 164.3, 141.4, 138.3, 126.0, 115.1, 114.5, 68.8, 33.4, 28.5, 25.3.

Synthesis of 1,3-Bis[4-(4-nitrophenoxy)butyl]-1,1,3,3-tetramethyldisiloxane (**2a**). To a solution of **1a** (0.519 g, 2.69 mmol) and 1,1,3,3-tetramethyldisiloxane (0.125 g, 0.934 mmol), in toluene (3 mL), Karstedt's catalyst (3 drops) (platinum divinyltetrametyhldisiloxane complex in 2 wt% xylene) was added. The reaction mixture was refluxed under nitrogen for 24 h, and then toluene was removed under reduced pressure. The residue was chromatographed (hexane: CH_2Cl_2, (6/4, v/v)) to give **2a**. The compound, **2a**, (0.321 g, 65% yield) was then isolated as a pale yellow oil after the vacuum. IR (NaCl), ν (cm^{-1}): 2951 (Alkyl C–H), 1593 (Ar C–C), 1516, 1338 ($–NO_2$), 1265 (Si–C). ^1H NMR (300 MHz, $CDCl_3$, δ, ppm, 25 °C): 8.19 (d, J=9.0 Hz, ArH, 4H), 6.93 (d, J=9.3 Hz, ArH, 4H), 4.04 (t, J=6.3 Hz, $–CH_2–$, 4H), 1.88–1.79 (m, $–CH_2–$, 4H), 1.54–1.45 (m, $–CH_2–$, 4H), 0.61–0.55 (m, $–CH_2–$, 4H), 0.06 (s, $Si–CH_3$, 12H). ^{13}C NMR (75 MHz, $CDCl_3$, δ, ppm, 25 °C): 164.3, 141.4, 126.0, 114.5, 68.6, 32.5, 19.9, 18.1, 0.503. Anal. Calcd For $C_{24}H_{36}N_2$: C, 55.36; H, 6.97; N, 5.38. Found: C, 55.10; H, 6.91; N, 5.23.

Synthesis of 1,5-Bis[4-(4-nitrophenoxy)butyl]-1,1,3,3,5,5-hexamethyltrisiloxane (**2b**). The title compound, **2b**, was synthesized by the same procedure as **2a** performed with 5.11 g (26.4 mmol) of **1a**, 2.10 g (10.1 mmol) of 1,1,3,3,5,5-hexamethyltrisiloxane,

30 drops of Karstedt's catalyst, and 20 mL of toluene. The compound, **2b**, (5.68 g, 95% yield) was then isolated as a pale yellow oil after the vacuum. IR (NaCl), ν (cm^{-1}): 2954 (Alkyl C–H), 1593 (Ar C–C), 1516, 1338 (–NO_2), 1261 (Si–C). ^1H NMR (300 MHz, $CDCl_3$, δ, ppm, 25 °C): 8.19 (d, J=9.3 Hz, ArH, 4H), 6.93 (d, J=9.0 Hz, ArH, 4H), 4.04 (t, J=6.3 Hz, –CH_2–, 4H), 1.89–1.80 (m, –CH_2–, 4H), 1.57–1.46 (m, –CH_2–, 4H), 0.62–0.57 (m, –CH_2–, 4H), 0.08 (s, Si–CH_3, 12H), 0.03 (s, Si–CH_3, 6H). ^{13}C NMR (75 MHz, $CDCl_3$, δ, ppm, 25 °C): 164.4, 141.4, 126.0, 114.5, 68.6, 32.5, 19.8, 18.0, 1.42, 0.315. Anal. Calcd For $C_{26}H_{42}N_2$: C, 52.49; H, 7.12; N, 4.71. Found: C, 52.88; H, 6.95; N, 4.71.

Synthesis of 1,7-Bis[4-(4-nitrophenoxy)butyl]-1,1,3,3,5,5,7,7-octamethyltetrasiloxane (**2c**). The title compound, **2c**, was synthesized by the same procedure as **2a** performed with 4.27 g (22.1 mmol) of **1a**, 2.82 g (9.98 mmol) of 1,1,3,3,5,5,7,7-octamethyltetrasiloxane, 30 drops of Karstedt's catalyst, and 20 mL of toluene. The compound, **2c**, (5.00 g, 75% yield) was then isolated as a pale yellow oil after the vacuum. IR (NaCl), ν (cm^{-1}): 2958 (Alkyl C–H), 1593 (Ar C–C), 1516, 1342 (–NO_2), 1261 (Si–C). ^1H NMR (300 MHz, $CDCl_3$, δ, ppm, 25 °C): 8.19 (d, J=9.3 Hz, ArH, 4H), 6.93 (d, J=9.3 Hz, ArH, 4H), 4.05 (t, J=6.3 Hz, –CH_2–, 4H), 1.89–1.80 (m, –CH_2–, 4H), 1.57–1.47 (m, –CH_2–, 4H), 0.63–0.57 (m, –CH_2–, 4H), 0.09 (s, Si–CH_3, 12H), 0.04 (s, Si–CH_3, 12H). ^{13}C NMR (75 MHz, $CDCl_3$, δ, ppm, 25 °C): 164.4, 141.4, 126.0, 114.5, 68.6, 32.5, 19.8, 18.0, 1.34, 0.314. Anal. Calcd For $C_{28}H_{48}N_2$: C, 50.27; H, 7.23; N, 4.19. Found: C, 50.37; H, 7.03; N, 4.21.

Synthesis of 1,7-Bis[6-(4-nitrophenoxy)hexyl]-1,1,3,3,5,5,7,7-octamethyltetrasiloxane (**2d**). The title compound, **2d**, was synthesized by the same procedure as **2a** performed with 3.32 g (15.0 mmol) of **1b**, 1.53 g (5.42 mmol) of 1,1,3,3,5,5,7,7-octamethyltetrasiloxane, 30 drops of Karstedt's catalyst, and 15 mL of toluene. The compound, **2d**, (3.79 g, 97% yield) was then isolated as a pale yellow oil after the vacuum. IR (NaCl), ν (cm^{-1}): 2924 (Alkyl C–H), 1593 (Ar C–C), 1516, 1342 ($–NO_2$), 1261 (Si–C). ^1H NMR (300 MHz, $CDCl_3$, δ, ppm, 25 °C): 8.19 (d, J=9.3 Hz, ArH, 4H), 6.93 (d, J=9.3 Hz, ArH, 4H), 4.04 (t, J=6.5 Hz, $–CH_2–$, 4H), 1.89–1.77 (m, $–CH_2–$, 4H), 1.53–1.33 (m, $–CH_2–$, 12H), 0.57–0.50 (m, $–CH_2–$, 4H), 0.07 (s, $Si–CH_3$, 12H), 0.04 (s, $Si–CH_3$, 12H). ^{13}C NMR (75 MHz, $CDCl_3$, δ, ppm, 25 °C): 164.6, 141.9, 126.2, 114.8, 69.3, 33.4, 29.3, 26.0, 23.5, 18.6, 1.56, 0.57. Anal. Calcd For $C_{32}H_{56}N_2$: C, 53.00; H, 7.78; N, 3.86. Found: C, 52.94; H, 7.58; N, 3.72.

Synthesis of 1,11-Bis[4-(4-nitrophenoxy)butyl]-1,1,3,3,5,5,7,7,9,9,11,11-dodecamethylhexasiloxane (**2e**). The title compound, **2e**, was synthesized by the same procedure as **2a** performed with 0.709 g (3.67 mmol) of **1a**, 0.647 g (1.50 mmol) of 1,1,3,3,5,5,7,7,9,9,11,11-dodecamethylhexasiloxane, 5 drops of Karstedt's catalyst, and 5 mL of toluene. The compound, **2e**, (1.18 g, 96% yield) was then isolated as a pale yellow oil after the vacuum. IR (NaCl), ν (cm^{-1}): 2958 (Alkyl C–H), 1593 (Ar C–C), 1516, 1342 ($–NO_2$), 1261 (Si–C). ^1H NMR (300 MHz, $CDCl_3$, δ, ppm, 25 °C): 8.18 (d, J=9.6 Hz, ArH, 4H), 6.93 (d, J=9.3 Hz, ArH, 4H), 4.05 (t, J=6.3 Hz, $–CH_2–$, 4H), 1.89–1.80 (m, $–CH_2–$, 4H), 1.57–1.47 (m, $–CH_2–$, 4H), 0.63–0.57 (m, $–CH_2–$, 4H), 0.09

(s, Si–CH_3, 12H), 0.06 (s, Si–CH_3, 12H), 0.05 (s, Si–CH_3, 12H). ^{13}C NMR (75 MHz, $CDCl_3$, δ, ppm, 25 °C): 164.4, 141.4, 126.0, 114.5, 68.6, 32.6, 19.8, 18.0, 1.33, 1.25, 0.314. Anal. Calcd For $C_{32}H_{60}N_2$: C, 47.02; H, 7.40; N, 3.43. Found: C, 46.91; H, 7.12; N, 3.43.

Synthesis of 1,3-Bis[4-(4-aminophenoxy)butyl]-1,1,3,3-tetramethyldisiloxane (**3a**). A mixture of nitro compound **2a** (1.35 g, 2.60 mmol) and Pd/C (0.0393 g, 10 wt%) in EtOAc (10 mL) was stirred at room temperature for 24 h under hydrogen atmosphere by using a balloon. The solution was filtered through celite and concentrated to give the diamine **3a** (1.18 g, 98% yield) as a light brown oil. IR (NaCl), v (cm^{-1}): 3356 (N–H), 2951 (Alkyl C–H), 1624 (N–H), 1512 (Ar C–C), 1238 (Si–C). ^1H NMR (300 MHz, $CDCl_3$, δ, ppm, 25 °C): 6.74 (d, J=9.0 Hz, ArH, 4H), 6.63 (d, J=9.0 Hz, ArH, 4H), 3.87 (t, J=6.3 Hz, –CH_2–, 4H), 3.40 (s, NH_2, 4H), 1.80–1.71 (m, –CH_2–, 4H), 1.54–1.42 (m, –CH_2–, 4H), 0.61–0.53 (m, –CH_2–, 4H), 0.05 (s, Si–CH_3, 12H). ^{13}C NMR (75 MHz, $CDCl_3$, δ, ppm, 25 °C): 152.5, 139.9, 116.5, 115.8, 68.4, 33.1, 20.0, 18.3, 0.510.

Synthesis of 1,5-Bis[4-(4-aminophenoxy)butyl]-1,1,3,3,5,5-hexamethyltrisiloxane (**3b**). The title compound, **3b**, was synthesized by the same procedure as **3a** performed with 2.79 g (4.69 mmol) of **2b**, 0.0262 g of Pd/C (10 wt%), and 15 mL of EtOAc. The compound, **3a**, (2.48 g, 99% yield) was then isolated as a light brown oil after the vacuum. IR (NaCl), v (cm^{-1}): 3359 (N–H), 2954 (Alkyl C–H), 1624 (N–H), 1512 (Ar C–C), 1238 (Si–C). ^1H NMR (300 MHz, $CDCl_3$, δ, ppm, 25 °C): 6.74 (d, J=8.7 Hz, ArH, 4H), 6.63 (d, J=9.0 Hz, ArH, 4H), 3.87 (t, J=6.3 Hz, –CH_2–, 4H), 3.39 (s, NH_2, 4H), 1.81–1.71 (m, –CH_2–, 4H), 1.54–1.43 (m, –CH_2–, 4H), 0.61–0.55 (m, –CH_2–, 4H), 0.07

(s, Si–CH_3, 12H), 0.02 (s, Si–CH_3, 6H). ^{13}C NMR (75 MHz, $CDCl_3$, δ, ppm, 25 °C): 152.5, 139.9, 116.5, 115.7, 68.4, 33.1, 19.9, 18.1, 1.45, 0.344.

Synthesis of 1,7-Bis[4-(4-aminophenoxy)butyl]-1,1,3,3,5,5,7,7-octamethyltetrasiloxane (**3c**). The title compound, **3c**, was synthesized by the same procedure as **3a** performed with 2.26 g (3.38 mmol) of **2c**, 0.0209 g of Pd/C (10 wt%), and 15 mL of EtOAc. The compound, **3c**, (2.05 g, 99% yield) was then isolated as a light brown oil after the vacuum. IR (NaCl), v (cm^{-1}): 3359 (N–H), 2958 (Alkyl C–H), 1624 (N–H), 1512 (Ar C–C), 1238 (Si–C). ^1H NMR (300 MHz, $CDCl_3$, δ, ppm, 25 °C): 6.74 (d, J=9.0 Hz, ArH, 4H), 6.63 (d, J=9.0 Hz, ArH, 4H), 3.88 (t, J=6.3 Hz, –CH_2–, 4H), 3.39 (s, NH_2, 4H), 1.81–1.72 (m, –CH_2–, 4H), 1.54–1.43 (m, –CH_2–, 4H), 0.62–0.56 (m, –CH_2–, 4H), 0.08 (s, Si–CH_3, 12H), 0.04 (s, Si–CH_3, 12H). ^{13}C NMR (75 MHz, $CDCl_3$, δ, ppm, 25 °C): 152.5, 139.9, 116.5, 115.8, 68.4, 33.1, 19.9, 18.1, 1.35, 0.334.

Synthesis of 1,7-Bis[6-(4-aminophenoxy)hexyl]-1,1,3,3,5,5,7,7-octamethyltetrasiloxane (**3d**). The title compound, **3d**, was synthesized by the same procedure as **3a** performed with 2.71 g (3.73 mmol) of **2d**, 0.0150 g of Pd/C (10 wt%), and 15 mL of EtOAc. The compound, **3d**, (2.47 g, 99% yield) was then isolated as a light brown oil after the vacuum. IR (NaCl), v (cm^{-1}): 3359 (N–H), 2924 (Alkyl C–H), 1624 (N–H), 1512 (Ar C–C), 1238 (Si–C). ^1H NMR (300 MHz, $CDCl_3$, δ, ppm, 25 °C): 6.74 (d, J=9.3 Hz, ArH, 4H), 6.63 (d, J=8.7 Hz, ArH, 4H), 3.87 (t, J=6.6 Hz, –CH_2–, 4H), 3.40 (s, NH_2, 4H), 1.78–1.68 (m, –CH_2–, 4H), 1.47–1.32 (m, –CH_2–, 12H), 0.57–0.51 (m, –CH_2–, 4H), 0.06 (s, Si–CH_3,

12H), 0.04 (s, Si–CH_3, 12H). ^{13}C NMR (75 MHz, $CDCl_3$, δ, ppm, 25 °C): 152.5, 139.9, 116.5, 115.8, 68.8, 33.3, 29.5, 25.9, 23.3, 18.4, 1.36, 0.347.

Synthesis of 1,7-Bis[4-(4-aminophenoxy)butyl]-1,1,3,3,5,5,7,7,9,9,11,11-dodecamethylhexasiloxane (**3e**). The title compound, **3e**, was synthesized by the same procedure as **3a** performed with 1.02 g (1.25 mmol) of **2e**, 0.0203 g of Pd/C (10 wt%), and 10 mL of EtOAc. The compound, **3e**, (0.943 g, 99% yield) was then isolated as a light brown oil after the vacuum. IR (NaCl), ν (cm^{-1}): 3363 (N–H), 2958 (Alkyl C–H), 1624 (N–H), 1512 (Ar C–C), 1257 (Si–C). ^1H NMR (300 MHz, $CDCl_3$, δ, ppm, 25 °C): 6.74 (d, J=9.0 Hz, ArH, 4H), 6.63 (d, J=8.7 Hz, ArH, 4H), 3.88 (t, J=6.3 Hz, –CH_2–, 4H), 3.41 (s, NH_2, 4H), 1.82–1.73 (m, –CH_2–, 4H), 1.55–1.44 (m, –CH_2–, 12H), 0.63–0.57 (m, –CH_2–, 4H), 0.09 (s, Si-CH_3, 12H), 0.08 (s, Si–CH_3, 12H), 0.06 (s, Si–CH_3, 12H). ^{13}C NMR (75 MHz, $CDCl_3$, δ, ppm, 25 °C): 152.5, 139.9, 116.5, 115.8, 68.4, 33.1, 19.9, 18.1, 1.33, 1.23, 0.314.

2-4-4. General Procedure for Polymer Synthesis

PMDA (**4a**) or BPDA (**4b**) was added to a solution of the diamines, **3**, in NMP, and the solution was stirred at room temperature for 12 h. Then a poly(amic acid) solution (15 wt%) was casted on a glass substrate and the imidization was carried out by heating in steps on hot-plate, finally the temperature was increased to 200 °C. Opaque yellow films, **6**, were obtained.

Synthesis of Polyimide **6a**. The above general procedure was applied using 0.258 g

(0.560 mmol) of **3a**, 0.122 g (0.559 mmol) of **4a**, and 2.15 g of NMP. IR (Si wafer), ν (cm^{-1}): 2954 (Alkyl C–H), 1782 (C=O), 1724 (C=O), 1400 (C–N), 1254 (Si–C). Anal. Calcd For $C_{34}H_{38}N_2$: C, 63.52; H, 5.96; N, 4.36. Found: C, 63.13; H, 6.00; N, 4.16.

Synthesis of Polyimide **6b**. The above general procedure was applied using 0.899 g (1.68 mmol) of **3b**, 0.366 g (1.68 mmol) of **4a**, and 7.15 g of NMP. IR (Si wafer), ν (cm^{-1}): 2958 (Alkyl C–H), 1782 (C=O), 1724 (C=O), 1400 (C–N), 1254 (Si–C). Anal. Calcd For $C_{36}H_{44}N_2$: C, 60.30; H, 6.19; N, 3.91. Found: C, 60.11; H, 6.14; N, 3.75.

Synthesis of Polyimide **6c**. The above general procedure was applied using 0.589 g (0.967 mmol) of **3c**, 0.211 g (0.967 mmol) of **4a**, and 4.54 g of NMP. IR (Si wafer), ν (cm^{-1}): 2958 (Alkyl C–H), 1782 (C=O), 1724 (C=O), 1396 (C–N), 1254 (Si–C). Anal. Calcd For $C_{38}H_{50}N_2$: C, 57.69; H, 6.37; N, 3.54. Found: C, 57.58; H, 6.27; N, 3.43.

Synthesis of Polyimide **6d**. The above general procedure was applied using 1.09 g (1.64 mmol) of **3d**, 0.357 g (1.64 mmol) of **4a**, and 8.20 g of NMP. IR (Si wafer), ν (cm^{-1}): 2958 (Alkyl C–H), 1782 (C=O), 1724 (C=O), 1400 (C–N), 1254 (Si–C). Anal. Calcd For $C_{42}H_{58}N_2$: C, 59.54; H, 6.90; N, 3.31. Found: C, 59.37; H, 6.80; N, 3.05.

Synthesis of Polyimide **6e**. The above general procedure was applied using 0.353 g (0.466 mmol) of **3e**, 0.102 g (0.466 mmol) of **4a**, and 2.56 g of NMP. IR (Si wafer), ν (cm^{-1}): 2958 (Alkyl C–H), 1774 (C=O), 1720 (C=O), 1381 (C–N), 1254 (Si–C). Anal. Calcd For $C_{40}H_{54}N_2$: C, 58.65; H, 6.64; N, 3.42. Found: C, 58.38; H, 6.65; N, 3.06.

Synthesis of Polyimide **6f**. The above general procedure was applied using 0.467 g (1.01 mmol) of **3a**, 0.298 g (1.01 mmol) of **4b**, and 3.01 g of NMP. IR (Si wafer), ν (cm^{-1}): 2954 (Alkyl C–H), 1770 (C=O), 1716 (C=O), 1389 (C–N), 1254 (Si–C). Anal. Calcd For $C_{40}H_{42}N_2$: C, 66.82; H, 5.89; N, 3.90. Found: C, 66.58; H, 5.96; N, 3.74.

Synthesis of Polyimide **6g**. The above general procedure was applied using 1.09 g (2.04 mmol) of **3b**, 0.599 g (2.04mmol) of **4b**, and 9.54 g of NMP. IR (Si wafer), ν (cm^{-1}): 2958 (Alkyl C–H), 1770 (C=O), 1712 (C=O), 1389 (C–N), 1257 (Si–C). Anal. Calcd For $C_{42}H_{48}N_2$: C, 63.61; H, 6.10; N, 3.53. Found: C, 63.71; H, 6.09; N, 3.48.

Synthesis of Polyimide **6h**. The above general procedure was applied using 0.306 g (0.502 mmol) of **3c**, 0.148 g (5.02 mmol) of **4b**, and 2.57 g of NMP. IR (Si wafer), ν (cm^{-1}): 2958 (Alkyl C–H), 1770 (C=O), 1712 (C=O), 1389 (C–N), 1257 (Si–C). Anal. Calcd For $C_{44}H_{54}N_2$: C, 60.94; H, 6.28; N, 3.23. Found: C, 60.81; H, 6.13; N, 3.04.

Synthesis of Polyimide **6i**. The above general procedure was applied using 0.994 g (1.49 mmol) of **3d**, 0.439 g (1.49 mmol) of **4b**, and 8.12 g of NMP. IR (Si wafer), ν (cm^{-1}): 2958 (Alkyl C–H), 1770 (C=O), 1712 (C=O), 1389 (C–N), 1254 (Si–C). Anal. Calcd For $C_{48}H_{62}N_2$: C, 62.44; H, 6.77; N, 3.03. Found: C, 62.01; H, 6.65; N, 2.77.

Synthesis of Polyimide **6j.** The above general procedure was applied using 0.485 g (0.641 mmol) of **3e**, 0.189 g (0.643 mmol) of **4b**, and 3.81 g of NMP. IR (Si wafer), ν (cm^{-1}): 2958 (Alkyl C–H), 1774 (C=O), 1720 (C=O), 1381 (C–N), 1254 (Si–C). Anal. Calcd For $C_{46}H_{58}N_2$: C, 61.71; H, 6.53; N, 3.13. Found: C, 61.56; H, 6.49; N, 2.83.

2-5. References and Notes

1. Akatsuka, M.; Takezawa, Y. *J. Appl. Polym. Sci.* **2003**, *89*, 2464.
2. Osada, K.; Niwano, H.; Tokita, M.; Kawauchi, S.; Watanabe, J. *Macromolecules* **2000**, *33*, 7420.
3. Patil, H. P.; Lentz, D. M.; Hedden, R. C. *Macromolecules* **2009**, *42*, 3525.
4. Kato, T.; Nagahara, T.; Agari, Y.; Ochi, M. *J. Appl. Polym. Sci.* **2007**, *104*, 3453.
5. Harada, M.; Ochi, M.; Tobita, M.; Kimura, T.; Ishigaki, T.; Shimayama, N.; Aoki, H. *J. Polym. Sci., Part B: Polym. Phys.* **2003**, *41*, 1739.
6. Bessonov, M. I.; Koton, M. M.; Kudryavstev, V. V.; Laius, L. A. In *Polyimides: Thermally Stable Polymers*; Consultants Bureau: New York, 1987.
7. Wilson, D.; Stenzenberger, H. D.; Hergenrother, P. *Polyimides*: Blackie: New York, 1990.
8. Inoue, T.; Kakimoto, M.; Imai, Y.; Watanabe, J. *Macromol. Chem. Phys.* **1997**, *198*, 519.
9. Kaneko, T. I.; Imamura, K.; Watanabe, J. *Macromolecules* **1997**, *30*, 4244.
10. Huang, H. W.; Kaneko, T. I.; Horie, K.; Watanabe, J. *Polymer* **1999**, *40*, 3821.
11. Coatat, G.; Eastmond, G. C.; Fairclough, J. P. A.; Paprotny, J.; Ryan, A. J.; Stagnaro, P. *Macromolecules* **2008**, *41*, 1034.
12. Watanabe, J.; Hayashi, M. *Macromolecules* **1988**, *21*, 278.
13. Braun, F.; Willner, L.; Hess, M.; Kosfeld, R. *Makromol. Chem.* **1990**, *191*, 1775.
14. We synthesized LC polyimide with 6 oxyethylene units (BPDA/6OE) according to the previous report (n=6) (see ref 11). Inherent viscosity was 1.04 dL/g. Transition temperatures of BPDA/6OE were determined to be $T_{cr\text{-}lc}$=239 °C and $T_{lc\text{-}i}$=282 °C

on the heating process.

15. Chandrasekhar, S.; Nair, G. G.; Rao, S. D.S.; Prasad, S.; Krishna, P. K.; Blunk, D. *Liq. Cryst.* **1998**, *24*, 67.
16. Li, Guo; Zhijie, Zhang; Yangping, Zhu; Junping, Li; Zemin, Xie *J. Appl. Polym. Sci.* **2008**, *108*, 1901.
17. Lipshutz, B. H.; Ghorai, S.; Boskovic, Z. V. *Tetrahedron* **2008**, *64*, 6949.

Chapter 3

Synthesis and Liquid Crystalline Behavior of Laterally Substituted Polyimides with Siloxane Linkages

Abstract.

Novel siloxane-containing liquid crystalline (LC) polyimides with methyl, chloro, and fluoro substituents on mesogenic units have been developed from siloxane-containing diamines with pyromellitic dianhydride (PMDA) or 3,3',4,4'-tetracarboxybiphenyl dianhydride (BPDA), and their thermotropic LC behavior was examined. Among these, chloro and fluoro substituents are effective for the formation of LC phases, particularly when those are substituted away from the center of the mesogenic unit: the isotropization temperature is not much affected, but the crystal-LC transition temperatures are significantly decreased. On the other hand, the methyl substituent tends to interrupt liquid crystallization as well as crystallization. Thus, the fluoro-substituted polyimide derived from BPDA exhibited the lowest crystalline-LC transition temperature ($T_{cr\text{-}lc}$=163 °C) among all polyimides, showing a wide liquid crystal temperature up to 238 °C. From the X-ray diffraction measurement conducted for the oriented mesophases of fibrous polyimides, they were found to form

SmA and SmC as high- and low-temperature mesophases, respectively.

3-1. Introduction

Liquid crystalline (LC) polyimides are expected as thermal conductivity materials because the alignment of LC polymers effectively conducts "phonon" which is the media of thermal conductivity for organic polymers.[1]

In chapter 2, the synthesis of thermotropic LC polyimides from diamines containing siloxane spacer units and pyromellitic dianhydride (PMDA) or 3,3',4,4'-tetracarboxybiphenyl dianhydride (BPDA) and their LC behavior are described. The crystal-LC transition temperatures ranged from 222 to 275 °C in the heating process, depending on the number of methylene or siloxane units. These LC transition temperatures were lower than those of corresponding polyimides with alkylene or oxyethylene spacer units. However, a further decrease in the transition temperatures of polyimides is required to avoid the destruction of semiconductor chips inside integrated circuits (ICs) during the fabrication process in practical application.

In this chapter, the synthesis of novel laterally substituted LC polyimides derived from PMDA or BPDA with diamines containing siloxane spacer units and their thermotropic LC behavior are described in detail. The purpose of this work is to determine which kinds and positions of substituents are effective for decreasing the crystal-LC transition temperatures of polyimides. The molecular designs of the substituents include methyl, fluoro, and chloro groups, expecting to reduce the molecular interaction of the mesogenic units.

3-2. Results and Discussion

3-2-1. Synthesis of Diamines and Polyimides

An LC polyimide backbone with octamethyltetrasiloxane spacer units was selected,

which showed the lowest crystal-LC transition temperature (222 °C) in chapter 2.2.3 Methyl-, fluoro-, or chloro-substituted diamine monomers containing octamethyltetrasiloxane units (**3b–f**) were newly synthesized under standard conditions for Williamson's ether synthesis, hydrosilylation, and reduction, as shown in Figure 3-1.

Figure 3-2 representatively shows the ^{1}H and ^{13}C NMR spectra for diamine **3d** in $CDCl_3$. The signal assignments in the ^{1}H NMR spectrum of **3d** are consistent with the proposed structures. The signals at 6.53 (b) and 6.76 ppm (a, c) correspond to aromatic protons. The resonances for methylene protons (g, f, e, and d) were clearly observed at 0.57–0.63, 1.47–1.58, 1.76–1.85, and 3.93 ppm, respectively. Furthermore, the signals of protons adjacent to the methylsilyl groups appeared at 0.05 and 0.08 ppm. The target structure of **3d** was also confirmed by the ^{13}C NMR spectrum, showing the expected 12 signals.

Table 3-1. Polymerization results and thermal stabilities.

polymer	Ar	R_1	R_2	η_{inh} [dL g^{-1}][a]	$T_{d1\%}$ [°C][b]	$T_{d5\%}$ [°C][b]
6a	**4a**	H	H	0.66	415	455
6b	**4a**	CH_3	H	0.67	421	443
6c	**4a**	F	H	0.62	412	443
6d	**4a**	Cl	H	0.86	414	444
6e	**4b**	H	H	1.43	430	457
6f	**4b**	CH_3	H	2.04	415	443
6g	**4b**	F	H	0.83	426	443
6h	**4b**	Cl	H	0.75	420	446
6i	**4b**	H	CH_3	0.78	408	452
6j	**4b**	H	F	1.60	392	440

[a] Inherent viscosities of PAAs **5** were measured at 30 °C in NMP at a PAA **5** concentration of 0.5 g dL^{-1}. [b] Decomposition temperature. $T_{d1\%}$: 1% weight loss temperature, $T_{d5\%}$: 5% weight loss temperature in the nitrogen atmosphere.

Polyimides **6** were synthesized by using a two-step polycondensation procedure, as shown in Figure 3-3. Poly(amic acid)s (PAAs) **5**, which are the precursors of polyimides, were prepared from each diamine **3** and tetracarboxydianhydride derivatives (PMDA (**4a**) or BPDA (**4b**)) at room temperature in *N*-methylpyrrolidone (NMP). The resulting PAAs had high inherent viscosities in the range 0.62–2.04 dL g^{-1} (Table 3-1). They were then cast and gradually heated up to 200 °C for 2 h on glass substrates under nitrogen to obtain polyimide films. In the representative FT-IR spectrum of obtained polyimide **6g**, the peaks for the amic acid groups disappeared and the characteristic imide peaks at 1770 (C=O asymmetric stretching), 1713 (C=O symmetric stretching), and 1389 cm^{-1} (C–N stretching) appeared, indicating complete imidization. The expected polyimide structures were also confirmed by elemental analysis.

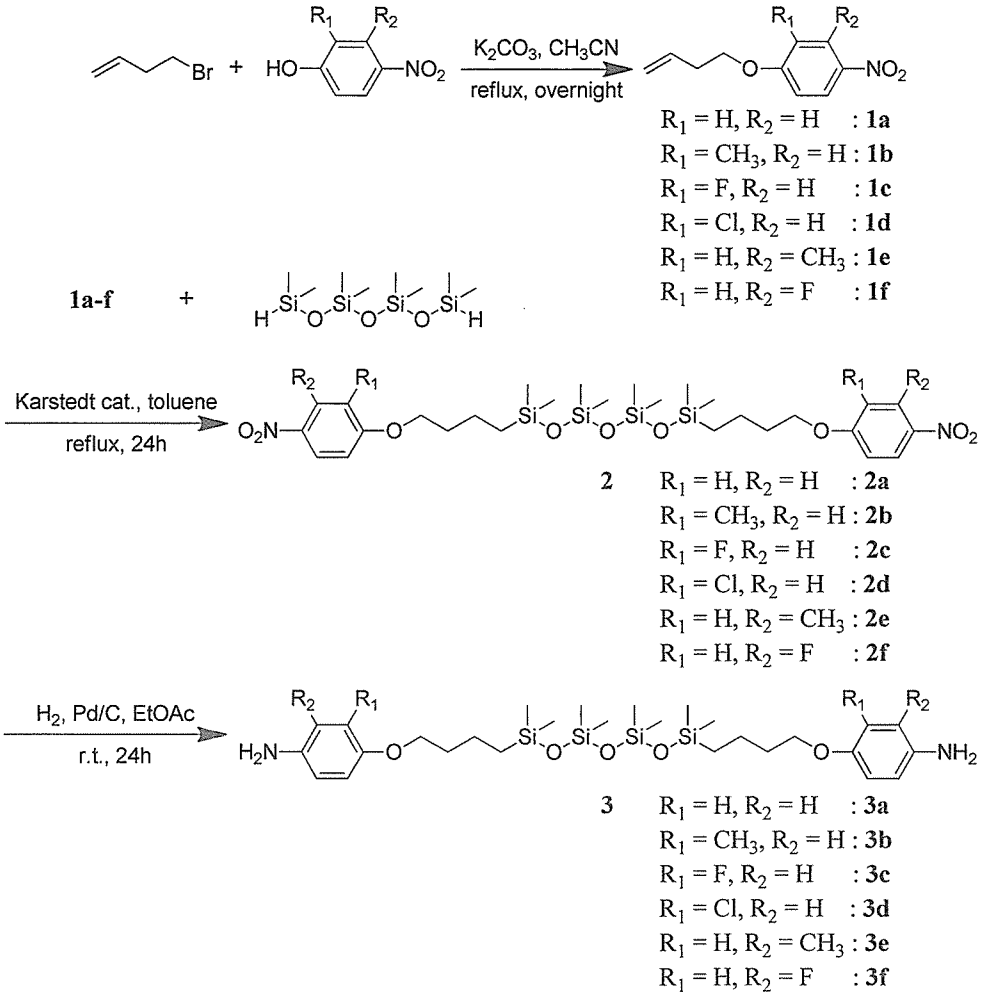

Figure 3-1. Synthetic routes of monomers and diamines **3**.

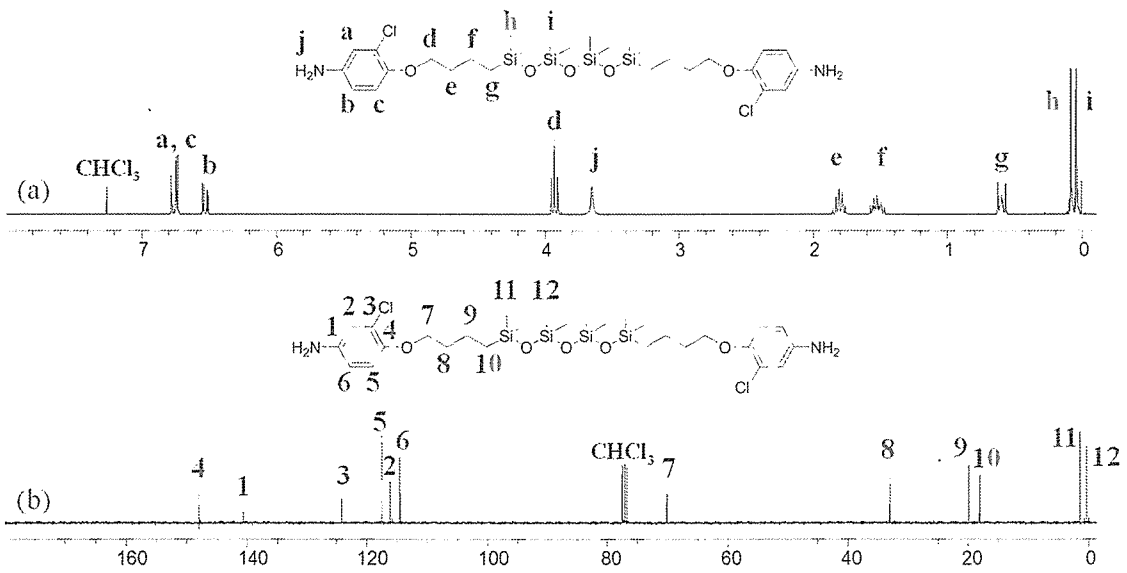

Figure 3-2. (a) ^{1}H and (b) ^{13}C NMR spectra of the diamine **3d**.

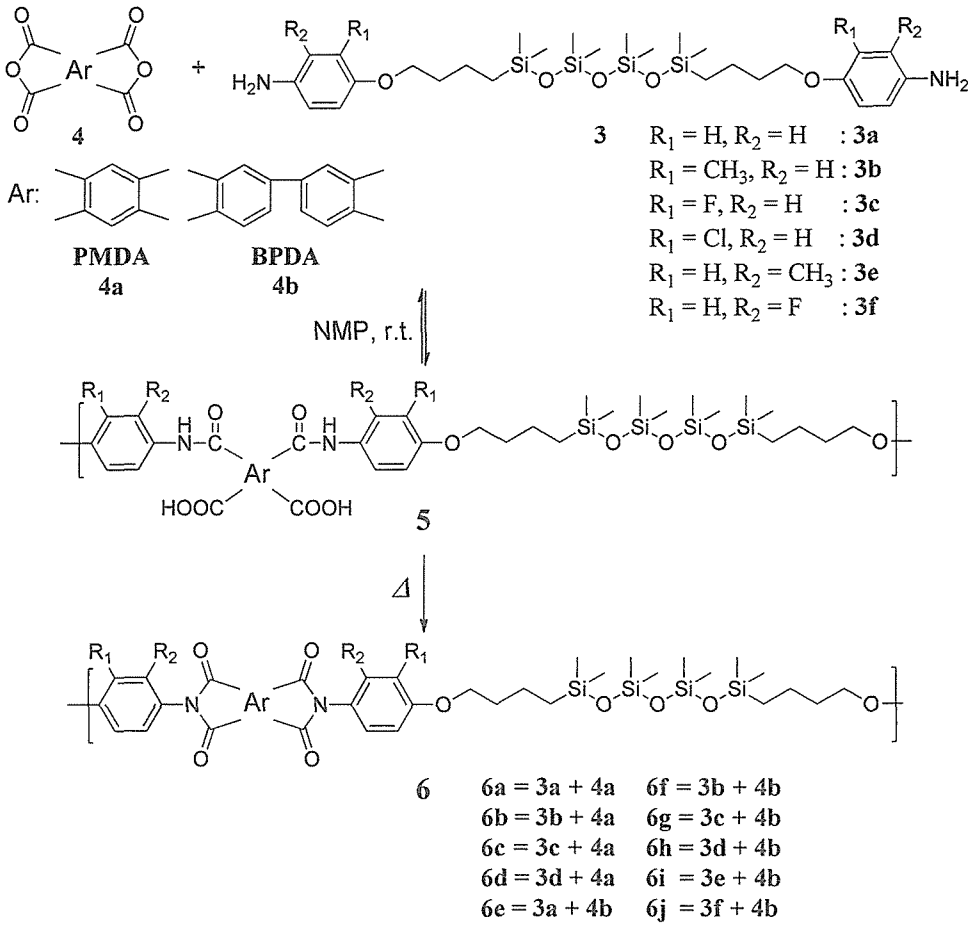

Figure 3-3. Synthetic routes of LC polyimides **6**.

3-2-2. Thermal Properties

All polyimides **6** possess high thermal stability over 440 °C ($T_{d5\%}$) according to thermogravimetric analysis (TGA) under nitrogen (Table 3-1). The differential scanning calorimetry (DSC) curves of all polyimides **6** are shown in Figure 3-4. The crystal melting temperatures in polyimides **6** were 237 (**6a**), 197 (**6b**), 237 (**6c**), 242 (**6d**), 222 (**6e**), 193 (**6f**), 163 (**6g**), 186 (**6h**), and 210 °C (**6j**) (Table 2-2, Figure 3-5), while polyimide **6i** showed an amorphous nature. Polyimides **6a** and **6c** derived from PMDA showed more than two exothermic peaks in the cooling process. In addition, birefringence and fluidity were observed in the temperature range between these peaks

by polarizing optical microscopy (POM). Therefore, the phase between the transition temperatures corresponds to the liquid crystalline phase. On the other hand, the methyl- or chloro-substituted polyimides, **6b** and **6d**, did not show the liquid crystallinity according to DSC trace and POM. With respect to the melting points of the polyimides derived from PMDA, there was no noticeable change among polyimides **6a**, **6c**, and **6d**. Only methyl-substituted polyimide **6b** had the lowest melting point among them, probably because the molecular interaction was reduced by a bulky substituent. The melting point of chloro-substituted polyimide **6d** was almost the same as non-substituted polyimide **6a** and fluoro-substituted **6c**, despite the similar bulkiness of the chlorine substituent of **6d** to the methyl one. The dipole moment of the chloro group might enhance the molecular interaction of mesogenic units.

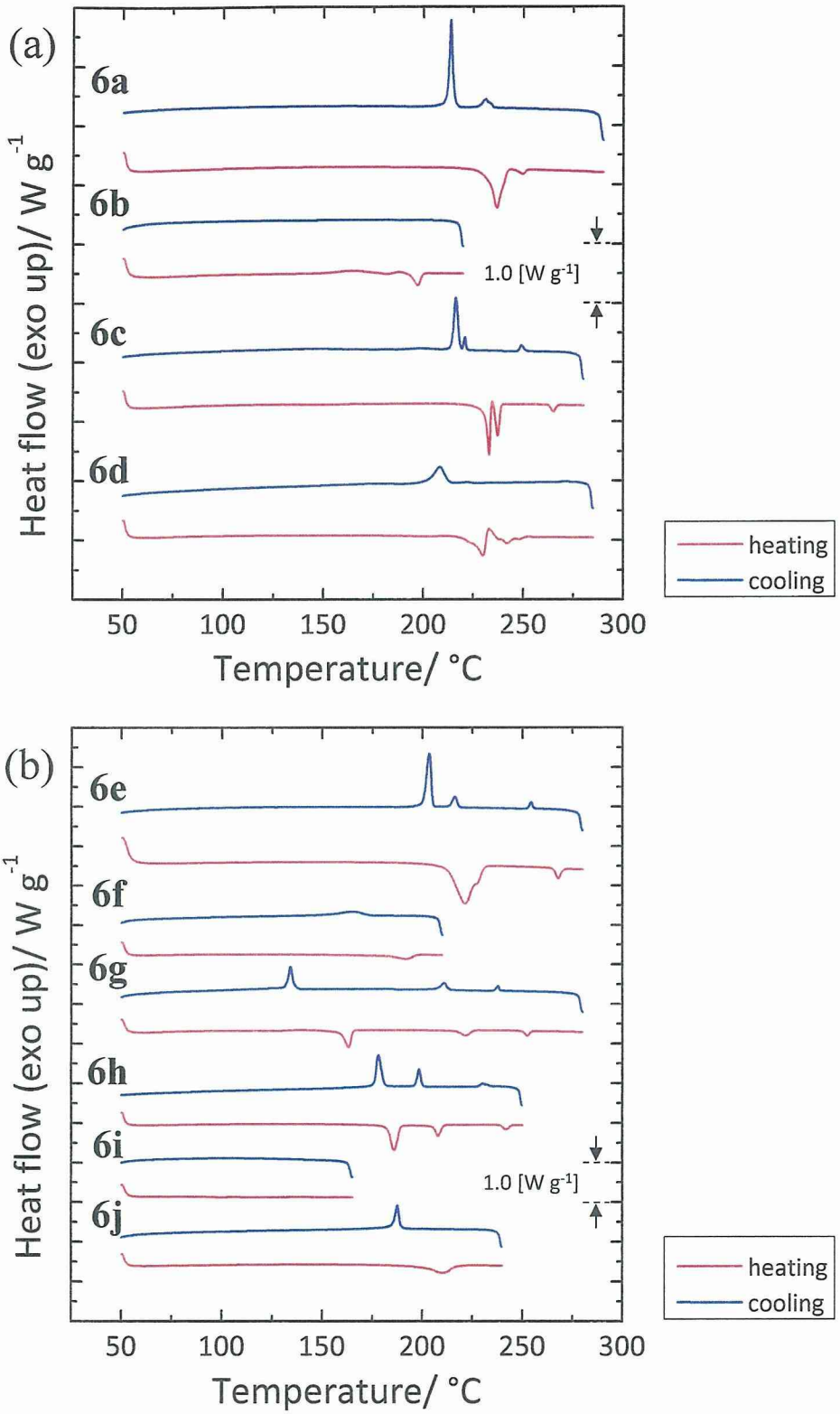

Figure 3-4. DSC heating and cooling curves of polyimides **6** derived from (a) PMDA and (b) BPDA by the measurement performed at a scanning rate of 10 °C min^{-1}.

Table 3-2. Thermal transition temperatures of polyimides **6**.

polymer	Ar	R_1	R_2	T_m [°C][a]	T_{cr-lc} [°C][a]	T_{lc-lc} [°C][a]	T_{lc-i} [°C][a]	ΔH [kJ mol^{-1}][a] lc–cr	lc–lc	iso–lc	d_{LC1} [Å]	d_{LC2} [Å]	Tilt angle [°][e]
6a	**4a**	H	H	237	214	*b*	231	16.2		2.7		32.7	
6b	**4a**	CH_3	H	197	*c*	*c*	*c*						
6c	**4a**	F	H	237	216	221	249	10.9	1.3	1.5		33.3	
6d	**4a**	Cl	H	242	*c*	*c*	*c*						
6e	**4b**	H	H	222	203	216	254	20.8	4.3	1.7	32.6	35.9	24
6f	**4b**	CH_3	H	192	*c*	*c*	*c*						
6g	**4b**	F	H	163	134	211	238	8.6	4.5	1.4	31.1	35.4	29
6h	**4b**	Cl	H	186	178	198	230	13.5	5.4	1.7	32.2	35.4	36
6i	**4b**	H	CH_3	*d*	*d*	*d*	*d*						
6j	**4b**	H	F	210	*c*	*c*	*c*						

[a] Peak-top temperatures determined by DSC at a second heating and cooling rate of 10 °C min^{-1}. T_m: melting points of polyimides **6** on the heating process. T_{cr-lc}: crystal-LC transition temperature, T_{lc-lc}: LC-LC transition temperature, T_{lc-i}: LC-isotropic transition temperature. [b] No detection of LC–LC transition temperature. [c] There are no LC phases. [d] Amorphous nature. [e] These tilt angles were measured from the splitting angle of inner layer reflections in oriented X-ray patterns taken for the fibrous SmC phases (refer to Figure 3-8a).

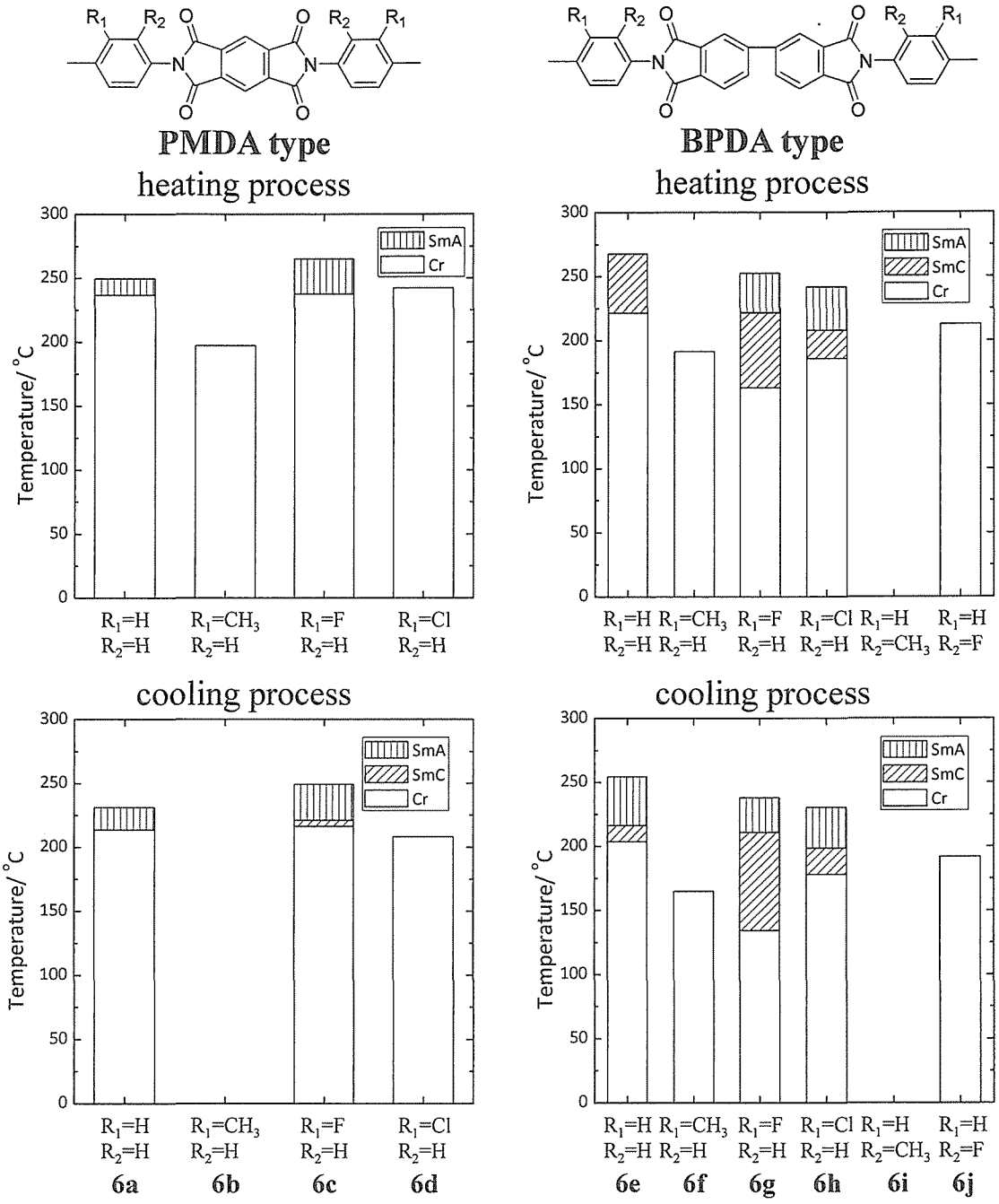

Figure 3-5. Comparison of mesomorphic properties for polyimides **6**.

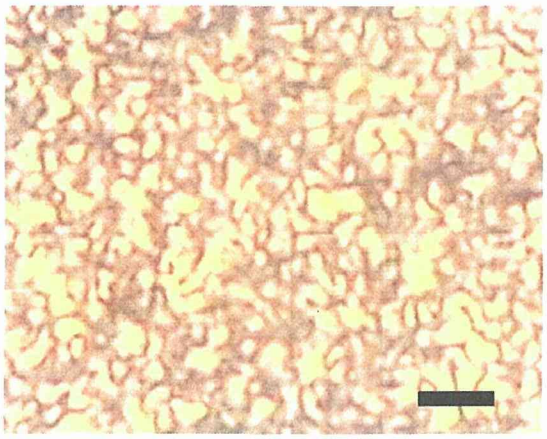

Figure 3-6. Polarized optical microscopic texture observed for SmC of polyimide **6h** at 225 °C (the scale bar indicates 25 μm).

Next, we investigated the effect of substituents at the R_1 position for polyimides **6e–h**, derived from BPDA. Polyimdes **6e**, **6g**, and **6h** also showed liquid crystallinity by DSC and POM, while polyimide **6f** did not. Figure 3-6 shows the optical microscopic texture observed for the mesophase of polyimide **6h** at 225 °C. Compared with the transition temperatures of polyimides **6e**, **6g**, and **6h**, fluoro-substituted polyimide **6g** had the lowest crystal-LC transition temperature (134 °C in the cooling process) among them, although the LC-isotropic transition temperatures were almost the same as the others. It probably means that the fluoro group effectively reduced the molecular interaction between the mesogens and prevented the highly ordered structure of the polyimides; in other words, it decreased the crystal melting temperature, leading to the expansion of the LC temperature range. To elucidate the effect of the substitution position, we synthesized polyimides **6i** and **6j**, which have a methyl- or fluoro-substituted group at the R_2 position and expected that the transition temperature of polyimide **6i** and **6j** would further be decreased compared with polyimide **6g**, which has a fluoro-substituted group at the R_1 position, by twisting the imide planes of the mesogenic units. However, polyimides **6i** and **6j** did not show LC properties, and their

isotropic transition temperatures decreased. This is probably because the methyl or fluoro substitution at the R_2 position twisted the imide plane and led to a significant decrease in the molecular interaction of the mesogenic units, destabilizing the crystalline phase or mesophase. To support this result, molecular simulation of the mesogenic units of polyimides **6e**, **6g**, and **6j** was carried out by density functional theory. The equilibrium structures of those polyimides were optimized and verified by frequency analysis at B3LYP/6-3/G(d) (Figure 3-7). The dihedral angle of the phenyl and imide groups for polyimide **6j** was 58.1°, which was wider than 42.7° for polyimide **6e** and 39.9° for polyimide **6g**. These results are similar to a previous report, wherein Coates suggested that a lateral substituent is the most efficient for producing a smectic C phase when it is substituted away from the center of the mesogen molecule and has reduced the occurrence of higher-ordered phases.[4] The fluoro group at the R_1 position was also the most effective substituent for decreasing the crystal-LC transition temperatures; in other words, the fluoro substituent properly destabilized the crystalline phase. Consequently, the fluoro or chloro substitutions at the R_1 position of polyimides **6** from BPDA reduce the crystal-LC transition temperatures almost without changing their LC-isotropic transition temperatures, while the substitutions at the R_2 position reduce the isotropic transition temperatures for destabilizing the crystalline or LC phase. There is no clear explanation for the reason why the methyl-substituted polyimide **6i** derived from BPDA exceptionally shows an amorphous nature.

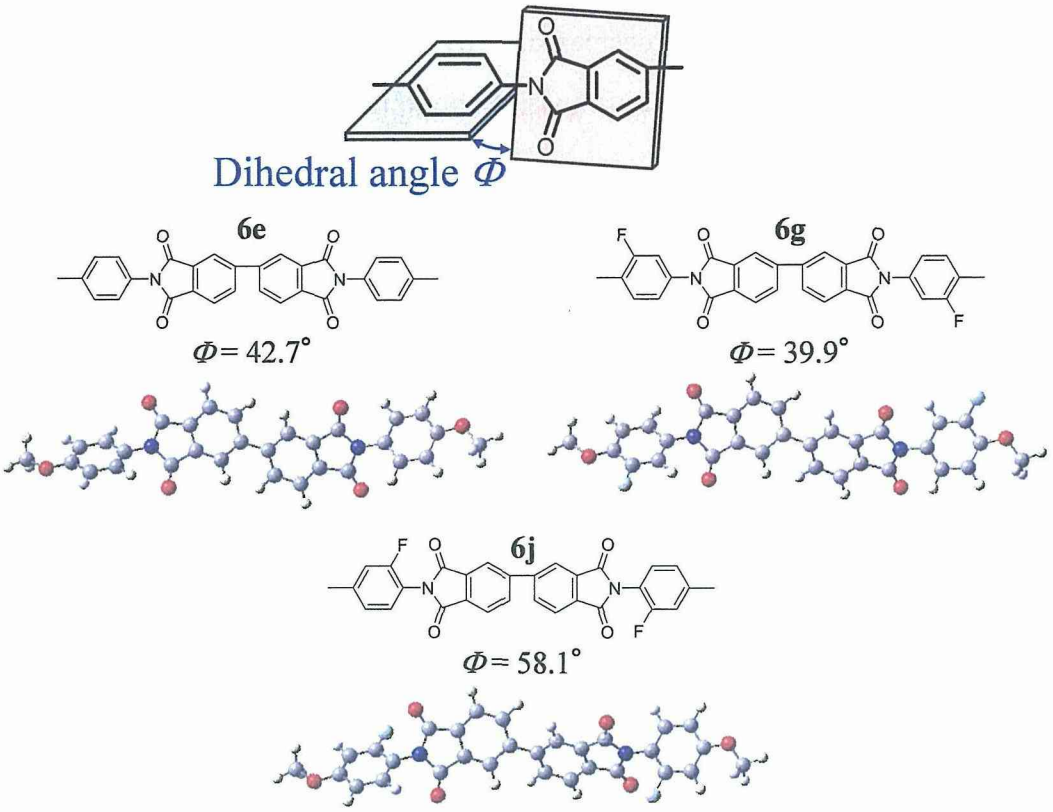

Figure 3-7. Optimized geometries of the mesogenic units of polyimides **6e**, **6g**, and **6j**.

From optical microscopic observation of the fanlike texture, all the liquid crystals formed are smectic phase. X-ray diffraction observation also identifies the smectic phase, showing an outer broad hallow and inner sharp reflections. For polyimides **6c**, **6e**, **6g**, and **6h**, forming two mesophases, the higher temperature mesophase is the SmA and the lower temperature mesophase is the SmC. The layer spacings of the SmA and SmC phases are listed in Table 3-2. The SmA layer spacings (32.7–33.3 Å) of **6a** and **6c** are relatively smaller than those (35.4–35.9 Å) of **6e**, **6g**, and **6h**, reflecting the difference in length in the central unit of the mesogenic group.

3-2-3. Wide-Angle X-ray Diffraction Measurements for Detailed LC Behavior

The detailed structural change in the SmA-SmC transition was investigated by

wide-angle X-ray diffraction (WAXD) measurement in polyimide **6g**, which forms enantiotropic mesophases in the widest temperature range. To obtain a uniaxial orientation of the mesophases, the fiber was spun from isotropic melt at 280 °C. Figure 3-8 shows a typical WAXD pattern observed in a low-temperature liquid-crystal phase (180 °C on the heating process). Here, the fiber axis is set in the vertical direction. In a small-angle region of the fiber pattern (see enlarged view of small angle region of Figure 3-8a), sharp layer reflections split on the left and right side of the meridian are observed with the spacing of 31.1 Å. On the other hand, an outer broad reflection with a spacing of 5.5 Å can be found on the equator. This diffraction profile gives just the luminescence of the SmC structure with the polymer chains lying parallel to the fiber axis and the layers normal tilted from the fiber axis.[5] Figure 3-8b shows the fiber pattern obtained for a high-temperature phase at 235 °C. This pattern has sharp reflections of the smectic layer on the meridian at 35.4 Å in the small-angle region and broad outer reflections whose intensity peak is on the equator at 6.6 Å. The orthogonal relationship between the layer reflection and outer broad reflection indicates that this high-temperature phase is the SmA phase followed by SmC-SmA transition. In addition, the other LC structures for **6a**, **6c**, **6e** and **6h** as representative examples were also assigned by the same manner for **6g**, as shown in Figure 3-9. The patterns of **6a** and **6c** were observed for the SmA phase (Figure 3-9a and Figure 3-9b), and **6e** and **6h** possess both the SmC and SmA phases (Figure 3-9c and Figure 3-9d), respectively. Furthermore, in Figure 3-10, the tilt angle of the layer corresponding to the split angle μ of the layer reflections is plotted against temperature. Of interest is that the tilt angle is somewhat independent of the SmC temperature and becomes zero discontinuously at the SmC-SmA transition, showing that the transition is of the first order. From a comparison

of the spacing between the SmC and SmA phases, we can estimate a tilt angle of 30° under the assumption that the repeating unit length is maintained throughout the transition. This value is nearly equal to the observed one of 29°.

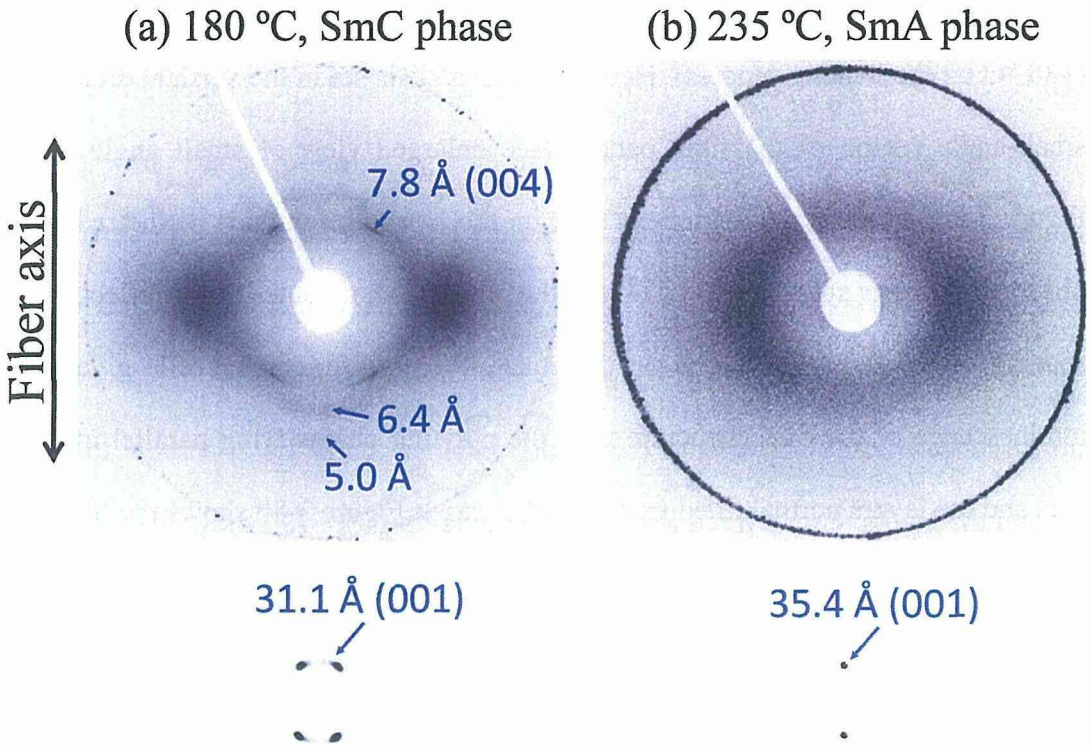

Figure 3-8. Wide-angle X-ray diffraction patterns of (a) SmC and (b) SmA phases observed in the fiber samples of **6g**. To show the smectic layer reflection, patterns in small-angle region are enlarged in the lower photographs. Fiber axis is set in a vertical direction.

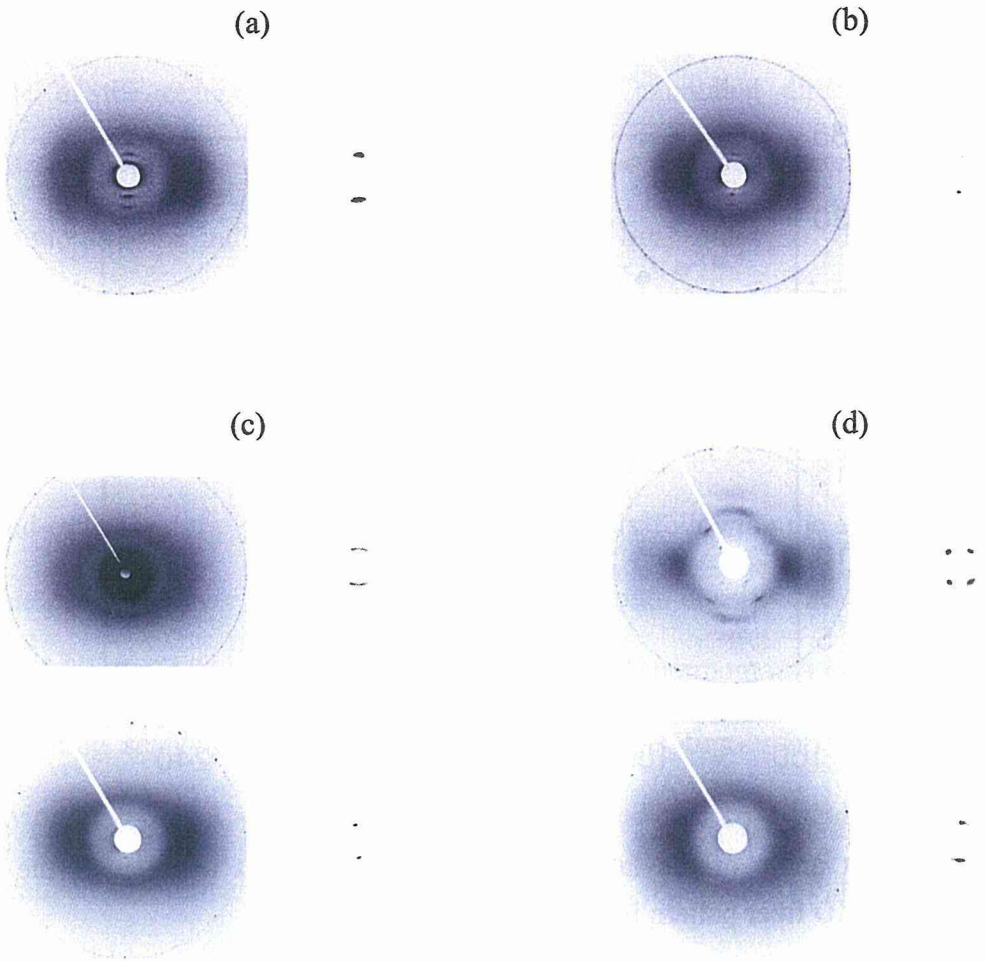

Figure 3-9. WAXD patterns of the fibrous samples. The patterns (a) and (b) were observed for the SmA phase of **6a** and **6c**, respectively. The upper and lower patterns of (c) **6e** and (d) **6h** were observed for SmC and SmA phases, respectively.

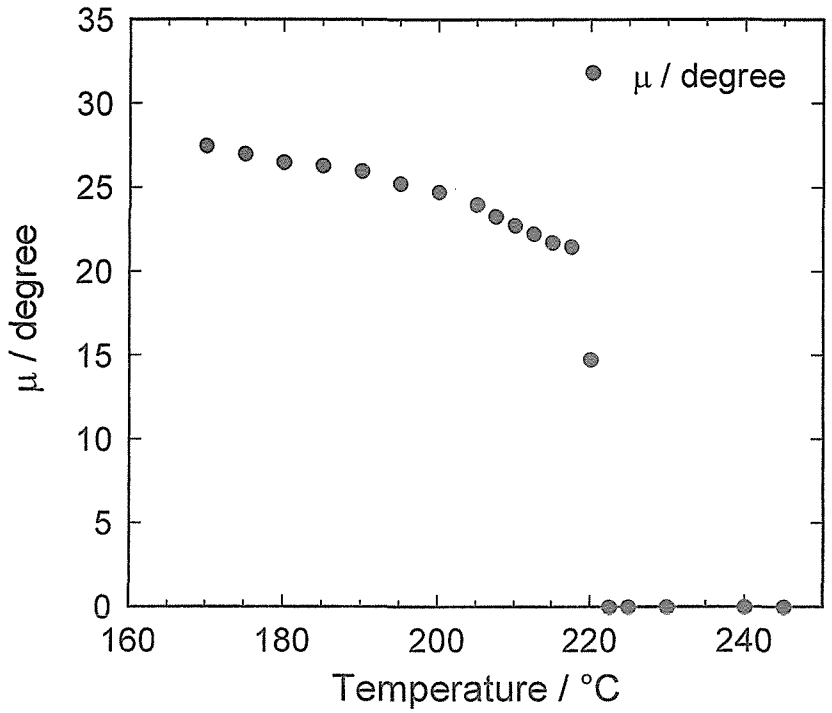

Figure 3-10. Tilt angle of the layer estimated from the split angle μ of the layer reflection in WAXD fiber pattern is plotted against temperature.

Although the SmA-SmC transformation is thus obvious, the present SmC and SmA phases possess some unusual structural features. First, the SmC phase shows a few of broad reflections along unusual directions in addition to the ordinal equatorial one with a spacing of 5.5 Å , that is, 6.4 and 5.0 Å ones along the meridional and off-meridional directions (see Figure 3-8). This unusual pattern may be attributable to the formation of a two dimensional pseudo lattice; the strong segregation takes place between the alkyl spacer part and dimethylsiloxane part,[6] giving a rise to short-range positional order along the layer plane direction. A second unusual feature is observed also on the broad outer reflection profile of the SmA phase. Irrespective of the high orientation of the layer, as can be found from the sharp inner reflection concentrated on the meridian, the

outer reflection is widely spread along the azimuthal direction. From the intensity profile of the outer broad reflection along the azimuthal direction, in fact, the orientational order parameter $<P_2>$ of the mesogenic part is evaluated as 0.4. This low orientational order indicates the "de Vries" type of SmA phase, in which the mesogens are significantly tilted to the layer normal, but their average axis is perpendicular to the layer. The average tilt angle is estimated as 37° from the layer normal. A third feature is the first-order SmA-SmC transition. Usually, the SmC-SmA phase transition is second-order, and the tilt angle changes continuously following the equation $(T_C\text{-}T)^{1/2}$.[5] In this case, however, the tilt angle changes discontinuously. The clear endothermic peak of the SmC-SmA transition observed on DSC thermograms on both the heating and cooling scan also supports that the transition is first-order. The first-transition behavior of the SmC-SmA transition has been predicted by Saunders *et al.* using a generalized theoretical Landau-de Gennes model.[7–9] As pointed out by Saunders, the fact that all known de Vries material does not form the nematic phase implies that the formation of the SmC phase is driven by an increase in the layering rather than orientation as the temperature decreases. In fact, our synthesized polyimide has a dimethylsiloxane group in the spacer which will be strongly segregated from the alkyl chains and aromatic mesogens, and this strong segregation is considered as a driving force to form the LC phase.

3-3. Conclusions

A new series of laterally substituted LC semialiphatic polyimides containing siloxane spacer units were synthesized, which showed high thermal stability ($T_{d5\%}$ >450 °C). Among the methyl, chloro, and fluoro substituents, the fluoro substituent was

the most effective in stabilizing the liquid crystal phase: it reduces the crystal melting temperature substantially, but not the isotropization temperature of LC. The chloro substituent was found to be effective as well, but the methyl substituent, irrespective of being the same size as the chloro one, substantially destabilizes the LC phase. We have also been concerned with the position of the substituent. The R_1 position, apart from the central part of the mesogen, was more effective than the R_2 position. The liquid crystals formed are the SmA and SmC phases, as found from the oriented X-ray patterns taken for the fibrous samples. The structural features of these phases and the SmA-SmC transition behavior were observed especially for the fluoro substituent polyimide based on BPDA, **6g** showing the widest LC temperature region. Of interest is that an anomalous diffraction profile is observed on the outer broad reflection both in the SmA and SmC phases, although inner layer reflections are observed ordinarily in the meridional direction. In the SmC phases, some other broad reflections appear along the meridional direction in addition to the ordinary equatorial one and in the SmA phase; the broad reflection is significantly spread along the azimuthal direction irrespective of the high orientation of the layer. Further, these features are considered to be caused by the segregation of the siloxane group from the other moieties in the polymer chain.

3-4. Experimental Section

3-4-1. Measurements

FT-IR spectra were measured on a Horiba FT-720 spectrometer. ^{1}H and ^{13}C NMR spectra were recorded with a Bruker DPX300S spectrometer. Inherent viscosities were measured at 30 °C in *N*-methylpyrrolidinone (NMP) at a polymer concentration of 0.5 g dL^{-1}. The transition characteristics were surveyed with a polarizing microscope (Olympus BX51), together with the use of a LINKAM LTS-350 hot stage equipped with a temperature controller by setting a polyimide film between crossed polarizers. Thermal analysis was performed on a Seiko EXSTAR 6000 TG/DTA 6300 thermal analyzer at a heating rate of 10 °C min^{-1} for thermogravimetry (TG) and a Perkin-Elmer DSC7 calorimeter connected to a cooling system at a heating rate of 10 °C min^{-1} for differential scanning calorimetry (DSC). WAXD measurements were performed at ambient temperature by using a Rigaku-Denki RINT-2500 X-ray generator with monochromic Cu Kα radiation (40 kV, 50 mA) from graphite crystal of monochromator and flat-plate type of imaging plate. Density functional theory calculations were carried out by using Gaussian09 program on TSUBAME supercomputer.

3-4-2. Materials

PMDA and BPDA were purified by sublimation prior to use. NMP, acetonitrile, and toluene were purified by distillation. Other reagents and solvents were purchased from TCI, Japan. The syntheses of diamine monomers **3a** as well as polyimides **6a** and **6e** were described in chapter 2.[3]

3-4-3. General Synthesis for Diamines

The diamine monomers containing siloxane linkages (**3b–3e**) were synthesized under the standard conditions for Williamson's ether synthesis, hydrosilylation, and reduction.

Synthesis of 4-(3-Butenyloxy)-3-methylnitrobenzene (**1b**). To a solution of 4-nitro-*o*-cresol (1.52 g, 9.96 mmol) and K_2CO_3 (2.10 g, 15.2 mmol) in CH_3CN (25 mL) was added 4-bromo-1-butene (2.17 g, 15.7 mmol), and the mixture was refluxed overnight. The solution was filtered through Celite and the filtrate was concentrated under reduced pressure. The residue was dissolved in CH_2Cl_2, washed with water, dried over $MgSO_4$, and the solvent was removed under reduced pressure to give a crude product, which was flash chromatographed (eluent: CH_2Cl_2) to give **1b** (yellow oil, 1.49 g, 72% yield). IR (NaCl), ν (cm^{-1}): 2927 (Alkyl C–H), 1643 (C=C), 1593 (Ar C–C), 1512, 1342 ($-NO_2$). ^1H NMR (300 MHz, $CDCl_3$, δ, ppm, 25 °C): 8.07 (dd, J=8.7 Hz, 2.7, ArH, 1H), 8.02 (d, J=2.4 Hz, ArH, 1H), 6.83 (d, J=9.3 Hz, ArH, 1H), 5.97–5.84 (m, –C*H*=CH_2, 1H), 5.23–5.11 (m, –CH=C*H*$_2$, 2H), 4.11 (t, J=6.3 Hz, –CH_2–, 2H), 2.64–2.56 (m, –CH_2–, 2H), 2.26 (s, –CH_3, 3H). ^{13}C NMR (75 MHz, $CDCl_3$, δ, ppm, 25 °C): 162.3, 141.0, 133.9, 128.1, 126.1, 123.7, 117.7, 110.0, 68.0, 33.6, 16.4.

Synthesis of 4-(3-Butenyloxy)-3-fluoronitrobenzene (**1c**). The title compound, **1c**, was synthesized by the same procedure as **1b** performed with 2.36 g (15.1 mmol) of 2-fluoro-4-nitrophenol, 2.77 g (20.1 mmol) of K_2CO_3, 2.81 g (20.4 mmol) of 4-bromo-1-butene, and 40 mL of CH_3CN. After purification by the flash column chromatography (eluent: CH_2Cl_2), the compound, **1c**, (2.57 g, 81% yield) was then

isolated as a yellow oil. IR (NaCl), ν (cm^{-1}): 2935 (Alkyl C–H), 1643 (C=C), 1581 (Ar C–C), 1512, 1338 (–NO_2). ^{1}H NMR (300 MHz, $CDCl_3$, δ, ppm, 25 °C): 8.06–8.01 (m, ArH, 1H), 7.96 (dd, J=11.0 Hz, 2.4, ArH, 1H), 7.02 (t, J=8.7 Hz, ArH, 1H), 5.96–5.94 (m, –C*H*=CH_2, 1H), 5.23–5.22 (m, –CH=C*H*$_2$, 2H), 4.18 (t, J=6.6 Hz, –CH_2–, 2H), 2.66–2.59 (m, –CH_2–, 2H). ^{13}C NMR (75 MHz, $CDCl_3$, δ, ppm, 25 °C): 153.0 (d, J=5.0 Hz), 151.3 (d, J=234.2 Hz), 140.9 (d, J=10.1 Hz), 133.3, 121.0 (d, J=3.5 Hz), 118.1, 113.1 (d, J=2.4 Hz), 112.4 (d, J=22.8 Hz), 69.1, 33.3.

Synthesis of 4-(3-Butenyloxy)-3-chloronitrobenzene (**1d**). The title compound, **1d**, was synthesized by the same procedure as **1b** performed with 2.60 g (15.0 mmol) of 2-chloro-4-nitrophenol, 2.74 g (19.8 mmol) of K_2CO_3, 2.81 g (20.4 mmol) of 4-bromo-1-butene, and 40 mL of CH_3CN. After purification by the flash column chromatography (eluent: CH_2Cl_2), the compound, **1d**, (2.32 g, 68% yield, m.p.=39–40 °C) was then isolated as a yellow solid. IR (KBr), ν (cm^{-1}): 2958 (Alkyl C–H), 1643 (C=C), 1585 (Ar C–C), 1512, 1342 (–NO_2). ^{1}H NMR (300 MHz, $CDCl_3$, δ, ppm, 25 °C): 8.28 (d, J=2.7 Hz, ArH, 1H), 8.14 (dd, J=9.0, 2.7 Hz, ArH, 1H), 6.97 (d, J=9.3 Hz, ArH, 1H), 5.99–5.85 (m, –C*H*=CH_2, 1H), 5.25–5.14 (m, –CH=C*H*$_2$, 2H), 4.18 (t, J=6.6 Hz, –CH_2–, 2H), 2.68–2.61 (m, –CH_2–, 2H). ^{13}C NMR (75 MHz, $CDCl_3$, δ, ppm, 25 °C): 159.6, 141.1, 133.3, 126.0, 124.0, 123.5, 118.0, 111.8, 69.2, 33.2.

Synthesis of 4-(3-Butenyloxy)-2-methylnitrobenzene (**1e**). The title compound, **1e**, was synthesized by the same procedure as **1b** performed with 3.05 g (19.9 mmol) of 3-methyl-4-nitrophenol, 4.27 g (30.9 mmol) of K_2CO_3, 4.02 g (29.8 mmol) of 4-bromo-1-butene, and 50 mL of CH_3CN. The compound, **1e**, (2.61 g, 63% yield) was

then isolated as a yellow oil after the vacuum. IR (NaCl), ν (cm^{-1}): 2935 (Alkyl C–H), 1643 (C=C), 1581 (Ar C–C), 1512, 1338 ($–NO_2$). ^1H NMR (300 MHz, $CDCl_3$, δ, ppm, 25 °C): 8.08 (d, J=9.9 Hz, ArH, 1H), 6.81–6.78 (m, ArH, 2H), 5.95–5.82 (m, $–CH=CH_2$, 1H), 5.22–5.11 (m, $–CH=CH_2$, 2H), 4.08 (t, J=6.9 Hz, $–CH_2–$, 2H), 2.62 (s, $–CH_3$, 3H), 2.61–2.53 (m, $–CH_2–$, 2H). ^{13}C NMR (75 MHz, $CDCl_3$, δ, ppm, 25 °C): 162.5, 142.2, 137.2, 133.8, 127.7, 118.1, 117.7, 112.3, 67.9, 33.5, 21.8.

Synthesis of 4-(3-Butenyloxy)-2-fluoronitrobenzene (**1f**). The title compound, **1f**, was synthesized by the same procedure as **1b** performed with 1.57 g (10.0 mmol) of 3-fluoro-4-nitrophenol, 2.09 g (15.1 mmol) of K_2CO_3, 2.21 g (16.0 mmol) of 4-bromo-1-butene, and 25 mL of CH_3CN. After purification by the column chromatography using hexane/CH_2Cl_2 (6/4, v/v) as an eluent, the compound, **1f**, (1.71 g, 81% yield) was then isolated as a yellow oil. IR (NaCl), ν (cm^{-1}): 2947 (Alkyl C–H), 1643 (C=C), 1612 (Ar C–C), 1520, 1346 ($–NO_2$). ^1H NMR (300 MHz, $CDCl_3$, δ, ppm, 25 °C): 8.11–8.05 (m, ArH, 1H), 6.77–6.70 (m, ArH, 2H), 5.93–5.80 (m, $–CH=CH_2$, 1H), 5.22–5.12 (m, $–CH=CH_2$, 2H), 4.09 (t, J=6.9 Hz, $–CH_2–$, 2H), 2.61–2.54 (m, $–CH_2–$, 2H). ^{13}C NMR (75 MHz, $CDCl_3$, δ, ppm, 25 °C): 164.8 (d, J=10.8 Hz), 157.6 (d, J=263.4 Hz), 133.4, 128.0 (d, J=1.9 Hz), 118.0, 110.9 (d, J=4.0 Hz), 103.9, 103.6, 68.6, 33.3.

Synthesis of 1,7-Bis[4-(2-methyl-4-nitrophenoxy)butyl]-1,1,3,3,5,5,7,7-octamethyltetrasiloxane (**2b**). To a solution of **1b** (2.08 g, 10.0 mmol) and 1,1,3,3,5,5,7,7-octamethyltetrasiloxane (1.09 g, 3.84 mmol), in toluene (10 mL), Karstedt's catalyst (20 drops) (platinum

divinyltetramethyldisiloxane complex in 2 wt% xylene) was added. The reaction mixture was refluxed under nitrogen for 24 h, and then toluene was removed under reduced pressure. The residue was chromatographed using hexane/CH_2Cl_2 (6/4, v/v) as an eluent to give **2b**. The compound, **2b**, (2.44 g, 91%yield) was then isolated as a pale yellow oil after the vacuum. IR (NaCl), ν (cm^{-1}): 2958 (Alkyl C–H), 1593 (Ar C–C), 1516, 1342 (–NO_2), 1261 (Si–C). ^{1}H NMR (300 MHz, $CDCl_3$, δ, ppm, 25 °C): 8.06 (dd, J=9.2 Hz, ArH, 2H), 8.02 (d, J=3.0 Hz, ArH, 2H), 6.83 (d, J=9.3 Hz, ArH, 2H), 4.06 (t, J=6.3 Hz, –CH_2–, 4H), 2.25 (s, –CH_3, 6H), 1.91–1.82 (m, –CH_2–, 4H), 1.60–1.49 (m, –CH_2–, 4H), 0.64–0.58 (m, –CH_2–, 4H), 0.09 (s, Si–CH_3, 12H), 0.04 (s, Si–CH_3, 12H). ^{13}C NMR (75 MHz, $CDCl_3$, δ, ppm, 25 °C): 162.5, 140.8, 127.9, 126.0, 123.7, 110.0, 68.5, 32.6, 19.9, 17.9, 16.4, 1.31, 0.269. Anal. Calcd For $C_{30}H_{52}N_2$: C, 51.69; H, 7.52; N, 4.02. Found: C, 51.78; H, 7.30; N, 3.96.

Synthesis of 1,7-Bis[4-(2-fluoro-4-nitrophenoxy)butyl]-1,1,3,3,5,5,7,7-octamethyltetrasiloxane (**2c**). The title compound, **2c**, was synthesized by the same procedure as **2b** performed with 2.12 g (10.0 mmol) of **1c**, 1.15 g (3.87 mmol) of 1,1,3,3,5,5,7,7-octamethyltetrasiloxane, 10 drops of Karstedt's catalyst, and 10 mL of toluene. The compound, **2c**, (2.46 g, 90% yield) was then isolated as a pale yellow oil after the vacuum. IR (NaCl), ν (cm^{-1}): 2958 (Alkyl C–H), 1605 (Ar C–C), 1524, 1346 (–NO_2) 1257 (Si–C). ^{1}H NMR (300 MHz, $CDCl_3$, δ, ppm, 25 °C): 8.05–8.01 (m, J=9.9 Hz, ArH, 2H), 7.96 (dd, J=10.5, 2.4 Hz, ArH, 2H), 7.01 (t, J=7.8 Hz, ArH, 2H), 4.13 (t, J=6.6 Hz, –CH_2–, 4H), 1.94–1.84 (m, –CH_2–, 4H), 1.61–1.48 (m, –CH_2–, 4H), 0.63–0.58 (m, –CH_2–, 4H), 0.08 (s, Si–CH_3, 12H), 0.04 (s, Si–CH_3, 12H). ^{13}C NMR (75 MHz, $CDCl_3$, δ, ppm, 25 °C): 153.2 (d,

J=17.9 Hz), 151.4 (d, *J*=257.1 Hz), 140.7 (d, *J*=6.8 Hz), 121.0 (d, *J*=4.0 Hz), 112.9 (d, *J*=2.1 Hz), 112.4 (d, *J*=23.0 Hz), 69.6, 32.4, 19.7, 18.0, 1.30, 0.291. Anal. Calcd For $C_{28}H_{48}N_2$: C, 47.70; H, 6.58; N, 3.97. Found: C, 47.84; H, 6.43; N, 3.90.

Synthesis of 1,7-Bis[4-(2-chloro-4-nitrophenoxy)butyl]-1,1,3,3,5,5,7,7-octamethyltetrasiloxane (**2d**). The title compound, **2d**, was synthesized by the same procedure as **2b** performed with 1.37 g (6.02 mmol) of **1d**, 0.544 g (1.92 mmol) of 1,1,3,3,5,5,7,7-octamethyltetrasiloxane, 10 drops of Karstedt's catalyst, and 7 mL of toluene. The compound, **2d**, (1.24 g, 87% yield) was then isolated as a pale yellow oil after the vacuum. IR (NaCl), ν (cm^{-1}): 2958 (Alkyl C–H), 1585 (Ar C–C), 1516, 1342 ($-NO_2$), 1257 (Si–C). ^1H NMR (300 MHz, $CDCl_3$, δ, ppm, 25 °C): 8.26 (d, *J*=3.0 Hz, ArH, 2H), 8.12 (dd, *J*=9.3, 3.0 Hz, ArH, 2H), 6.96 (d, *J*=9.0 Hz, ArH, 2H), 4.13 (t, *J*=6.3 Hz, $-CH_2-$, 4H), 1.95–1.86 (m, $-CH_2-$, 4H), 1.62–1.52 (m, $-CH_2-$, 4H), 0.64–0.59 (m, $-CH_2-$, 4H), 0.09 (s, Si–CH_3, 12H), 0.04 (s, Si–CH_3, 12H). ^{13}C NMR (75 MHz, $CDCl_3$, δ, ppm, 25 °C):159.9, 141.1, 126.1, 124.1, 123.5, 111.8, 69.7, 32.3, 19.8, 17.9, 1.33, 0.275. Anal. Calcd For $C_{28}H_{46}N_2$: C, 45.57; H, 6.28; N, 3.80. Found: C, 45.58; H, 6.13; N, 3.78.

Synthesis of 1,7-Bis[4-(3-methyl-4-nitrophenoxy)butyl]-1,1,3,3,5,5,7,7-octamethyltetrasiloxane (**2e**). The title compound, **2e**, was synthesized by the same procedure as **2b** performed with 2.37 g (11.4 mmol) of **1e**, 1.44 g (5.09 mmol) of 1,1,3,3,5,5,7,7-octamethyltetrasiloxane, 20 drops of Karstedt's catalyst, and 12 mL of toluene. The compound, **2e**, (3.05 g, 86%

yield) was then isolated as a pale yellow oil after the vacuum. IR (NaCl), ν (cm^{-1}): 2958 (Alkyl C-H), 1581 (Ar C–C), 1512, 1338 (–NO_2), 1257 (Si–C). ^1H NMR (300 MHz, $CDCl_3$, δ, ppm, 25 °C): 8.07 (d, *J*=9.3 Hz, ArH, 2H), 6.79–6.76 (m, ArH, 4H), 4.02 (t, *J*=6.5 Hz, –CH_2–, 4H), 2.62 (s, –CH_3, 6H), 1.87–1.78 (m, –CH_2–, 4H), 1.57–1.46 (m, –CH_2–, 4H), 0.63–0.57 (m, –CH_2–, 4H), 0.09 (s, Si–CH_3, 12H), 0.05 (s, Si–CH_3, 12H). ^{13}C NMR (75 MHz, $CDCl_3$, δ, ppm, 25 °C): 162.9, 142.1, 137.2, 127.7, 118.0, 112.3, 68.4, 32.6, 21.9, 19.8, 18.0, 1.36, 0.329. Anal. Calcd For $C_{30}H_{52}N_2$: C, 51.69; H, 7.52; N, 4.02. Found: C, 51.52; H, 7.28; N, 3.83.

Synthesis of 1,7-Bis[4-(3-fluoro-4-nitrophenoxy)butyl]-1,1,3,3,5,5,7,7-octamethyltetrasiloxane (**2f**). The title compound, **2f**, was synthesized by the same procedure as **2b** performed with 1.55 g (7.34 mmol) of **1e**, 0.705 g (2.49 mmol) of 1,1,3,3,5,5,7,7-octamethyltetrasiloxane, 10 drops of Karstedt's catalyst, and 8 mL of toluene. The compound, **2f**, (1.66 g, 95% yield) was then isolated as a pale yellow oil after the vacuum. IR (NaCl), *ν* (cm^{-1}): 2958 (Alkyl C–H), 1612 (Ar C–C), 1520, 1346 (–NO_2), 1257 (Si–C). ^1H NMR (300 MHz, $CDCl_3$, *δ*, ppm, 25 °C): 8.10–8.04 (m, ArH, 2H), 6.76–6.68 (m, ArH, 4H), 4.03 (t, *J*=6.3 Hz, –CH_2–, 4H), 1.89–1.79 (m, –CH_2–, 4H), 1.56–1.46 (m, –CH_2–, 4H), 0.62–0.57 (m, –CH_2–, 4H), 0.08 (s, Si–CH_3, 12H), 0.04 (s, Si–CH_3, 12H). ^{13}C NMR (75 MHz, $CDCl_3$, *δ*, ppm, 25 °C): 165.1 (d, *J*=10.4 Hz), 157.6 (d, *J*=262.9 Hz), 128.0 (d, *J*=2.4 Hz), 110.9 (d, *J*=3.0 Hz), 103.8, 103.4, 69.1, 32.4, 19.8, 17.9, 1.34, 0.304. Anal. Calcd For $C_{28}H_{48}N_2$: C, 47.70; H, 6.58; N, 3.97. Found: C, 48.08; H, 6.53; N, 3.91.

Synthesis of 1,7-Bis[4-(4-amino-2-methylphenoxy)butyl]-1,1,3,3,5,5,7,7-octamethyltetrasiloxane (**3b**). A mixture of nitro compound **2b** (2.19 g, 3.15 mmol) and Pd/C (0.0206 g, 10 wt %) in EtOAc (10 mL) was stirred at room temperature for 24 h under hydrogen atmosphere by using a balloon. The solution was filtered through Celite and concentrated to give the diamine **3b** (2.00 g, 99% yield) as a light brown oil. IR (NaCl), ν (cm^{-1}): 3356 (N–H), 2958 (Alkyl C–H), 1624 (N–H), 1593 (Ar C–C), 1257 (Si–C). ^1H NMR (300 MHz, $CDCl_3$, δ, ppm, 25 °C): 6.66 (d, J=8.1 Hz, ArH, 2H), 6.53 (d, J=2.7 Hz, ArH, 2H), 6.48 (dd, J=8.4, 2.7 Hz, ArH, 2H), 3.89 (t, J=6.0 Hz, $-CH_2-$, 4H), 3.18 (s, NH_2, 4H), 2.17 (s, $-CH_3$, 3H) 1.83–1.74 (m, $-CH_2-$, 4H), 1.58–1.47 (m, $-CH_2-$, 4H), 0.63–0.58 (m, $-CH_2-$, 4H), 0.09 (s, Si–CH_3, 12H) , 0.05 (s, Si–CH_3, 12H). ^{13}C NMR (75 MHz, $CDCl_3$, δ, ppm, 25 °C): 150.7, 139.6, 128.2, 118.6, 113.2, 113.1, 68.7, 33.2, 20.0, 18.1, 16.4, 1.34, 0.300.

Synthesis of 1,7-Bis[4-(4-amino-2-fluorophenoxy)butyl]-1,1,3,3,5,5,7,7-octamethyltetrasiloxane (**3c**). The title compound, **3c**, was synthesized by the same procedure as **3b** performed with 2.18 g (3.09 mmol) of **2c**, 0.0233 g of Pd/C (10 wt%), and 10 mL of EtOAc. The compound, **3c**, (1.98 g, 99% yield) was then isolated as a light brown oil after the vacuum. IR (NaCl), ν (cm^{-1}): 3375 (N–H), 2958 (Alkyl C–H), 1639 (N–H), 1589 (Ar C–C), 1257 (Si–C). ^1H NMR (300 MHz, $CDCl_3$, δ, ppm, 25 °C): 6.79 (t, J=9.0 Hz, ArH, 2H), 6.44 (dd, J=12.6, 2.4 Hz, ArH, 2H), 6.37–6.33 (m, ArH, 2H), 3.94 (t, J=6.6 Hz, $-CH_2-$, 4H), 3.49 (s, NH_2, 4H), 1.83–1.73 (m, $-CH_2-$, 4H), 1.55–1.44 (m, $-CH_2-$, 4H), 0.62–0.56 (m, $-CH_2-$, 4H), 0.08 (s, Si–CH_3, 12H), 0.05 (s, Si–CH_3, 12H). ^{13}C NMR (75

MHz, $CDCl_3$, δ, ppm, 25 °C): 153.9 (d, J=244.2 Hz), 141.3 (d, J=9.3 Hz), 139.6 (d, J=11.3 Hz), 118.0 (d, J=2.6 Hz), 110.5 (d, J=3.2 Hz), 104.2 (d, J=21.8 Hz), 70.8, 33.1, 19.8, 18.1, 1.31, 0.284.

Synthesis of 1,7-Bis[4-(4-amino-2-chlorophenoxy)butyl]-1,1,3,3,5,5,7,7-octamethyltetrasiloxane (**3d**). The title compound, **3d**, was synthesized by the same procedure as **3b** performed with 0.936 g (1.38 mmol) of **2d**, 0.0469 g of Pd/C (10 wt%), and 10 mL of EtOAc. The compound, **3d**, (0.860 g, 99% yield) was then isolated as a light brown oil after the vacuum. IR (NaCl), ν (cm^{-1}): 3371 (N–H), 2958 (Alkyl C–H), 1624 (N–H), 1500 (Ar C–C), 1257 (Si–C). ^1H NMR (300 MHz, $CDCl_3$, δ, ppm, 25 °C): 6.78–6.74 (m, ArH, 4H), 6.53 (dd, J=8.6, 3.0 Hz, ArH, 2H), 3.93 (t, J=6.3 Hz, $-CH_2-$, 4H), 3.65 (s, NH_2, 4H), 1.85–1.76 (m, $-CH_2-$, 4H), 1.58–1.47 (m, $-CH_2-$, 12H), 0.63–0.57 (m, $-CH_2-$, 4H), 0.08 (s, $Si-CH_3$, 12H), 0.05 (s, $Si-CH_3$, 12H). ^{13}C NMR (75 MHz, $CDCl_3$, δ, ppm, 25 °C): 148.0, 140.6, 124.3, 117.5, 116.2, 114.6, 70.2, 33.0, 19.8, 18.1, 1.36, 0.333.

Synthesis of 1,7-Bis[4-(4-amino-3-methylphenoxy)butyl]-1,1,3,3,5,5,7,7-octamethyltetrasiloxane (**3e**). The title compound, **3e**, was synthesized by the same procedure as **3b** performed with 2.62 g (3.76 mmol) of **2e**, 0.0230 g of Pd/C (10 wt%), and 10 mL of EtOAc. The compound, **3e**, (2.38 g, 99% yield) was then isolated as a light brown oil after the vacuum. IR (NaCl), ν (cm^{-1}): 3363 (N–H), 2935 (Alkyl C–H), 1608 (N–H), 1504 (Ar C–C), 1238 (Si–C). ^1H NMR (300 MHz, $CDCl_3$, δ, ppm, 25 °C): 6.67–6.60 (m, ArH, 6H), 3.87 (t, J=6.5 Hz, $-CH_2-$, 4H), 3.33 (s, NH_2, 4H), 2.15 (s, $-CH_3$, 6H), 1.81–1.71

(m, $-CH_2-$, 4H), 1.53–1.43 (m, $-CH_2-$, 4H), 0.62–0.56 (m, $-CH_2-$, 4H), 0.08 (s, Si–CH_3, 12H), 0.04 (s, Si–CH_3, 12H). ^{13}C NMR (75 MHz, $CDCl_3$, δ, ppm, 25 °C): 152.4, 138.1, 124.1, 117.4, 116.1, 113,1, 68.4, 33.2, 20.0, 18.1, 17.8, 1.36, 0.334.

Synthesis of 1,7-Bis[4-(4-amino-3-fluorophenoxy)butyl]-1,1,3,3,5,5,7,7-octamethyltetrasiloxane (**3f**). The title compound, **3f**, was synthesized by the same procedure as **3b** performed with 1.66 g (2.35 mmol) of **2f**, 0.0275 g of Pd/C (10 wt%), and 10 mL of EtOAc. The compound, **3f**, (1.51 g, 99% yield) was then isolated as a light brown oil after the vacuum. IR (NaCl), ν (cm^{-1}): 3371 (N–-H), 2958 (Alkyl C–H), 1639 (N–H), 1593 (Ar C–C), 1238 (Si–C). ^1H NMR (300 MHz, $CDCl_3$, δ, ppm, 25 °C): 6.70 (t, J=8.4 Hz, ArH, 2H), 6.61 (dd, J=12.5, 2.4 Hz, ArH, 2H), 6.55–6.51 (m, ArH, 2H), 3.86 (t, J=6.3 Hz, $-CH_2-$, 4H), 3.41 (s, NH_2, 4H), 1.81–1.72 (m, $-CH_2-$, 4H), 1.54–1.43 (m, $-CH_2-$, 4H), 0.62–0.56 (m, $-CH_2-$, 4H), 0.08 (s, Si–CH_3, 12H), 0.05 (s, Si–CH_3, 12H). ^{13}C NMR (75 MHz, $CDCl_3$, δ, ppm, 25 °C): 152.5 (d, J=9.3 Hz), 152.1 (d, J=237.6 Hz), 127.6 (d, J=13.6 Hz), 117.7 (d, J=5.0 Hz), 110.7 (d, J=3.5 Hz), 103.1 (d, J=21.6 Hz), 68.5, 32.9, 19.9, 18.1, 1.35, 0.332.

3-4-4. General Procedure for Polymer Synthesis.

PMDA (**4a**) or BPDA (**4b**) was added to a solution of the diamines **3** in NMP, and the solution was stirred at room temperature for 12 h. Then a poly(amic acid) solution (15 wt%) was casted on a glass substrate and the imidization was carried out by heating in steps on a hot plate, finally the temperature was increased to 200 °C. Yellow films of polyimides **6** were obtained.

Synthesis of Polyimide **6b**. IR (Si wafer), ν (cm^{-1}): 2958 (Alkyl C–H), 1774 (C=O), 1720 (C=O), 1385 (C–N), 1254 (Si–C). Anal. Calcd For $C_{40}H_{54}N_2$: C, 58.65; H, 6.64; N, 3.42. Found: C, 58.55; H, 6.62; N, 3.33.

Synthesis of Polyimide **6c**. IR (Si wafer), ν (cm^{-1}): 2958 (Alkyl C–H), 1774 (C=O), 1709 (C=O), 1385 (C–N), 1261 (Si–C). Anal. Calcd For $C_{38}H_{48}N_2$: C, 55.18; H, 5.85; N, 3.39. Found: C, 55.21; H, 5.86; N, 3.40.

Synthesis of Polyimide **6d**. IR (Si wafer), ν (cm^{-1}): 2958 (Alkyl C–H), 1774 (C=O), 1720 (C=O), 1385 (C–N), 1257 (Si–C). Anal. Calcd For $C_{38}H_{48}N_2$: C, 53.07; H, 5.63; N, 3.26. Found: C, 53.16; H, 5.59; N, 3.21.

Synthesis of Polyimide **6f**. IR (Si wafer), ν (cm^{-1}): 2958 (Alkyl C–H), 1770 (C=O), 1728 (C=O), 1381 (C–N), 1257 (Si–C). Anal. Calcd For $C_{46}H_{58}N_2$: C, 61.71; H, 6.53; N, 3.13. Found: C, 61.62; H, 6.50; N, 3.10.

Synthesis of Polyimide **6g**. IR (Si wafer), ν (cm^{-1}): 2958 (Alkyl C–H), 1770 (C=O), 1713 (C=O), 1389 (C–N), 1261 (Si–C). Anal. Calcd For $C_{44}H_{52}N_2$: C, 58.51; H, 5.80; N, 3.10. Found: C, 58.74; H, 5.59; N, 3.09.

Synthesis of Polyimide **6h**. IR (Si wafer), ν (cm^{-1}): 2958 (Alkyl C–H), 1770 (C=O), 1724 (C=O), 1389 (C–N), 1261 (Si–C). Anal. Calcd For $C_{44}H_{52}N_2$: C, 56.45; H, 5.60; N, 2.99. Found: C, 56.86; H, 5.55; N, 2.96.

Synthesis of Polyimide **6i.** IR (Si wafer), ν (cm^{-1}): 2958 (Alkyl C–H), 1774 (C=O), 1720 (C=O), 1381 (C–N), 1254 (Si–C). Anal. Calcd For $C_{46}H_{58}N_2$: C, 61.71; H, 6.53; N, 3.13. Found: C, 61.56; H, 6.49; N, 2.83.

Synthesis of Polyimide **6j**. IR (Si wafer), ν (cm^{-1}): 2958 (Alkyl C–H), 1774 (C=O), 1724 (C=O), 1400 (C–N), 1257 (Si–C). Anal. Calcd For $C_{44}H_{52}N_2$: C, 58.51; H, 5.80; N, 3.10. Found: C, 58.31; H, 5.87; N, 3.06.

3-5. References and Notes

1. Akatsuka, M.; Takezawa, Y. *J. Appl. Polym. Sci.* **2003**, *89*, 2464.
2. Shoji, Y.; Higashihara, T.; Watanabe, J.; Ueda, M. *Chem. Lett.* **2009**, *38*, 716.
3. Shoji, Y.; Ishige, R.; Higashihara, T.; Watanabe, J.; Ueda, M. *Macromolecules* **2010**, *43*, 805.
4. Coates, D. *Liq. Cryst.* **1987**, *2*, 423.
5. Watanabe, J.; Hayashi, M.; Tokita, M. *React. Funct. Polym.* **1996**, *30*, 191.
6. Corsellis, E.; Guillon, D.; Kloess, P.; Coles, H. *Liq. Cryst.* **1997**, *23*, 235.
7. Saunders, K. *Phys. Rev. E* **2008**, *77*, 061708.
8. Saunders, K.; Hernandez, D.; Pearson, S.; Toner, J. *Phys. Rev. Lett.* **2007**, *98*, 197801.
9. Saunders, K. *Phys. Rev. E* **2009**, *80*, 011703.

Chapter 4

Cross-Linked Liquid Crystalline Polyimides with Siloxane Units: Their Morphology and Thermal Diffusivity

Abstract.

Cross-linked liquid crystalline (LC) polyimides with siloxane units have been developed as high thermally conductive materials. The relationship between their thermal diffusivities and film morphologies was investigated. The cross-linking reaction of the LC polyimides was monitored by Fourier transform infrared spectroscopy and differential scanning calorimetry. It was found that the cross-linked LC polyimides successfully maintained their LC structures at room temperature as confirmed by polarized optical microscopy and wide-angle X-ray diffraction (WAXD). The thermal diffusivity of the films in the thickness direction measured by a temperature wave analysis method increased gradually from 0.116 to 0.185 $mm^2 s^{-1}$ with the increasing extent of the cross-linking. In the detailed WAXD study, the obtained cross-linked LC polyimide films showed that the polymer chains vertically aligned in the thickness direction of the films, and the increase in the extent of the cross-linking expanded the

areas of chain alignment. Such a chain alignment plays an important role in the phonon conduction in the thickness direction of the films.

4-1. Introduction

In chapter 3, the synthesis of novel laterally substituted LC polyimides derived from PMDA or BPDA with diamines containing siloxane spacer units was described.[1–4] The lowest crystal-LC transition temperature was 163 °C during a heating process that originated from long siloxane units and the fluoro substituent on the mesogenic units to reduce the polymer packing interaction. This LC transition temperature was lower than those of the reported LC polyimides containing similar mesogenic units.[5–11] However, the morphology of their LC structures was not maintained for the measurement of the heat transporting property at room temperature because of the crystallization during the cooling process to room temperature. Therefore, cross-linking would be a suitable method for maintaining their LC structures at room temperature.

In this chapter, the cross-linked LC polyimides containing siloxane spacer units by the cross-linking reaction of the ethynyl end-groups introduced at the chain end were developed, with controlling the extent of the degree of cross-linking by changing the molar ratio of the ethynyl end-group to the monomer units. The ethynyl group was selected as a thermally cross-linkable moiety around 250 °C,[12–16] corresponding to the temperature of LC phase for our reported LC polyimides.[1–4] The purpose of this study is to clarify the relationship between the morphology and thermal diffusivity of the LC polyimides maintaining the LC structure at room temperature via cross-linking at elevated temperature. It should be mentioned that there were no reports on the detailed relationship between the LC structures of polyimides and their thermal diffusivity at room temperature. Indeed, the cross-linked LC polyimide films were successfully obtained, as confirmed by their FT-IR spectra and elemental analysis. It was found that the thermal diffusivity in the thickness direction of the cross-linked LC polyimide films

was enhanced with the increasing extent of the cross-linking. The X-ray diffraction patterns clearly show the smectic LC structure with vertical alignment of the polymer main chains to the film substrate side after the cross-linking reaction. The orientation of the chains leads an enhanced thermal diffusivity of the films gradually from 0.116 to 0.185 $mm^2 s^{-1}$ in the same direction.

4-2. Results and Discussion

4-2-1. Synthesis of Cross-Linked Liquid Crystalline Polyimides

An LC polyimide **5** with octamethyltetrasiloxane spacer units was synthesized using a two-step polymerization procedure, as shown in Figure 4-1 according to previous reports.[1–4] As we clarified in a previous report,[3] the methyl-substituted polyimide in Figure 4-1 showed an amorphous nature, which was synthesized for comparison of its thermal diffusivity to that of the LC polyimides. The ethynyl end-groups of the resulting PAAs **4** were assigned based on the ^1H NMR spectra (Figure 4-2). The signals at 4.31, 4.39, and 4.56 ppm correspond to the ethynyl protons. The PAA films cast from the DMAc solution were heated to 150 °C for 30 min to obtain polyimide films **5** without cross-linking of the ethynyl groups. In the FT-IR spectra of the LC polyimides **5**, the characteristic peaks for the amide groups of PAA were not observed and the characteristic imide peaks at 1770 cm^{-1} (C=O asymmetric stretching), 1713 cm^{-1} (C=O symmetric stretching), and 1389 cm^{-1} (C–N stretching) appeared, indicating completion of the imidization, although the ethynyl peaks around 3250 cm^{-1} (C–H stretching) and 2106 cm^{-1} (C≡C stretching) are still observed. The properties of the resulting PAAs **4** and polyimides **5** are summarized in Table 4-1. In addition to the FT-IR spectra results, the measured elemental compositions of the C, H, and N elements

agreed well with the calculated values. These results clearly support the formation of the polyimides **5**.

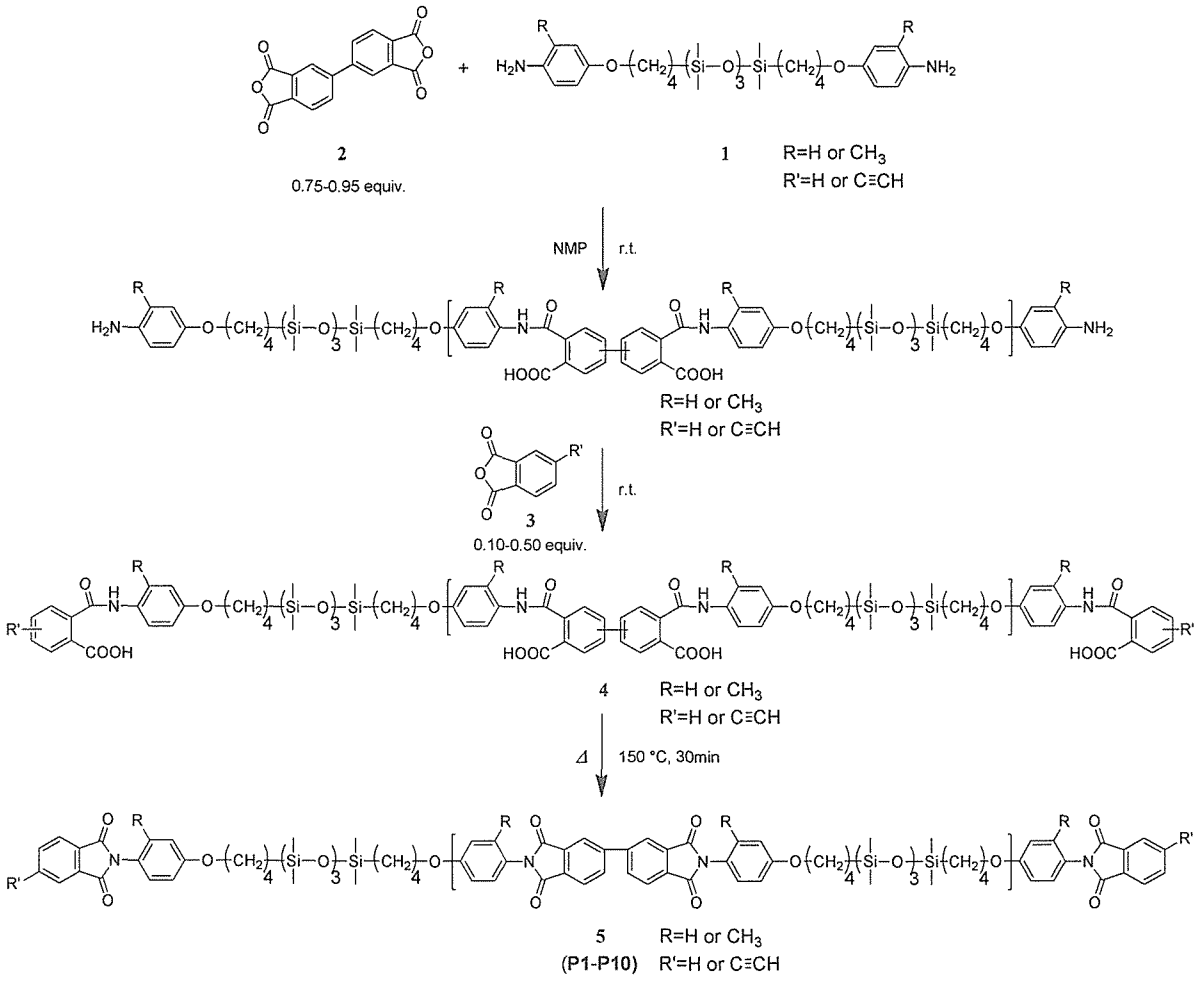

Figure 4-1. Synthesis of LC polyimides **5** from diamines **1** and BPDA (**2**).

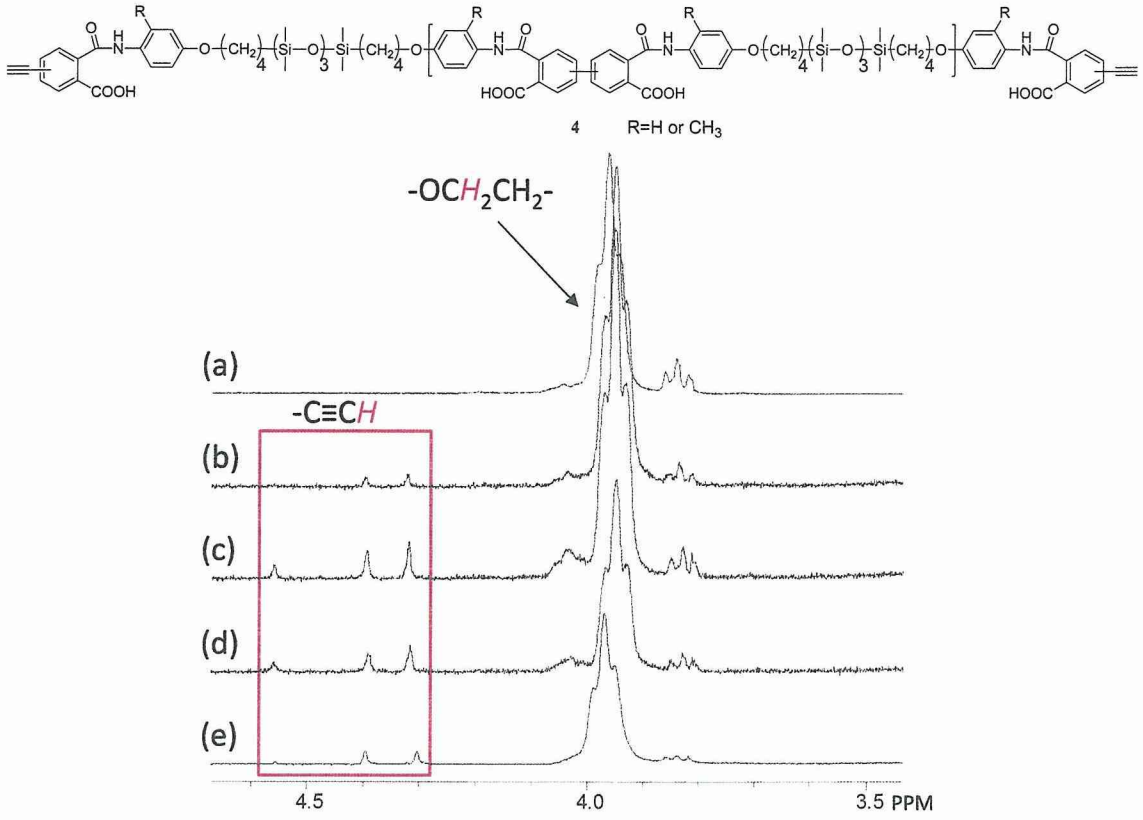

Figure 4-2. ^{1}H-NMR spectra for precursor PAAs **4** of (a) **P1**, (b) **P2**, (c) **P4**, (d) **P6**, and (e) **P10** in DMSO-d_6.

4-2-2. Thermal Properties

All polyimides **5** before the cross-linking reaction possess a high thermal stability over 440 °C ($T_{d5\%}$) according to the thermogravimetric analysis (TGA) under nitrogen, and show two exothermic peaks in the cooling process determined by differential scanning calorimetry (DSC) (Table 4-1). In addition, birefringence and fluidity were observed in the temperature range between these peaks by polarizing optical microscopy (POM, Figure 4-3, Figure 4-4). Therefore, the phase between the transition temperatures corresponds to the LC phase.

Table 4-1. Properties for LC polyimides **5**.

Entry	R	R'	**2** [equiv.][a]	**3** [equiv.][a]	η_{inh} [dL g^{-1}][b]	Elemental analysis [%][c] C	H	N	$T_{d5\%}$ [°C][d]	$T_{lc\text{-}cr}$ [°C][e]	$T_{iso\text{-}lc}$ [°C][e]
P1	H	H	0.90	0.20	0.28	60.37	5.96	3.28	446	195	219
P2	H	C≡CH	0.95	0.10	0.36	60.37	6.18	3.13	459	195	234
P3	H	C≡CH	0.90	0.20	0.32	60.36	6.14	3.17	458	199	237
P4	H	C≡CH	0.85	0.30	0.25	60.55	6.16	3.16	457	186	225
P5	H	C≡CH	0.80	0.40	0.23	60.43	6.14	3.19	457	182	221
P6	H	C≡CH	0.75	0.50	0.23	60.50	6.18	3.11	455	170	207
P7	CH_3	H	0.95	0.10	0.37	61.00	6.25	3.12	448	–[f]	–[f]
P8	CH_3	C≡CH	0.95	0.10	0.35	61.00	6.38	3.00	453	–[f]	–[f]
P9	CH_3	C≡CH	0.85	0.30	0.27	61.10	6.19	3.12	452	–[f]	–[f]
P10	CH_3	C≡CH	0.75	0.50	0.24	61.02	6.34	3.03	452	–[f]	–[f]

[a] Polymerization was carried out under each molar ratio to **1**. The terminal group was an aromatic amine after the polymerization, and then **3** with the equivalent amount to the terminal amine group was added to the reaction mixture. [b] Inherent viscosities were measured at 30 °C in NMP at a PAA **4** concentration of 0.5 g dL^{-1}. [c] Experimental values for the elemental analysis. Theoretically calculated values of the repeating units for the polyimides **5** are shown as follows: for $-(C_{44}H_{54}N_2)_n-$ (**P1**–**P6**), C, 60.94; H, 6.28; N, 3.23; for $-(C_{46}H_{58}N_2)_n-$ (**P7**–**P10**), C, 61.71; H, 6.53; N, 3.13. [d] Decomposition temperature of the polyimides **5**. $T_{d5\%}$: 5% weight loss temperature. [e] Transition temperatures of the uncross-linked LC polyimides **5** were determined as those peak tops by the DSC during the cooling scan at 10 °C min^{-1}. $T_{lc\text{-}cr}$: LC-crystal transition temperature; $T_{iso\text{-}lc}$: isotropic-LC transition temperature. [f] Amorphous nature at room temperature.

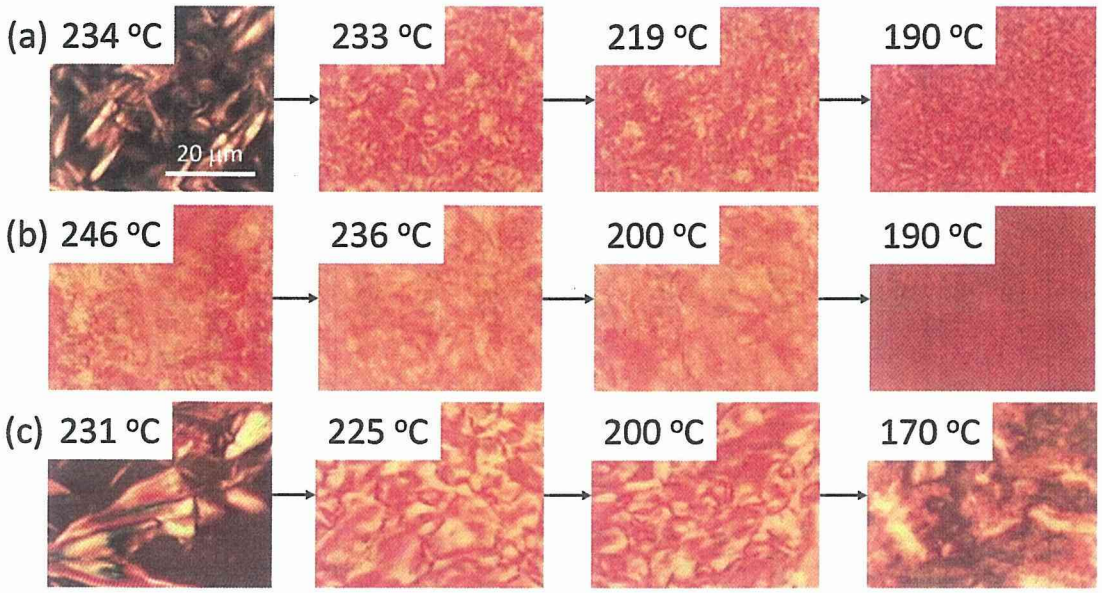

Figure 4-3. POM images of (a) **P1**, (b) **P2**, and (c) **P6** during a cooling process at 5 °C min^{-1} from their isotropic states.

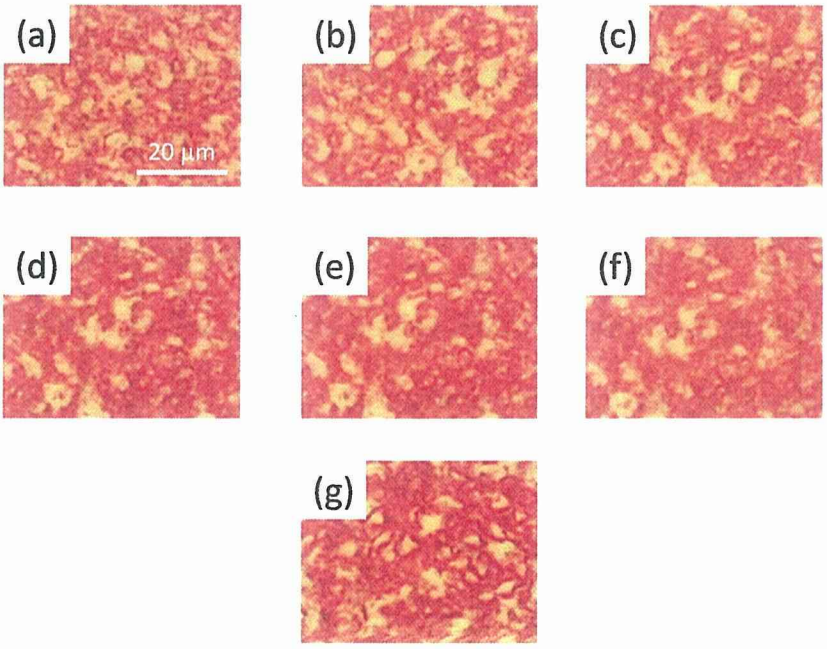

Figure 4-4. POM images of **P6** during annealing at 200 °C for (a) 0h, (b) 0.5h, (c) 1h, (d) 2h, (e) 3h, and (f) 5h. (g) The microscopic textures still remain at room temperature after the cross-linking reaction for 5h.

4-2-3. Preparation of Cross-Linked Liquid Crystalline Polyimide Films

The optimized condition of the cross-linking and annealing temperatures for the LC polyimides **5** was determined by FT-IR and DSC measurements. The FT-IR spectra (Figure 4-5) during the imidization of the PAA films at 150 °C for 30 min on a KBr substrate showed the temperature dependence of the cross-linking reaction. The characteristic peaks of the ethynyl group at 2106 and 3250 cm^{-1} disappeared in the range of 200–230 °C for 30 min, which corresponded to the LC phase of the polyimides **5** (Table 4-1 and Figure 4-6), indicating that the cross-linking proceeded. Moreover, the exothermic peaks of the LC-crystal transition from the DSC thermograms gradually broadened (no broadening observation for **P1** without a cross-linker, Figure 4-7a) after the cross-linking reaction because the relaxation of cross-linked chains became slow (Figure 4-7b). The broadened exothermic peaks remained unchanged with the increase in the annealing time at 200–230 °C for 5 h, suggesting completion of the cross-linking reaction and annealing. On the basis of the optimized condition at 200–230 °C for 5 h, the cross-linked polyimide films **5** (thickness: 100–150 μm) were successfully obtained after removal from the KBr substrate.

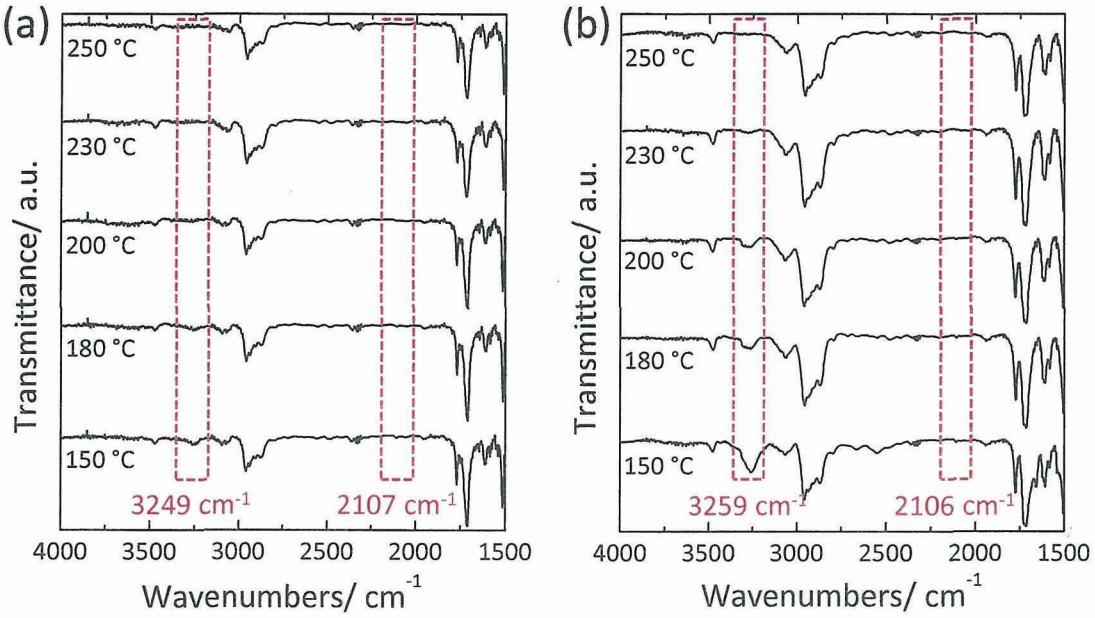

Figure 4-5. Temperature dependence of the cross-linking reaction for (a) **P6** and (b) **P10** by FT-IR spectra.

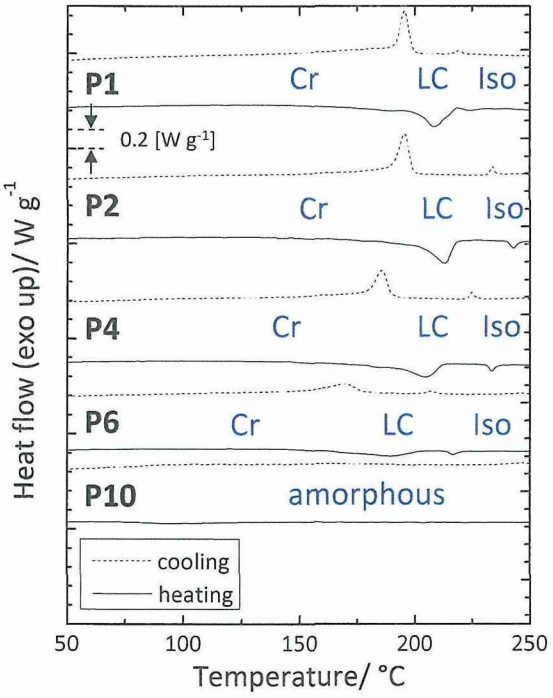

Figure 4-6. DSC trace for the polyimides **5** before the cross-linking.

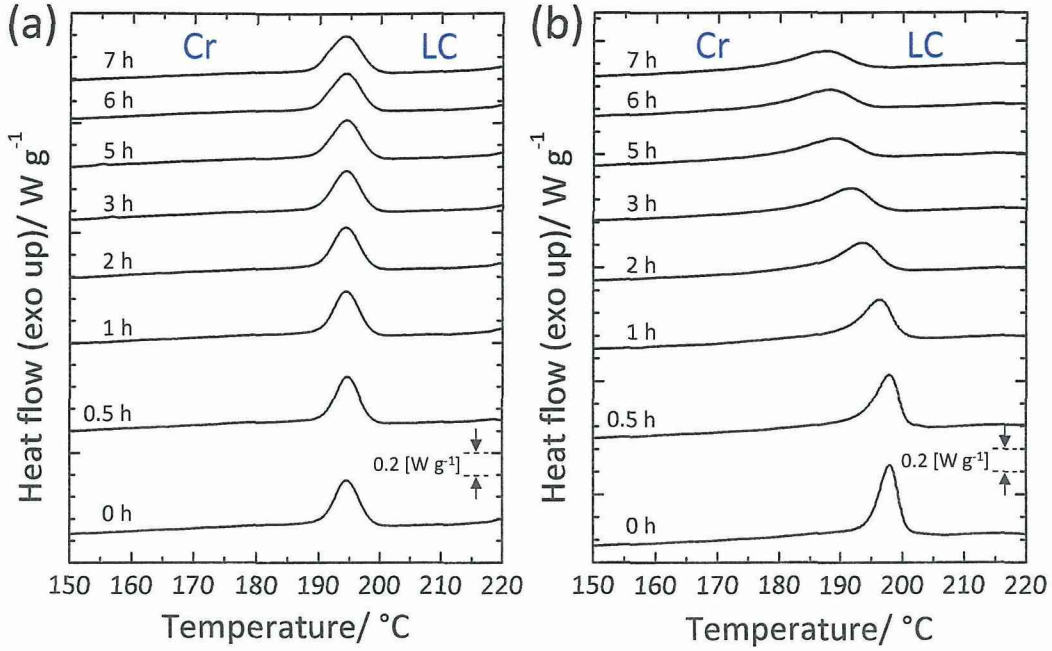

Figure 4-7. Time dependence of the phase transition behavior for the (a) **P1** and (b) **P2** by the DSC thermograms during the cooling scan at 10 °C min^{-1}.

4-2-4. Thermal Diffusivity in the Thickness Direction of Cross-Linked LC Polyimide Films

The thermal diffusivity of the cross-linked LC polyimide films in the thickness direction was measured by the temperature wave analysis (TWA) method[17] at room temperature. The principle of TWA is based on the solution of the heat diffusion equation for the thin and flat plane specimen with the thickness of d, assuming a one-dimensional heat flux. Thermal diffusivity is related to the phase shift ($\Delta\theta$) from the generated temperature wave on a heater in the front surface to that on a sensor in the rear surface as

$$\Delta\theta = -\sqrt{\frac{\omega}{2\alpha}}d - \frac{\pi}{4} \quad (1),$$

where ω is the angular frequency of the temperature wave and α is the thermal

diffusivity. The thermal diffusivity, α, is calculated from the slope in the plot of $\Delta\theta$ versus $\omega^{1/2}$, when d is already known. The values of the thermal diffusivity for cross-linked polyimides increased with the increasing molar ratio of the ethynyl end-group, and the **P6** film showed the highest value of 0.185 $mm^2\ s^{-1}$ (Table 4-2 and Figure 4-8). The morphology of the cross-linked films was investigated in detail to clarify this 50% increase in the thermal diffusivity of the cross-linked LC polyimide films compared to that of the uncross-linked film **P1** or the cross-linked amorphous films **P7**–**P10** with the varied extents of the cross-linking, in which the phenyl ring in the polyimide **5** is substituted with a methyl group (Table 4-1).

Table 4-2. Thermal diffusivities for the LC polyimides **5**.

Entry	R	R'	**2** [equiv.][a]	**3** [equiv.][a]	α [$mm^2\ s^{-1}$][b]	σ [$mm^2\ s^{-1}$][b]
P1	H	H	0.90	0.20	0.116	0.0055
P2	H	C≡CH	0.95	0.10	0.128	0.0056
P3	H	C≡CH	0.90	0.20	0.138	0.0054
P4	H	C≡CH	0.85	0.30	0.142	0.0047
P5	H	C≡CH	0.80	0.40	0.160	0.0167
P6	H	C≡CH	0.75	0.50	0.185	0.0204
P7	CH_3	H	0.95	0.10	0.131	0.0013
P8	CH_3	C≡CH	0.95	0.10	0.119	0.0031
P9	CH_3	C≡CH	0.85	0.30	0.126	0.0040
P10	CH_3	C≡CH	0.75	0.50	0.123	0.0032
Ref. Kapton film[c]					0.124	0.0029

[a] Polymerization was carried out under each molar ratio to **1**. [b] Thermal diffusivity of the films in the thickness direction was measured by the TWA.[17] α: thermal diffusivity, σ: standard deviation. α shows the average value collected from 10 positions (sensor size: 0.25 mm × 0.5 mm) for the films. [c] Kapton H (125 μm thickness) was purchased from DU PONT-TORAY CO., LTD.

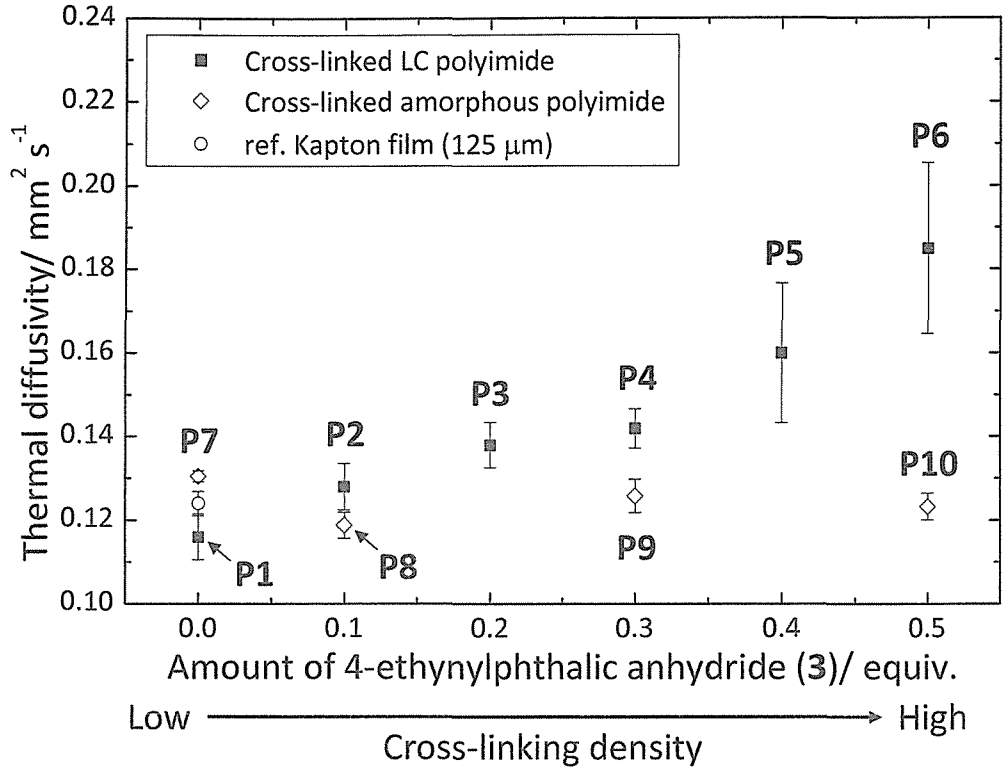

Figure 4-8. Plots of the thermal diffusivity in the thickness direction of the cross-linked polyimides at room temperature vs the amount of 4-ethynylphthalic anhydride (**3**) as a cross-linkable end-capping agent.

4-2-5. Wide-Angle X-ray Diffraction Measurements for Cross-Linked LC Polyimide Films

In order to identify the morphology of the cross-linked LC polyimides **5** at room temperature, wide-angle X-ray diffraction (WAXD) measurements were performed for the films after the cross-linking and annealing processes (Figure 4-9). The typical WAXD patterns of the annealed films obtained by the beam irradiation perpendicular to the film surface are shown in Figure 4-9, as representatively observed for **P1**, **P2**, **P4**, **P6**, and **P10**. A strong layer reflection with a spacing of 29.0 Å and the outer reflections with spacings of 7.4 and 4.9 Å were observed in the uncross-linked LC polyimide **P1** (Figure 4-9a). For the cross-linked LC polyimides, **P2**, **P4**, or **P6**, strong layer

reflections were observed at room temperature with a spacing of 34.4–34.5 Å and broad outer reflections indicating the liquid-like packing of molecules within a layer, corresponding to the typical smectic LC structure (Figure 4-9b–d). The smectic nature of the liquid crystals was accurately identified from the microscopic fan-shaped texture by the POM (Figure 4-3 and Figure 4-4). Moreover, the patterns in Figure 4-9 were assigned to the SmC phase at room temperature in comparison to the *d*-spacing of the patterns for **P2** and **P6** taken at 200 °C, corresponding to the SmC phase (Figure 4-10). These results indicated that the cross-linked LC polyimides successfully maintained their SmC LC structures at room temperature. On the other hand, the WAXD pattern of the cross-linked polyimide **P10** did not show the strong layer reflection, but the broad halo due to its amorphous nature, as expected (Figure 4-9, parts e and j).

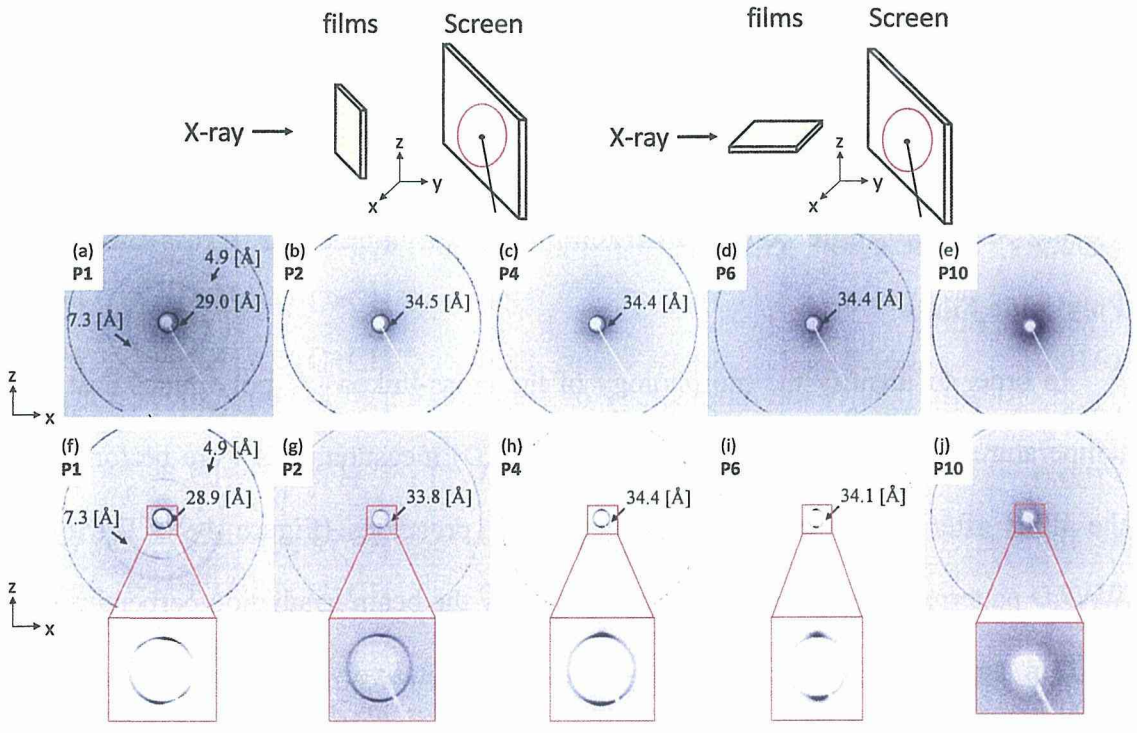

Figure 4-9. WAXD patterns for the cross-linked polyimide films, **P1**, **P2**, **P4**, **P6**, and **P10**, by beam irradiation (a)–(e) perpendicular to the film surface and (f)–(j) parallel to the film surface.

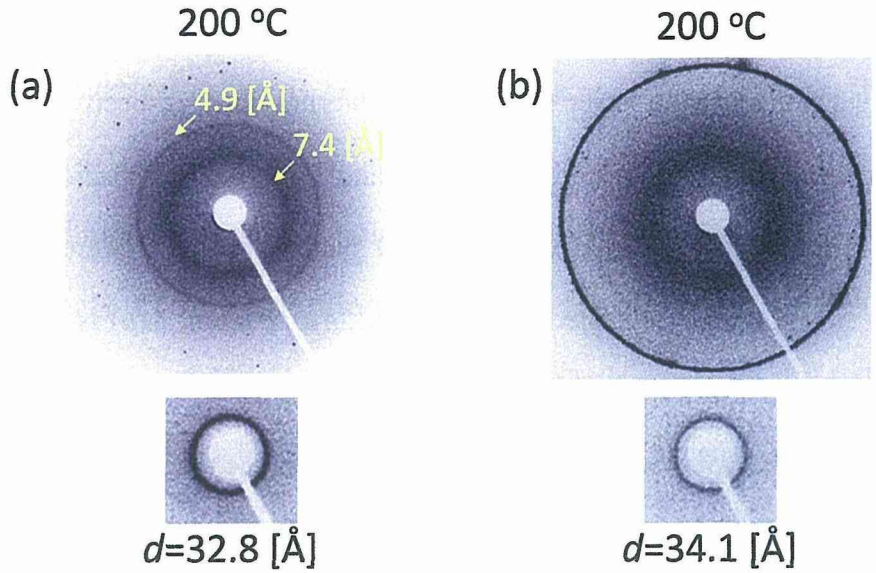

Figure 4-10. WAXD patterns of LC polyimide film (a) **P2** and (b) **P6** at 200 °C with beam irradiation from parallel to the film surface.

Parts f–j of Figure 4-9 show the WAXD patterns of the annealed films taken with the beam irradiation parallel to the film surface. The layer reflections on the meridian gradually became strong with the increasing extent of the cross-linking, although the sharp inner reflections and broad outer reflections were similar to the patterns with the incident X-ray beam perpendicular to the film surface, indicating the fixed smectic LC structure at room temperature (Figure 4-9g–i). In addition, these results indicated that the smectic layers have preferred alignment parallel to the film surface, that is, the polymer chains are aligned in the direction normal to the films.

Furthermore, to clarify how large areas of polymer chains are aligned in the films, we operated the microbeam (beam size: 2.9 μm × 3.5 μm) WAXD (BL40XU beamline in SPring-8 at Hyogo, Japan) at each position of the cross-sectional direction of the **P2** and **P6** films in the thickness direction (z-direction), scanning from the KBr plate side to the air interface side (Figure 4-11). Parts a and d of Figure 4-11 are the optical

microscope images of the **P2** and **P6** thin films. The upper surface is corresponding to the KBr substrate and the lower one is the air interface side, respectively. Figure 4-11c and 4-11f are the WAXD patterns of the **P2** and **P6** at each z position. The intensity profiles in azimuthal angle μ of the WAXD patterns c and f were fitted with the Gaussian functions and separated into $I_0(\mu)$ and $I_1(\mu)$. Herein, $I_0(\mu)$ is corresponding to the intensity of the diffraction of the nonoriented region without the μ-dependence, and $I_1(\mu)$ is that of the oriented region concentrated around the meridian, respectively. Parts b and e of Figure 4-11 show the orientational order parameter S (▲), the integral intensity of oriented region (▼) and the nonoriented region (○) were plotted versus the z-position, for (b) **P2** and (e) **P6**, respectively. The orientational order parameter S is defined as the eq 2.[18]

$$S = \frac{1}{2}(3\langle\cos^2\mu\rangle - 1), \langle\cos^2\mu\rangle = \frac{\int_0^\pi I_1(\mu)\cos^2\mu|\sin\mu|d\mu}{\int_0^\pi I_1(\mu)|\sin\mu|d\mu} \quad (2)$$

The integrated intensity Q is defined as the eq 3, which is proportional to the fraction of the oriented or nonoriented region.

$$Q = \int_0^\pi I_i(\mu)\,|\sin\mu|d\mu \quad i = 0 \text{ or } 1 \quad (3)$$

The results clearly show that the layer reflections of both **P2** and **P6** are highly concentrated on the meridian near the KBr substrate side compared with the air surface side to give the higher intensity. These reflections are gradually broadened in the azimuthal direction and the Debye–Scherrer ring overlapped, resulting in the decrease of intensity. The reason why the intensity gradually increased at the KBr surface side can be found in some undulation of the surface. These results demonstrate that the smectic layers are almost perfectly aligned near the KBr substrate, but become progressively more disordered further away from the substrate, forming the

polydomain-like smectic structure close to the air surface. In addition, the extent of the cross-linkers influenced the areas of the aligned chains in the thickness direction of films. In Figure 4-11b and 4-11e, ca. 50% range in thickness for the **P6** film was filled with the aligned region and there is little nonoriented region, while only ca. 30% range in thickness for the **P2** film was filled with the aligned region and there exists about 30% of the nonoriented region. Herein, three possible explanations for these phenomena are offered. (1) The smectic layers aligned perpendicular to the surface are affected by the KBr substrate during the imidization and cross-linking process. This alignment occurred, at least partly, during the imidization considering the pattern with the incident X-ray beam parallel to the surface of the **P6** film after imidization (Figure 4-12). (2) The vertical alignment of the layers near the air surface side is difficult to occur during annealing, while that near the KBr side preferentially occurs. (3) The alignment of the layers could be maintained by the cross-linking, expanding ts area in the thickness direction of the films. For the **P6** with a large content of cross-linkers, the cross-linking reaction of **P6** should be faster than that of **P2**, therefore the areas of the aligned chains in the thickness direction of **P6** were larger than those of **P2**.

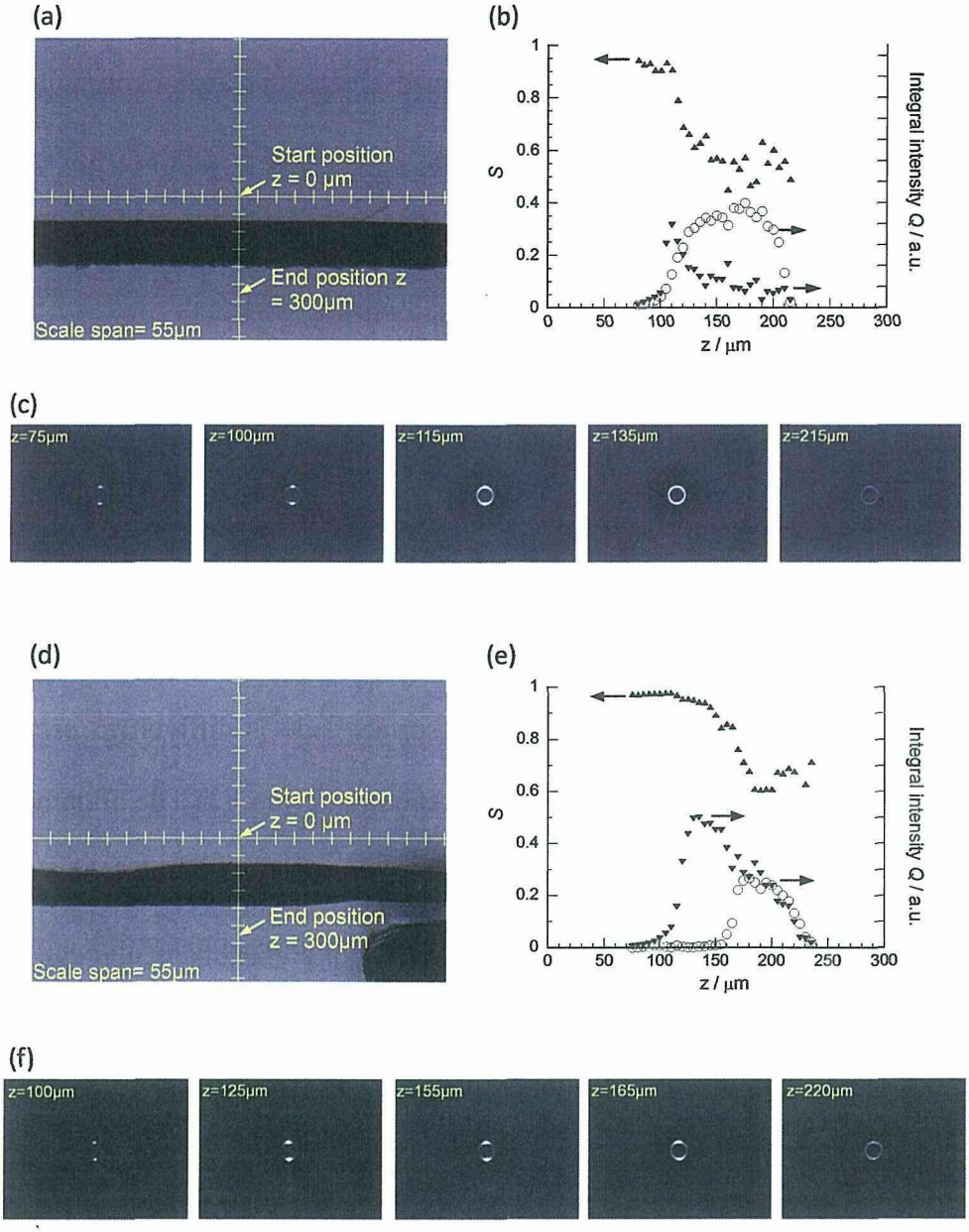

Figure 4-11. Optical microscope images of the (a) **P2** and (d) **P6** thin films. The upper surface is corresponding to the KBr substrate side and the lower one is the air interface side, respectively. The X-ray with 2.9 μm × 3.5 μm size was scanned from the start and end position at the same interval of 5μm. (c and f) WAXD patterns of the (c) **P2** and (f) **P6** at each z-position. (b and e) Orientational order parameter S (▲ symbol), integral intensity of oriented region (▼) and nonoriented region (○) for the (b) **P2** and (e) **P6**, were plotted versus z-position, respectively.

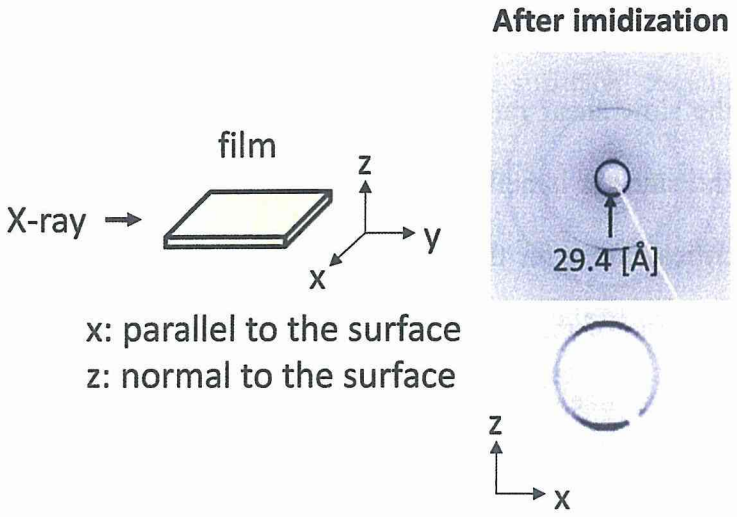

Figure 4-12. WAXD pattern of LC polyimide film **P6** after imidization without cross-linking at room temperature irradiated from parallel to the film surface.

The smectic layer normal aligned near the KBr substrate after the film fabrication process can be explained by the shear deformation near the substrate rather than some interactions between the polyimides and the KBr substrate. If the interaction is the main driving force of the homeotropic alignment, the polymer chains would align along the substrate, because the mesogenic imide rings with a higher surface free energy will preferentially lie on the substrate. It should be noted that the evaporation of the DMAc in PAAs simultaneously occurred during the imidization and smectic phase formation process. Fukunaga *et al.* reported that the mechanical strain fields generated during the solvent evaporation process helped to form the lamellar alignment of the block copolymer films in which the bottom surface was affected by shear deformation causing sample shrinkage. It should also be noted that the film will not uniformly shrink near the substrate, because the lateral shrinkage of the bottom film layer is hindered by silicon substrate interactions.[19] Our cross-linked LC polyimides would be in similar shear flow fields. In the case of the smectic phase of the main-chain LC polymers, the

smectic layer normal is easily aligned parallel to the velocity gradient direction of the shear flow in the slow shear rate region, similar to the usual smectic systems.[20–22] In these reports, the smectic lamellar spacing of the main-chain polymer smectic LC is related to the critical stress for the layer collapse and the lamellar binding energy, and the parallel orientation of the smectic layer normal is attributed to the mutual slide of the chain-folded lamellae. Therefore, it can be concluded that the homeotropic alignment of the LC polyimides to the KBr substrate was induced by a shearing motion in the vicinity of the KBr substrate during imidization and formation of the smectic LC structure (Figure 4-13). The preformed homeotropic orientation will be better maintained for a faster cross-linking reaction and may be amplified by further shear deformation caused by volume shrinkage during the cross-linking process.

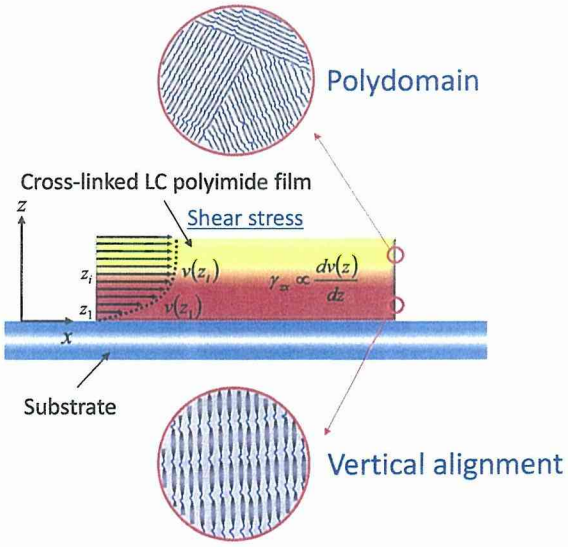

Figure 4-13. Schematic illustration of the mechanism of the homeotropic orientation for the cross-liked LC polyimides.

In practical use, the high thermally conductive materials can be used between the semiconductor chips as adhesives. The cross-linked LC polyimides might be aligned well, influenced by the sandwiched substrates through the out-of-direction of the films to enhance the thermal conductivity in the thickness direction. Also, when the high

thermally conductive composites are prepared based on the cross-linked LC polyimides and inorganic fillers, a small amount of fillers can be sufficient to achieve the desired thermal conductivity (3–5 W m^{-1} K^{-1}) of the composites.

4-3. Conclusions

The relationship between the morphology of the cross-linked LC polymide films and their thermal diffusivity has been clarified. The optimized cross-linking condition in their LC phase at 200–230 °C for 5 h was determined by the FT-IR spectra and DSC thermograms, respectively. The WAXD patterns of the cross-linked films obtained by the beam irradiation perpendicular to the film surface corresponded to the typical smectic LC structures at room temperature. The thermal diffusivity in the thickness direction of the cross-linked LC polyimide films was measured by the TWA method at room temperature. The thermal diffusivity values increased with the increasing extent of the cross-linking, and the **P6** film showed the highest value of 0.185 mm^2 s^{-1} compared to that of 0.116 mm^2 s^{-1} for the **P1** film. Moreover, for the results of the WAXD patterns by the beam irradiation parallel to the film surface, the layer reflections on the meridian gradually became strong with the increasing extent of the cross-linking. These results indicated that the smectic layer comparatively formed the vertical alignment of the polymer chains in the thickness direction of the films. The scanning WAXD profiles indicated that the homeotropic alignment of chains near the KBr substrate side was maintained compared to that near the air surface side probably due to a shearing motion in the vicinity of the KBr substrate and the cross-linking for a film with a large number of cross-linking sites before disordering. This homeotropic alignment of the chains in the thickness direction and the increase in the areas for the aligned chains can be related

to the 50% increase in the thermal diffusivity of the cross-linked LC polyimide films. For the first time, the fixing the morphology of the LC polyimide films at room temperature was demonstrated, clarifying the relationship between their morphological structures and the thermal diffusivity. It can be expected that future materials with a high thermal conductivity, such as LC polyimides, will lead to the production of highly functional and density-packed electric devices.

4-4. Experimental Section

4-4-1. Measurements

Inherent viscosities were measured at 30 °C in NMP at a polymer concentration of 0.5 g dL^{-1}. FT-IR spectra were measured on a Horiba FT-720 spectrometer. ^{1}H and ^{13}C NMR spectra were recorded with a Bruker DPX300S spectrometer. The phase transitions behavior was observed with a polarizing optical microscope (Olympus BX51), together with the use of a LINKAM LTS-350 hot stage equipped with a temperature controller by setting a polyimide film between crossed polarizers. Thermal analysis was performed on a Seiko EXSTAR 6000 TG/DTA 6300 thermal analyzer at a heating rate of 10 °C min^{-1} for thermogravimetry (TG) and a Seiko EXSTAR 6000 DSC 6200 connected to a cooling system at a heating rate of 10 °C min^{-1} for differential scanning calorimetry (DSC). Elemental analysis was carried out on a YANACO CHN cord er MT-6. Wide-angle X-ray diffraction (WAXD) measurements were performed at ambient temperature by using a Rigaku-Denki UltraX-18 X-ray generator with monochromic Cu Kα radiation (40 kV, 50 mA) from graphite crystal of monochromator and flat-plate type of imaging plate. Thermal diffusivity of the films in the thickness direction was measured by using ai-Phase Mobile 1u, ai-Phase Co. Ltd., based on the TWA method.[17] Microbeam WAXD measurements were carried out on BL40XU beamline of SPring-8 in Hyogo, Japan. The wavelength of the X-ray beam was 1.55 Å, the beam size was 2.9 μm × 3.5 μm as half-width, and the diffraction pattern was recorded with an X-ray image intensifier (Hamamatsu Photonics, V5445P) and a fast CCD camera (Hamamatsu Photonics, C4880–80). The samples were moved stepwise at 5 μm interval and irradiated with the X-ray for 0.1 s.

4-4-2. Materials

BPDA was purified by the sublimation prior to use. The other materials and solvents were obtained commercially and used as received.

4-4-3. General Synthesis for Diamines and Poly(amic acid) 4

The diamine monomers containing the siloxane linkages were synthesized according to the previous reports[21–23] under the standard condition for Williamson's ether synthesis, hydrosilylation, and reduction.

Synthesis of PAA for **P1**

The PAA as a precursor of the **P1** was synthesized from BPDA (0.194 g, 0.660 mmol) with 1,7-bis[4-(4-aminophenoxy)butyl]-1,1,3,3,5,5,7,7-octamethyltetrasiloxane (0.447 g, 0.733 mmol) and phthalic anhydride (0.0216 g, 0.146 mmol) by the solution polymerization in 20 wt% NMP (2.65 g). After the reaction, the reaction mixture was poured into water containing 10 vol% methanol (200 mL), then the precipitate was collected and dried under the reduced pressure at 70 °C to obtain the PAA as a precursor of polyimide (0.619 g, 85% yield).

Synthesis of PAA for **P2**

The title compound, the PAA for the **P2**, was synthesized by the same procedure as the PAA for the **P1** performed with 0.452 g (1.54 mmol) of BPDA, 0.986 g (1.62 mmol) of 1,7-bis[4-(4-aminophenoxy)butyl]-1,1,3,3,5,5,7,7-octamethyltetrasiloxane, 0.0284 g (0.165 mmol) of 4-ethynylphthalic anhydride, and 5.83 g of NMP. After the reaction, the compound, the PAA for the **P2**, (1.43 g, 54% yield) was isolated as a pale yellow

solid.

Synthesis of PAA for **P3**

The title compound, the PAA for the **P3**, was synthesized by the same procedure as the PAA for the **P1** performed with 0.342 g (1.16 mmol) of BPDA, 0.786 g (1.29 mmol) of 1,7-bis[4-(4-aminophenoxy)butyl]-1,1,3,3,5,5,7,7-octamethyltetrasiloxane, 0.0443 g (0.257 mmol) of 4-ethynylphthalic anhydride, and 4.59 g of NMP. After the reaction, the compound, the PAA for the **P3**, (0.967 g, 73% yield) was isolated as a pale yellow solid.

Synthesis of PAA for **P4**

The title compound, the PAA for the **P4**, was synthesized by the same procedure as the PAA for the **P1** performed with 0.240 g (0.817 mmol) of BPDA, 0.585 g (0.961 mmol) of 1,7-bis[4-(4-aminophenoxy)butyl]-1,1,3,3,5,5,7,7-octamethyltetrasiloxane, 0.0493 g (0.286 mmol) of 4-ethynylphthalic anhydride, and 3.49 g of NMP. After the reaction, the compound, the PAA for the **P4**, (0.761 g, 86% yield) was isolated as a pale yellow solid.

Synthesis of PAA for **P5**

The title compound, the PAA for the **P5**, was synthesized by the same procedure as the PAA for the **P1** performed with 0.179 g (0.607 mmol) of BPDA, 0.463 g (0.760 mmol) of 1,7-bis[4-(4-aminophenoxy)butyl]-1,1,3,3,5,5,7,7-octamethyltetrasiloxane, 0.0529 g (0.307 mmol) of 4-ethynylphthalic anhydride, and 2.82 g of NMP. After the reaction, the compound, the PAA for the **P5**, (0.481 g, 73% yield) was isolated as a pale

yellow solid.

Synthesis of PAA for **P6**

The title compound, the PAA for the **P6**, was synthesized by the same procedure as the PAA for the **P1** performed with 0.127 g (0.431 mmol) of BPDA, 0.350 g (0.575 mmol) of 1,7-bis[4-(4-aminophenoxy)butyl]-1,1,3,3,5,5,7,7-octamethyltetrasiloxane, 0.0493 g (0.286 mmol) of 4-ethynylphthalic anhydride, and 2.14 g of NMP. After the reaction, the compound, the PAA for the **P6**, (0.358 g, 67% yield) was isolated as a pale yellow solid.

Synthesis of PAA for **P7**

The title compound, the PAA for the **P7**, was synthesized by the same procedure as the PAA for the **P1** performed with 0.491 g (1.67 mmol) of BPDA, 1.12 g (1.75 mmol) of 1,7-bis[4-(4-amino-3-methylphenoxy)butyl]-1,1,3,3,5,5,7,7-octamethyltetrasiloxane, 0.0258 g (0.174 mmol) of phthalic anhydride, and 6.53 g of NMP. After the reaction, the compound, the PAA for the **P7**, (1.57 g, 91% yield) was isolated as a pale yellow solid.

Synthesis of PAA for **P8**

The title compound, the PAA for the **P8**, was synthesized by the same procedure as the PAA for the **P1** performed with 0.510 g (1.73 mmol) of BPDA, 1.16 g (1.82 mmol) of 1,7-bis[4-(4-amino-3-methylphenoxy)butyl]-1,1,3,3,5,5,7,7-octamethyltetrasiloxane, 0.0319 g (0.185 mmol) of 4-ethynylphthalic anhydride, and 6.94 g of NMP. After the reaction, the compound, the PAA for the **P8**, (1.63 g, 91% yield) was isolated as a pale yellow solid.

Synthesis of PAA for **P9**

The title compound, the PAA for the **P9**, was synthesized by the same procedure as the PAA for the **P1** performed with 0.345 g (1.17 mmol) of BPDA, 0.879 g (1.38 mmol) of 1,7-bis[4-(4-amino-3-methylphenoxy)butyl]-1,1,3,3,5,5,7,7-octamethyltetrasiloxane, 0.0721 g (0.419 mmol) of 4-ethynylphthalic anhydride, and 5.23 g of NMP. After the reaction, the compound, the PAA for the **P9**, (1.08 g, 73% yield) was isolated as a pale yellow solid.

Synthesis of PAA for **P10**

The title compound, the PAA for the **P10**, was synthesized by the same procedure as the PAA for the **P1** performed with 0.259 g (0.880 mmol) of BPDA, 0.748 g (1.17 mmol) of 1,7-bis[4-(4-amino-3-methylphenoxy)butyl]-1,1,3,3,5,5,7,7-octamethyltetrasiloxane, 0.101 g (0.588 mmol) of 4-ethynylphthalic anhydride, and 4.46 g of NMP. After the reaction, the compound, the PAA for the **P10**, (0.436 g, 32% yield) was isolated as a pale yellow solid.

4-4-4. Preparation of Cross-Linked Liquid Crystalline Polyimides

Cross-linked polyimides were prepared by casting the 20 wt% *N*,*N*-dimethylacetoamide (DMAc) solution of PAAs on the KBr plate, drying solvent, thermally imidizing the PAAs at 150 °C for 30 min, and finally the cross-linking ethynyl groups on the chain end of the polyimides at the LC phase temperature. After the cross-linking reaction, the films with the KBr substrate were immersed into water to

remove from the substrate, and the strong free-standing films were finally obtained.

4-5. References and Notes

1. Shoji, Y.; Higashihara, T.; Watanabe, J.; Ueda, M. *Chem. Lett.* **2009**, *38*, 716–717.
2. Shoji, Y.; Ishige, R.; Higashihara, T.; Watanabe, J.; Ueda, M. *Macromolecules* **2010**, *43*, 805.
3. Shoji, Y.; Ishige, R.; Higashihara, T.; Kawauchi, S.; Watanabe, J.; Ueda, M. *Macromolecules* **2010**, *43*, 8950.
4. Ishige, R.; Shoji, Y.; Higashihara, T.; Ueda, M.; Watanabe, J. *J. Mater. Chem.* **2012**, *22*, 1532.
5. Ho, C.-Y.; Lee, J.-Y. *J. Appl. Polym. Sci.* **2006**, *100*, 1688.
6. Pramoda, K. P.; Liu, S.; Chung, T.-S. *Macromol. Mater. Eng.* **2002**, *287*, 931.
7. Huang, H. W.; Kaneko, T. I.; Horie, K.; Watanabe, J. *Polymer* **1999**, *40*, 3821.
8. Kaneko, T. I.; Imamura, K.; Watanabe, J. *Macromolecules* **1997**, *30*, 4244.
9. Inoue, T.; Kakimoto, M.; Imai, Y.; Watanabe, J. *Macromol. Chem. Phys.* **1997**, *198*, 519.
10. Schab-Balcerzak, E.; Wegrzyn, M.; Janeczek, H.; Jarzabek, B.; Rannou, P.; Iwan, A. *Liq. Cryst.* **2010**, *37*, 1347.
11. Coatat, G.; Eastmond, G. C.; Fairclough, J. P. A.; Paprotny, J.; Ryan, A. J.; Stagnaro, P. *Macromolecules* **2008**, *41*, 1034.
12. Kim, J.-P.; Lee, W.-Y.; Kang, J.-W.; Kwon, S.-K.; Kim, J.-J.; Lee, J.-S. *Macromolecules* **2001**, *34*, 7817.
13. Kwon, S.-K.; Lee, J.-S. *Chem. Mater.* **2006**, *18*, 4519.
14. Kwon, S.-K.; Jeong, M.-H.; Lee, J.-P.; Lee, J.-S. *Macromolecules* **2009**, *42*, 584.

15. Jeong, M.-H.; Kwon, S.-K.; Lee, J.-S. *Macromolecules* **2009**, *42*, 1652.

16. Kwon, S.-K.; Jeong, M.-H.; Lee, J.-P.; Lee, J.-P.; Kim, Y.-J.; Lee, J.-S. *Chem. Mater.* **2010**, *22*, 5500.

17. Morikawa, J.; Hashimoto, T. *J. Appl. Phys.* **2009**, *105*, 113506.

18. Ortiz, C.; Wagner, M.; Bhargave, N.; Ober, C. K.; Kramer, E. J. *Macromlecules* **1998**, *31*, 8531.

19. Fukunaga, K.; Elbs, H.; Magerle, R.; Krausch, G. *Macromolecules* **2000**, *33*, 947.

20. Tokita, M.; Osada, K.; Kawauchi, S.; Watanabe, J. *Polym. J.* **1998**, *30*, 687.

21. Tokita, M.; Tokunaga, K.; Funaoka, S.; Osada, K.; Watanabe, J. *Macromolecules* **2004**, *37*, 2527.

22. Tokita, M.; Watanabe, J. *Polym. J.* **2006**, *38*, 611.

Chapter 5

Thermal Diffusivity of Hexagonal Boron Nitride Composites Based on Cross-Linked Liquid Crystalline Polyimides

Abstract.

Hexagonal boron nitride (h-BN) composites with the oriented cross-linked liquid crystalline (LC) polyimide have been developed as high thermally conductive materials. Well-dispersed h-BN composite films were obtained, as observed by scanning electron microscopy. The morphology of the composite films was further investigated in detail by the wide-angle X-ray diffraction. The obtained composite films based on the cross-linked LC polyimide showed that the polymer chains vertically aligned in the thickness direction of the films, while those based on the amorphous polyimide showed an isotropic nature. Moreover, the alignment of the cross-linked LC polyimides was maintained, even after increasing the volume fraction of h-BN. This alignment plays an important role in the effective phonon conduction between h-BN and the matrices. Indeed, the thermal diffusivity in the thickness direction of the composite films based on the LC polyimide measured by a temperature wave analysis method was increased to

0.679 mm^2 s^{-1} at a 30 vol% h-BN loading, which was higher than that based on the amorphous polyimide.

5-1. Introduction

In chapter 4, the oriented cross-linked liquid crystalline (LC) polyimides with siloxane units were prepared by the cross-linking reaction of the ethynyl end-groups introduced at the chain end, increasing their thermal diffusivity in the thickness direction of the films.[1] It was found that the cross-linked LC polyimides formed a continuous smectic alignment from the substrate side with the increasing extent of cross-linking and this alignment gradually became disordered near the air interface side. The thermal diffusivity of the cross-linked LC polyimides in the thickness direction of the films was enhanced from 0.116 to 0.185 $mm^2 s^{-1}$. The relationship between the chain alignments and thermal diffusivity has been clarified. However, the effect of the filler addition to the cross-linked LC polyimides has not been investigated yet.

In this chapter, high thermal conductive h-BN composites using the cross-linked LC polyimides as matrices, which show a vertical alignment of the smectic structures, have been developed. The purpose of this work is to confirm the advantage of the oriented LC polyimide, **P1**, compared with the amorphous one, **P2**, in the composite systems (Figure 1). Indeed, the h-BN composite films of the cross-linked LC polyimide and amorphous polyimide were successfully obtained, as characterized by FT-IR spectra and SEM observation. The smectic orientation of the LC polyimide matrices was maintained even in the composites, as confirmed by wide-angle X-ray diffraction (WAXD). In the case of the cross-linked LC polyimide, the orientation of the chains did not become disordered on increasing the content of h-BN. As a result, the composites based on the cross-linked LC polyimides possess higher thermal diffusivity than the composites based on amorphous polyimides.

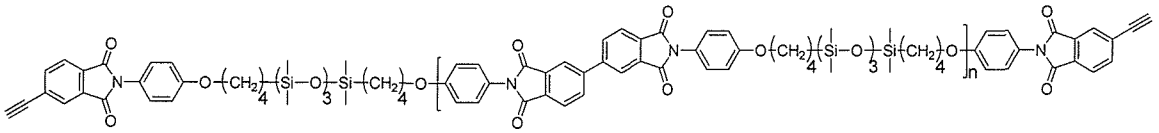

P1: cross-linked LC polyimide

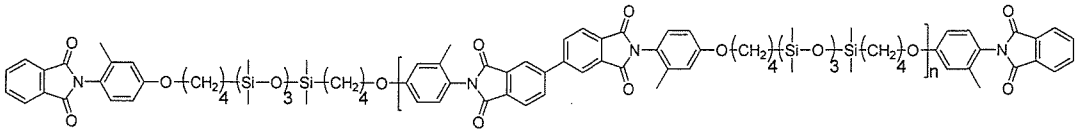

P2: amorphous polyimide

Figure 5-1. Cross-linked LC polyimide, **P1** and amorphous polyimide, **P2**.

5-2. Results and Discussion

5-2-1. Synthesis of Polyimide Matrices.

A cross-linked LC polyimide (**P1**) and an amorphous polyimide (**P2**) with octamethyltetrasiloxane spacer units were synthesized according to the previous chapters by using a two-step polymerization procedure (Figure 5-1 and Table 5-1).[1,2] The chemical structures of **P1** and **P2** before cross-linking reaction were assigned by ^{1}H NMR, ^{13}C NMR (Figure 5-2 and Figure 4-2), and FT-IR spectra. In addition, the results of elemental analysis agreed well with the analytical calculation values.[1] The viscosities of the resulting PAAs, which are the precursors of **P1** and **P2**, were 0.18 and 0.37 dL g^{-1}, respectively (Table 5-1). The number-average molecular weight and polydispersity indices (M_n; PDI) of **P1** and **P2** before the cross-linking reaction were determined to be (7,800; 2.36) and (30,500; 2.58), respectively, determined by SEC in $CHCl_3$ with calibration using polystyrene standards, as listed in Table 5-1. Moreover, **P1** and **P2** possessed high thermal stability over around 440 °C ($T_{d5\%}$) according to thermogravimetric analysis (TGA) under nitrogen and showed the LC and amorphous natures, respectively, as determined by differential scanning calorimetry (DSC) and polarized optical microscopy (POM) (Table 5-1 and Figure 5-4).[1,2c]

Table 5-1. Properties of polyimide matrices.

Entry	η_{inh} [dL g^{-1}][a]	M_n[b]	PDI[b]	$T_{d5\%}$ [°C][c]	$T_{lc\text{-}cr}$ [°C][d]	$T_{iso\text{-}lc}$ [°C][d]
P1	0.18	7,800	2.36	448	158	192
P2	0.37	30,500	2.58	439	*f*	*f*

[a] Inherent viscosities of precursor PAAs of polyimides were measured at 30 °C in NMP at a concentration of 0.5 g dL^{-1}. [b] M_n and PDI were determined by SEC in $CHCl_3$ using polystyrene standards. [c] Decomposition temperature of the polyimide matrices. $T_{d5\%}$: 5% weight loss temperature. [d] Transition temperature of the polyimide matrices were determined as those peak tops by DSC during a cooling scan at 10 °C min^{-1}. $T_{lc\text{-}cr}$: LC-crystal transition temperature, $T_{iso\text{-}lc}$: isotropic-LC transition temperature. [e] Amorphous nature at room temperature. T_g=76 °C, T_c=123 °C, and T_m=167 °C determined by the DSC trace during a heating process at 10 °C min^{-1}.

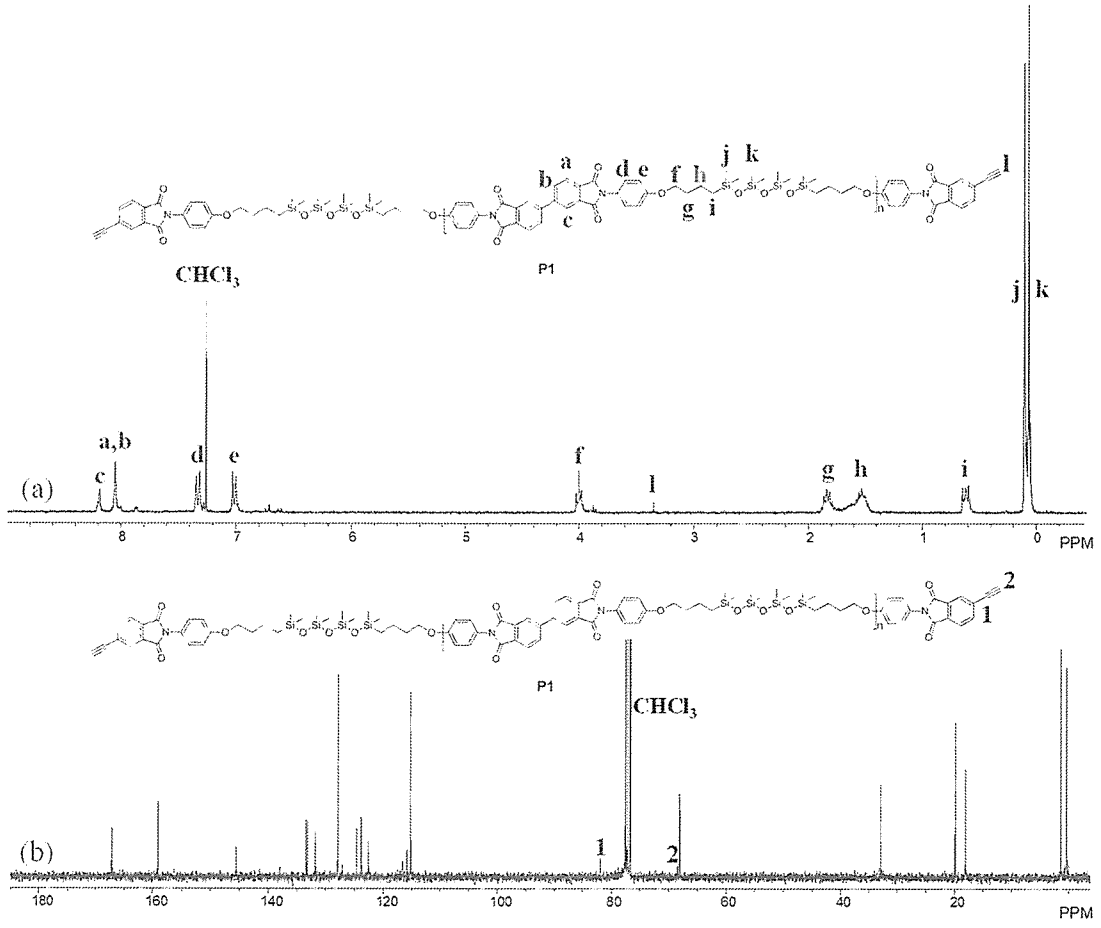

Figure 5-2. (a) ^1H and (b) ^{13}C NMR spectra of non cross-linked **P1** in $CDCl_3$.

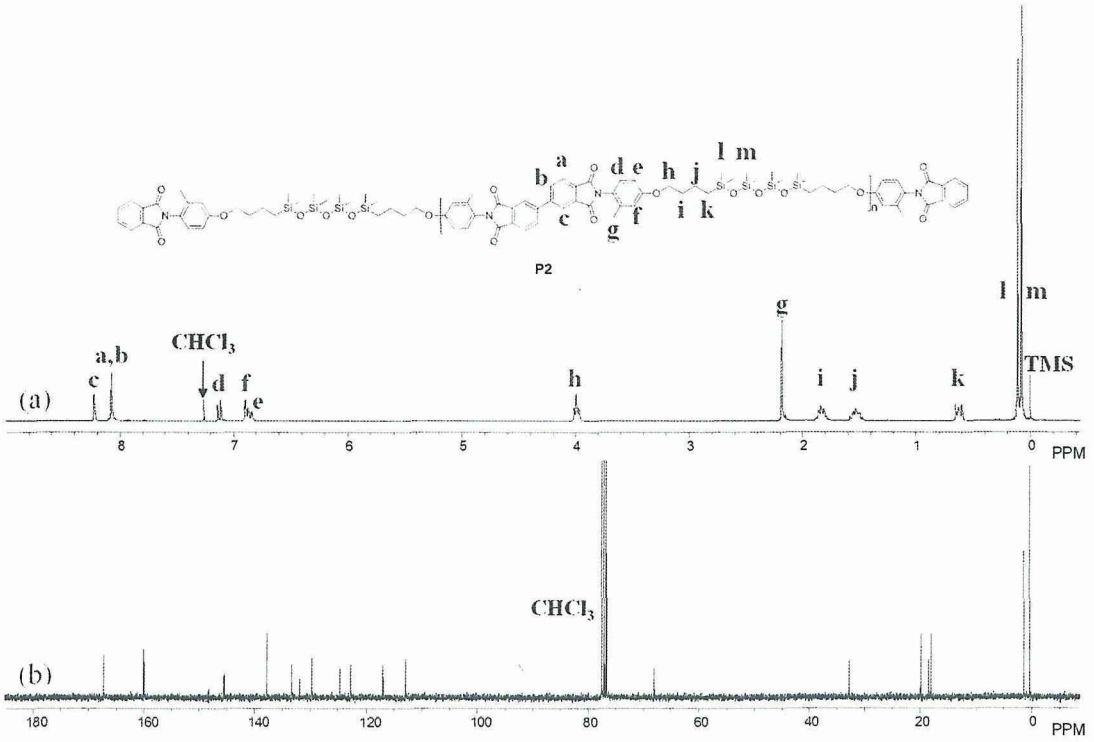

Figure 5-3. (a) ^{1}H and (b) ^{13}C NMR spectra of **P2** in $CDCl_3$.

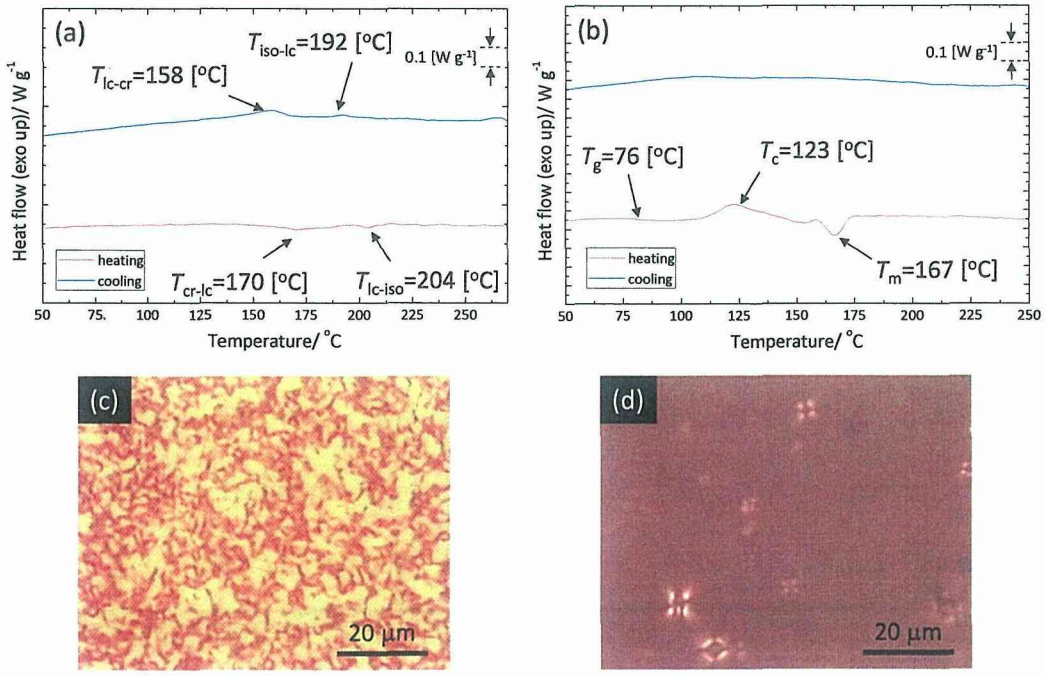

Figure 5-4. DSC traces for polyimide (a) **P1** and (b) **P2**. POM images of (c) **P1** and (d) **P2** at room temperature.

5-2-2. Preparation of Polyimide Composite Films

The h-BN composite solutions were prepared by mixing h-BN with the PAAs of **P1** or **P2** in *N*,*N*-dimethylacetamide (DMAc), changing the volume fraction of h-BN from 0 to 50 vol%. They were then cast and gradually heated to 200 °C on the KBr substrates to obtain the polyimide composite films. In the case of the composite films of **P1**, the cross-linking reaction and annealing treatment were carried out at 200 °C for 5 h according to the previous report,[1] while the composite films of **P2** were treated at 200 °C for 30 min after imidization.[3] Finally, the polyimide composite films (thickness: 125–275 μm) were successfully obtained after removal from the KBr substrates. For the characterization of the composite films (Figure 5-5), the FT-IR spectra of the composite thin films of **P1** spin-coated on a Si wafer are shown in Figure 4-4. The absorption band at 1381 cm^{-1}, which corresponds to the B–N stretching, is clearly observed with the increasing volume fraction of the h-BN. Moreover, the volume fraction of h-BN was estimated by calculation of the chars after TGA measurement up to 900 °C (Figure 5-7). Because the weight loss did not change over 700 °C, the weight ratio values of the chars at 700 °C were estimated to determine the volume fraction of h-BN. As a result, the volume faction values were in good agreement with that of the feed values (Table 5-2).

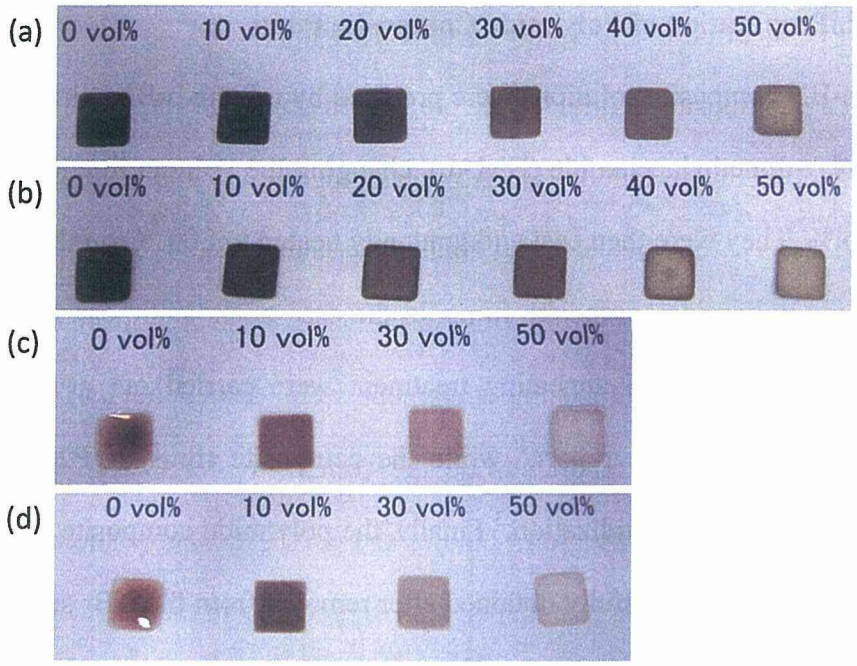

Figure 5-5. The photos of the obtained h-BN composite films: (a) air surface side of composite films of **P1**, (b) KBr substrate side of composite films of **P1**, (c) air surface side of composite films of **P2**, (d) KBr substrate side of composite films of **P2**.

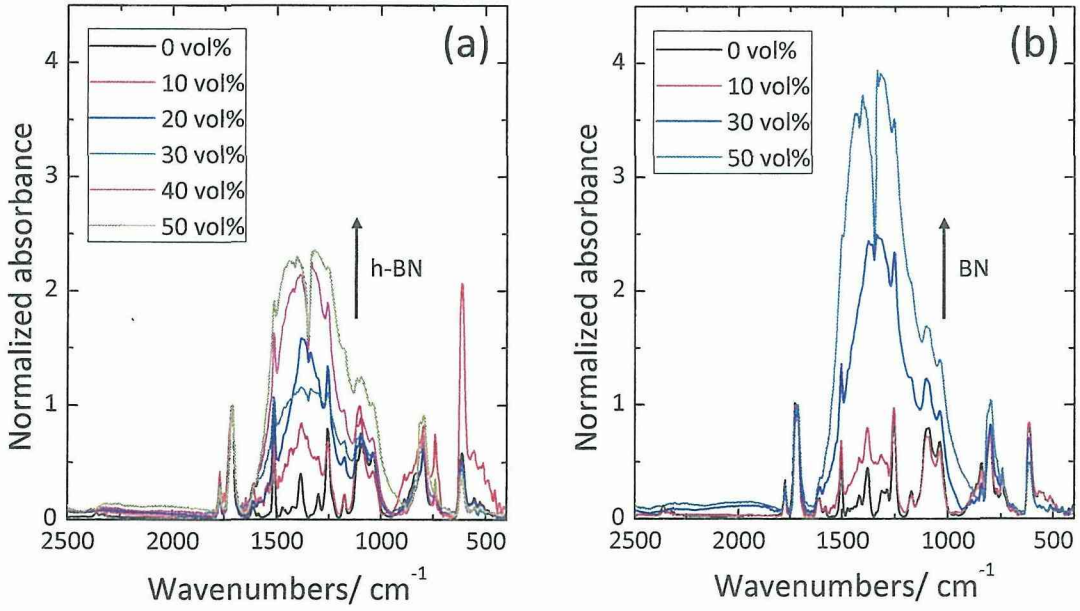

Figure 5-6. FT-IR spectra of the h-BN composites of (a) **P1** and (b) **P2**.

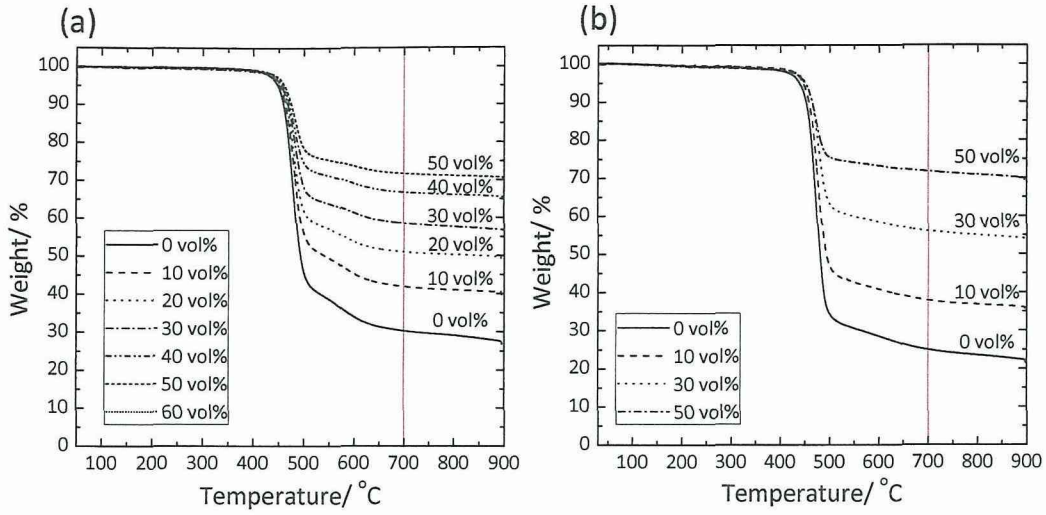

Figure 5-7. TGA curves of the composite films of (a) **P1** and (b) **P2**.

Table 5-2. Properties of the h-BN composite films of the polyimides.

Entry	Volume fraction of h-BN [vol%]	Volume fraction of h-BN (TGA) [vol%][a]	$T_{d5\%}$ [°C][b]	α [mm^2 s^{-1}][c]	σ [mm^2 s^{-1}][c]
P1	0	0	448	0.147	0.0230
	10	11.4	452	0.313	0.0414
	20	20.4	454	0.512	0.0690
	30	28.3	455	0.679	0.0406
	40	36.4	458	1.17[d]	0.0452[d]
	50	41.3	462	1.15[d]	0.0787[d]
P2	0	0	439	0.113	0.0038
	10	12.6	446	0.275	0.0215
	30	30.4	452	0.644	0.0291
	50	45.9	451	1.41[d]	0.0887[d]

[a] The volume fraction of h-BN was estimated by the calculation of the char weight after TGA measurement at 700 °C using the density of the graphite as a char, 2.20 g cm^{-3} and h-BN, 2.27 g cm^{-3}. [b] Decomposition temperature of the composite films. $T_{d5\%}$: 5% weight loss temperature. [c] Thermal diffusivity was measured by TWA method. α: thermal diffusivity, σ: standard deviation. [d] The voids were found inside the composite films.

5-2-3. Scanning Electron Microscope (SEM) Observation of the Cross-Sectional Area of Composite Films

The morphology of composite films with different h-BN contents was observed by SEM. Figure 4-7a–c, f and g show that the h-BN flakes are almost homogeneously dispersed through the thickness direction of the films of both polyimides **P1** and **P2** with less than 30 vol% h-BN. There is no largely aggregated h-BN in the films, although the h-BN flakes are comparatively accumulated near the KBr substrate side due to the difference in the density between h-BN and the polyimide matrices. However, a large amount of h-BN over 40 vol% leads to the production of voids inside the composite films, which appear from the KBr substrate side because of the densely dispersed h-BN at the bottom of the composite films compared to the air interface (Figure 4-7d). 50 vol% h-BN finally caused widely spread voids in the entire composite films (Figure 4-7e and h). The void formation was probably caused during the imidization process of the composite films, when the water molecules eliminated by the thermal dehydration of the PAAs could not come out from the composite films because of the hindrance by the large h-BN flakes.[4] For a reliable experiment, the investigation of the thermal diffusivity for the composite films was carried out using the films without any voids and with less than 30 vol% content of h-BN.

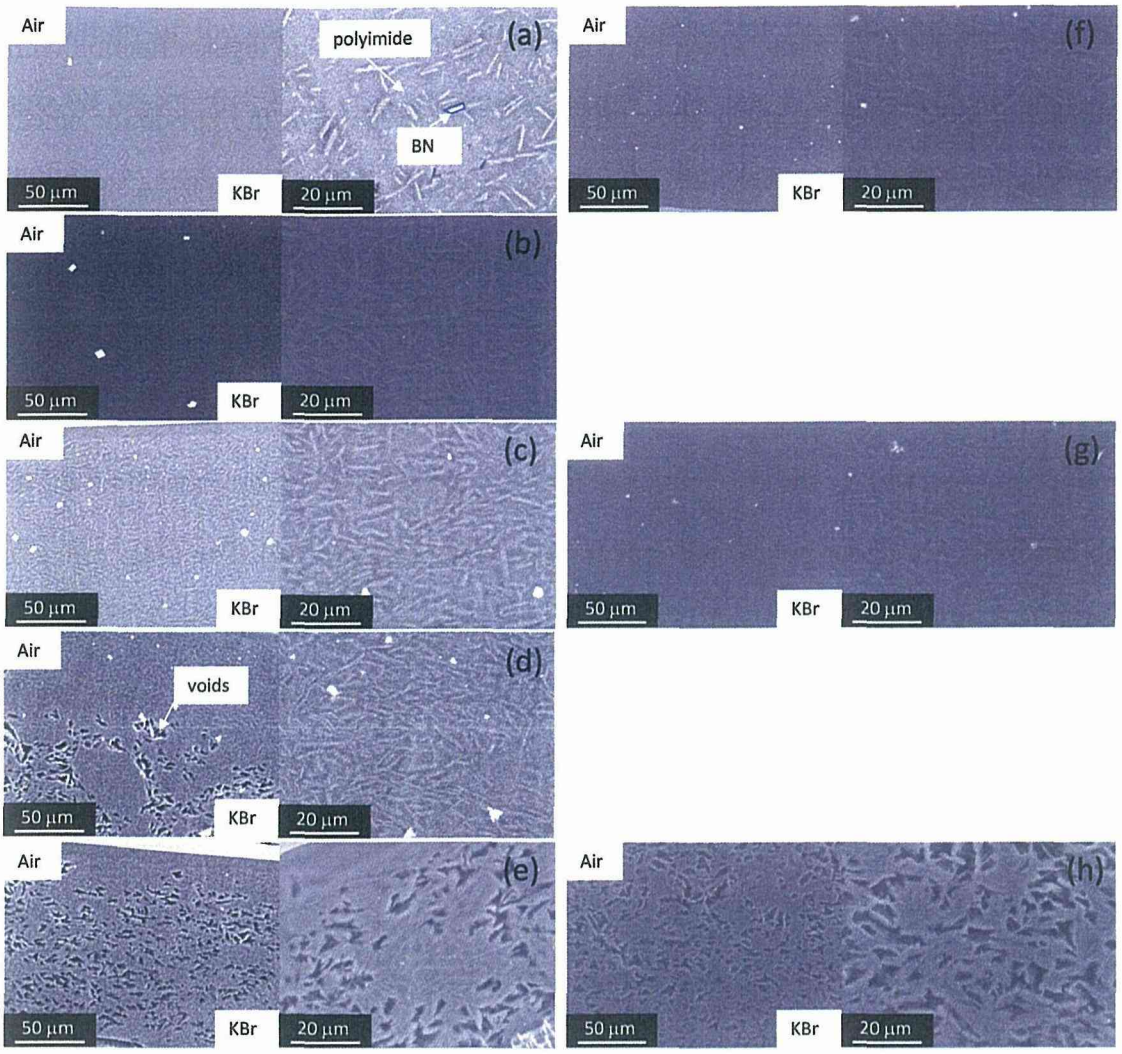

Figure 5-8. SEM images of cross-sectional area for the (a) 10 vol%, (b) 20 vol%, (c) 30 vol%, (d) 40 vol% and (e) 50 vol% h-BN composite films of **P1**, and the (f) 10 vol%, (g) 30 vol% and (h) 50 vol% h-BN composite films of **P2** (15.0 kV, ×600 (left) and ×1,500 (right)). Air interface side (upper) and KBr substrate side (bottom) in each image.

5-2-4. Wide-Angle X-ray Diffraction Measurements for Composite Films

In order to identify the morphology of the composite polyimides at room temperature before the thermal diffusivity measurements, WAXD measurements were performed for the composite films. The typical WAXD patterns of the composite films with different volume fractions of h-BN were obtained by the beam irradiation perpendicular to the film surface (Figure 5-9 and Figure 5-10). The composite films of

P1 display WAXD patterns, which include a strong (001) smectic layer reflection with a *d*-spacing of 32 Å and a broad outer reflection, characteristic to the polyimide smectic LC structure reported in our previous work.[1] Besides these reflections, the (002) reflection of h-BN with a *d*-spacing of 3.3 Å appears as the most outer Debye–Scherrer ring. The WAXD patterns of the composite films of **P2** are similar to that of **P1** composite films; however, the inner reflection is not as sharp as the smectic layer reflection observed for the **P1** composite films. Besides, the **P2** composite films showed no birefringence under polarizing optical microscopy (Figure 5-4). The inner reflection could be assigned to the micro-segregated layer structure (ca. 30 Å) of each component of the aromatic mesogens, the alkyl groups, and the siloxane units in the matrix **P2**.[2b–d] The bulky methyl-substituent on the mesogenic moiety may twist the imide plane to prevent the aromatic groups from forming smectic layers. Thus, the **P2** matrix is amorphous rather than liquid crystal.

While the WAXD pattern of **P1** composite films measured with beam irradiation perpendicular to the film surface includes ring-shaped reflections with isotropic intensities, that measured with beam irradiation parallel to the film surface show ring-shaped reflections with anisotropic intensities (Figure 5-11). The composite films of **P1**, the (001) smectic layer reflection is somewhat concentrated on the meridian, indicating that the smectic layers tend to lie parallel to the film surface, in other words, the polymer main chains align in the film normal direction.[1]

Figure 5-12 shows the normalized intensity profiles of the (001) smectic layer in each of the diffraction patterns of the composite films of **P1** against the azimuthal angle β. It was found that the (001) smectic layer alignment in the thickness direction of the films did not become disordered even on increasing the amount of h-BN, where the

orientation of the mesogenic units might be independent because the size of h-BN (around 20-μm flakes) was 3- or 4-orders larger than that of the mesogenic units. In contrast, no preferential orientation is observed for the micro-segregated layer structure in the **P2** composite films (compare Figure 5-9d–f with Figure 5-11d–f). Thus, the polymer backbones of the liquid crystal **P1** matrix lie preferentially along the film normal direction, whereas that of the amorphous **P2** matrix is isotropic in the film.

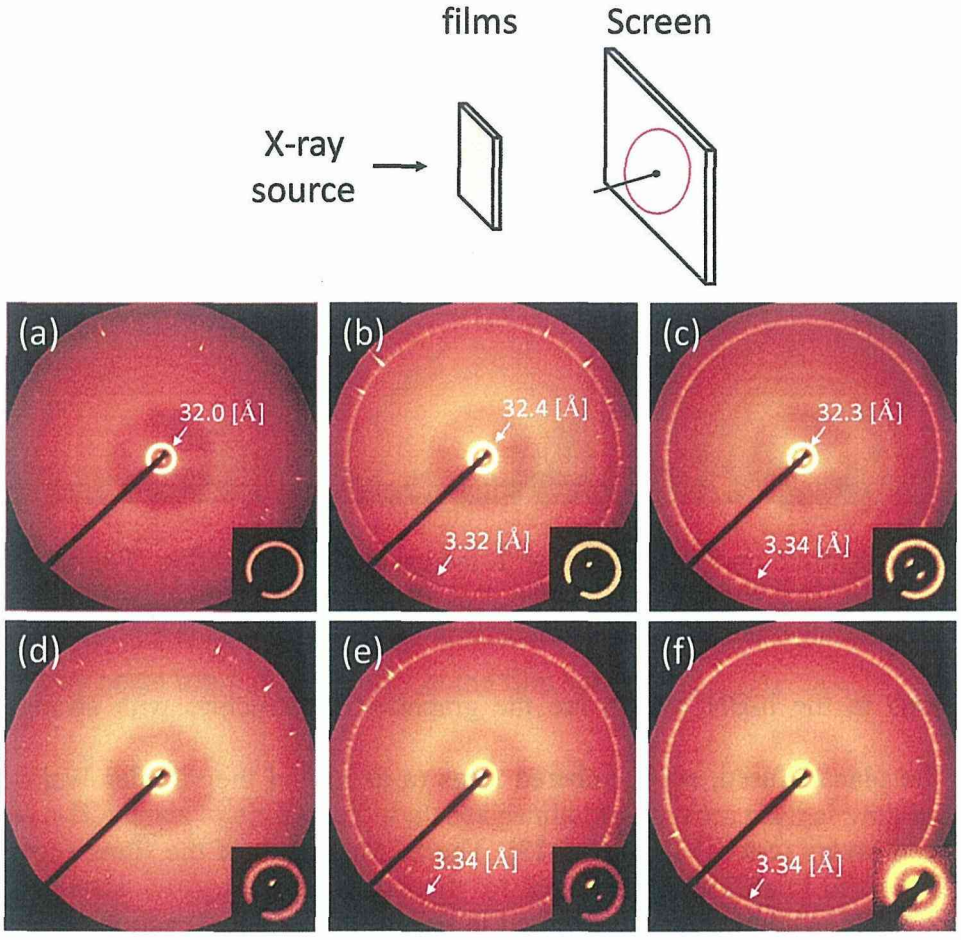

Figure 5-9. WAXD patterns for the (a) 0 vol%, (b) 10 vol%, and (c) 30 vol% h-BN composite films of **P1**, and the (d) 0 vol%, (e) 10 vol%, and (f) 30 vol% h-BN composite films of **P2** by beam irradiation perpendicular to the film surface.

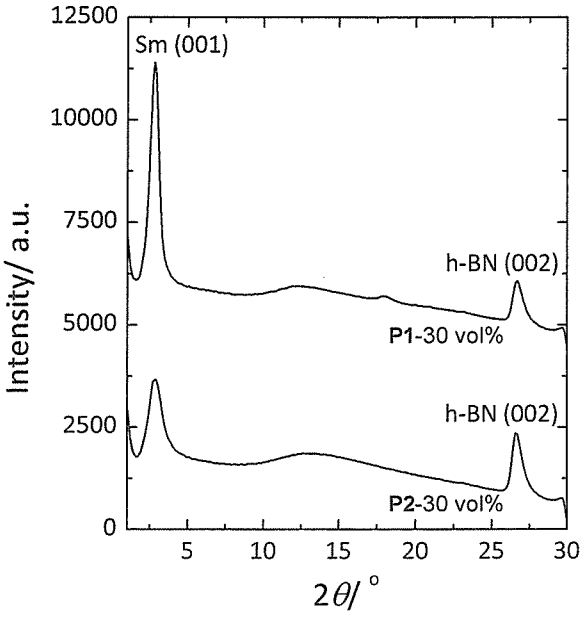

Figure 5-10. The intensity profiles of WAXD patterns by the beam irradiation perpendicular to the film surface for the 30 vol% h-BN composite films of **P1** (upper) and **P2** (bottom) against 2θ.

On the other hand, the (002) reflection of h-BN in both series of composite films tends to concentrate on the meridian with increasing h-BN fraction (Figure 5-11b, c, e, and f), indicating the anisotropic dispersion of flake-shaped h-BN. There are two dimensions in the h-BN, which are the graphite-like structure with strong bonding within the planar, fused, six-membered rings (a-axis) and the van der Waals bonding in-between layers (c-axis) (Figure 5-13). The SEM images of the films show that the c-axis of h-BN is comparatively oriented in the film thickness direction, corresponding to the anisotropic (002) reflection of h-BN in the WAXD patterns.

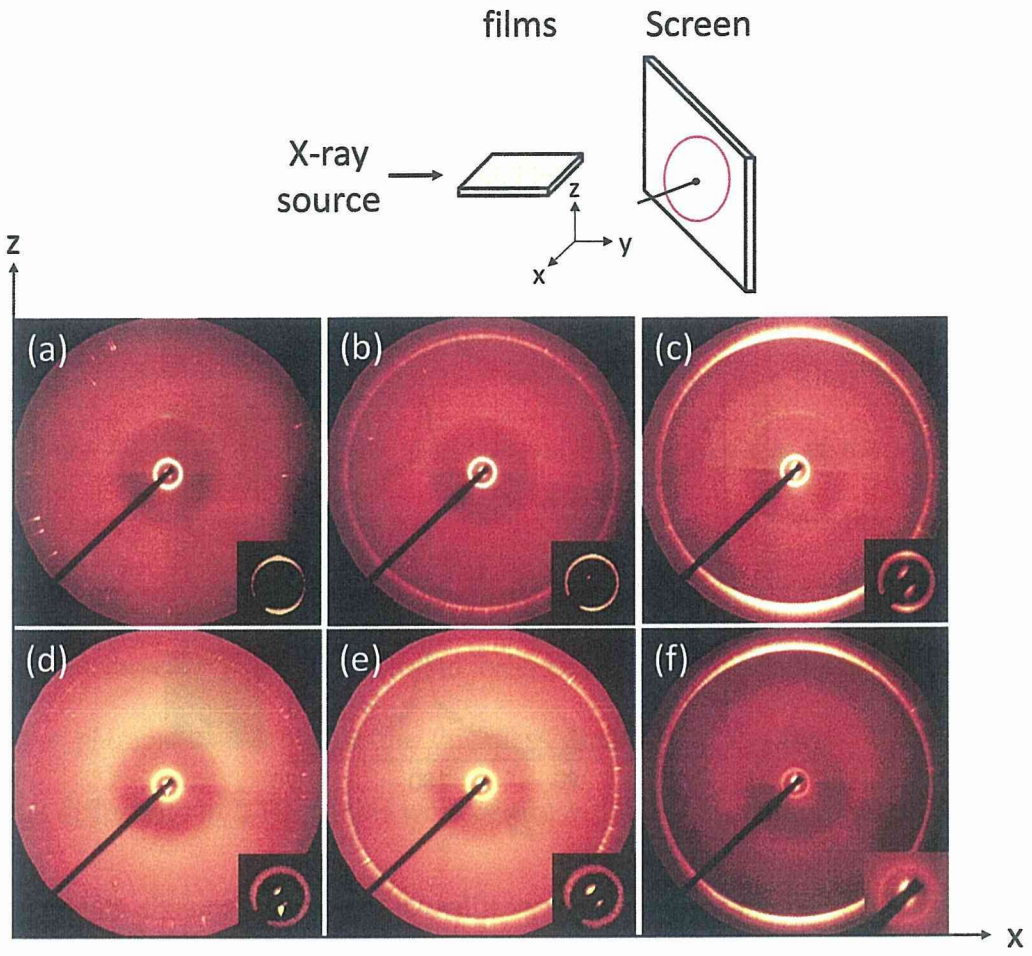

Figure 5-11. WAXD patterns for the (a) 0 vol%, (b) 10 vol%, and (c) 30 vol% h-BN composite films of **P1**, and the (d) 0 vol%, (e) 10 vol%, and (f) 30 vol% h-BN composite films of **P2** by beam irradiation parallel to the film surface.

Thus, h-BN tends to align the 00*l* planes parallel to the film normal with increasing its fraction in the composite independently of the liquid crystallinity of the polyimide matrix which makes the polyimide chain backbones lie in the film thickness direction. As a result, the two types of composite films have been prepared and characterized by WAXD measurement. One is the composite film of the anisotropic polyimide matrix in the thickness direction of the film using cross-linked LC polyimides **P1**, and the other is the composite film using the amorphous polyimide matrix **P2**. The thermal diffusivity

would be strongly influenced by these morphological differences in the polyimide matrices, and the anisotropic orientation could enhance the thermal diffusivity in the composite system.

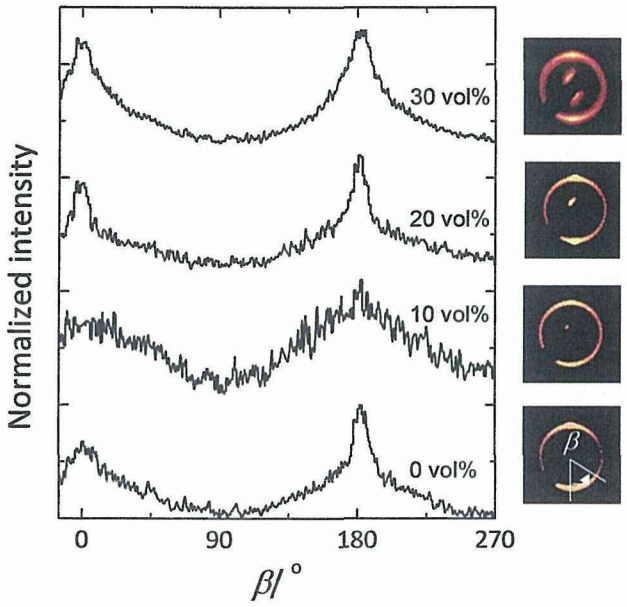

Figure 5-12. The normalized intensity profiles of the (001) smectic layer in each diffraction pattern for the composite films of **P1** against the azimuthal angle β.

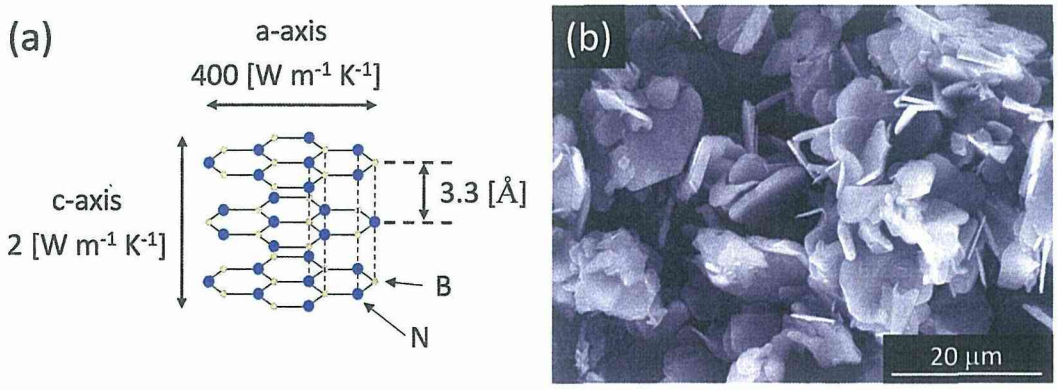

Figure 5-13. (a) The schematic illustration of the h-BN lattice structure and (b) the SEM image of the h-BN flakes.

5-2-5. Thermal Diffusivity of Composite Films

The thermal diffusivity in the thickness direction of the composite films was measured by the temperature wave analysis (TWA) method[5] at room temperature. The values of the thermal diffusivity for composite films were enhanced with the increasing volume fraction of h-BN, and the 30 vol% h-BN composite film of **P1** showed 0.679 $mm^2\ s^{-1}$, which was ca. 10 % higher than that of the composite films of **P2** (Table 5-2 and Figure 4-9). As a result, the high thermal diffusivity value at the low content of h-BN in the composite films was successfully obtained by using the oriented polyimide matrix **P1**, approximately 5 times higher than that of the pristine film of **P1**. This result can be attributed to the homeotropic orientation of the polyimide matrix and the effective phonon conduction in the thickness direction of the films. Furthermore, the thermal diffusivity of h-BN in this work can be estimated from the equation:

$$\alpha = \frac{\lambda}{\rho C_p},$$

where α is the thermal diffusivity, λ is the thermal conductivity (a-axis: 400 $W\ m^{-1}\ K^{-1}$, c-axis: 2 $W\ m^{-1}\ K^{-1}$), ρ is the density (2.27 $g\ cm^{-3}$) and C_p is the specific heat (0.8 $J\ g^{-1}\ K^{-1}$).[6,7] The thermal diffusivity values of h-BN are determined to be approximately 220 $mm^2\ s^{-1}$ in the a-axis and 1.1 $mm^2\ s^{-1}$ in the c-axis, respectively. The c-axis of h-BN aligns in almost the same direction as the thickness one of films observed by SEM and WAXD measurements. In spite of the relatively low thermal diffusivity of h-BN in the c-axis compared with that in the a-axis, high thermal diffusivity values were obtained in the thickness direction of the films using the anisotropic polyimide matrix **P1**. This is due not only to the existence of the a-axis of h-BN along the thickness direction of the films but also to the homeotropic alignment of the polymer chains serving the enhancement of the thermal diffusivity in the thickness direction of the films. Therefore,

it can be concluded that controlling the anisotropic orientation of the LC polyimide matrices leads to enhancing their thermal diffusivity in the oriented direction of the films when filled with h-BN. In addition, these homeotropic alignments possibly enhance not only the thermal diffusivity in the thickness direction of films but also the one parallel to the film surface.[7] However, the TWA method is difficult to apply to the thermal diffusivity parallel to the thin film. Therefore, a laser method[7] may possibly be applicable for estimating the thermal diffusivity parallel to the film surface.

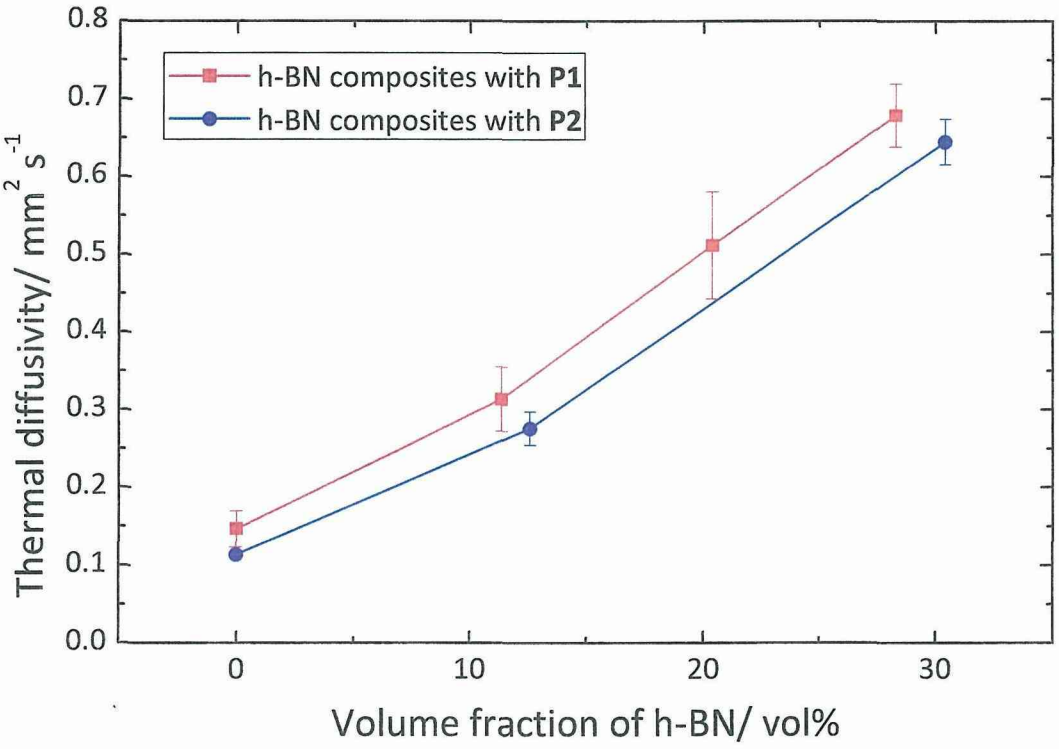

Figure 5-14. Plots of the thermal diffusivity in the thickness direction of the composite films at room temperature vs the volume fraction of h-BN calculated by TGA.

5-3. Conclusions

The h-BN composite films with high thermal diffusivity have been prepared using the cross-linked LC polyimide aligned in the thickness direction of the film as a matrix.

The composite films were successfully prepared, as characterized by FT-IR, TGA, and SEM, in which the h-BN flakes were almost homogeneously dispersed in the composite films. The WAXD patterns of the composite films **P1** and **P2** obtained by beam irradiation perpendicular to the film surface corresponded to the typical smectic LC structures and the amorphous nature at room temperature, respectively. On the other hand, in the case of the results of the WAXD patterns by the beam irradiation parallel to the film surface, the layer reflections on the meridian became comparatively strong, where the smectic layer formed the vertical alignment of the polymer chains in the thickness direction of the films. Even after increasing the volume fraction of h-BN, these alignments were maintained. The thermal diffusivity in the thickness direction of the composite films was measured by the TWA method at room temperature. The thermal diffusivity values were enhanced with the increasing amount of h-BN in the anisotropic polyimide matrix **P1**, and the 30 vol% h-BN composite film of **P1** showed the highest value of 0.679 $mm^2 s^{-1}$. The advantage of the oriented LC polyimide over the amorphous one in the composite system has been demonstrated, showing effective phonon conduction along the oriented direction.

5-4. Experimental Section

5-4-1. Measurements

Inherent viscosities were measured at 30 °C in NMP at a polymer concentration of 0.5 g dL^{-1}. Number- and weight-average molecular weights (M_n and M_w) were evaluated by SEC on a HITACHI UV Dectector L-2400 equipped with a pump, an absorbance detector (UV, λ=254 nm), and two polystyrene gel columns based on a conventional calibration curve using polystyrene standards. $CHCl_3$ (40 °C) was used as a carrier solvent at a flow rate of 1.0 mL min^{-1}. FT-IR spectra were measured on a Horiba FT-720 spectrometer. ^1H NMR spectrum was recorded with a Bruker DPX300S spectrometer. The phase transitions behavior was observed with a polarizing optical microscope (Olympus BX51), together with the use of a LINKAM LTS-350 hot stage equipped with a temperature controller by setting a polyimide film between crossed polarizers. Thermal analysis was performed on a Seiko EXSTAR 6000 TG/DTA 6300 thermal analyzer at a heating rate of 10 °C min^{-1} for thermogravimetry (TG) and a Seiko EXSTAR 6000 DSC 6200 connected to a cooling system at a heating rate of 10 °C min^{-1} for differential scanning calorimetry (DSC). To observe the cross-sectional morphology using a scanning electron microscope (SEM) with reflected electrons (FE-SEM S4500, Hitachi Ltd.), the specimens were polished by cross-section polisher with argon ion beam (SM-09020CP, JEOL Ltd.) to achieve a flat cross-section area, and then treated to carbon deposition. Wide-angle X-ray diffraction (WAXD) measurements were performed at ambient temperature by using Cu Kα radiation (50 kV, 100 mA) with a Bruker D8 DISCOVER equipped with a Vantec 500 detector. Thermal diffusivity in the thickness direction of films was measured by using ai-Phase Mobile 1u, ai-Phase Co. Ltd., based on the TWA method.[5]

5-4-2. Materials

Cross-linked LC and amorphous polyimides were synthesized according to the previous reports.[1,2] The h-BN filler (size: around 20 μm) was UHP-1 manufactured by Showa Denko K. K., Japan. The other materials and solvents were obtained commercially and used as received.

5-4-3. General Synthesis for Diamines and Poly(amic acid) 4

The composite films were prepared by mixing the h-BN fillers with the precursor PAAs of **P1** or **P2**. First, h-BN flakes were well dispersed in DMAc by the sonication for 3 h. Then, to a dispersed solution, the precursor PAAs were added and stirred for 24 h. The resulting PAA composite solutions were cast on a KBr substrate (7 × 7 × 1 mm) and the obtained films were cured in the air at 200 °C. After dissolving the KBr substrate into water, the free-standing composite films were obtained with the thicknesses of 125–275 μm.

5-5. References and Notes

1. Shoji. Y,; Ishige, R.; Higashihara, T.; Morikawa, J.; Hashimoto, T.; Takahara, A.; Watanabe, J.; Ueda, M. *Submitted to Macromolecules*.
2. (a) Shoji, Y.; Higashihara, T.; Watanabe, J.; Ueda, M. *Chem. Lett.* **2009**, *38*, 716. (b) Shoji, Y.; Ishige, R.; Higashihara, T.; Watanabe, J.; Ueda, M. *Macromolecules* **2010**, *43*, 805. (c) Shoji, Y.; Ishige, R.; Higashihara, T.; Kawauchi, S.; Watanabe, J.; Ueda, M. *Macromolecules* **2010**, *43*, 8950. (d) Ishige, R.; Shoji, Y.; Higashihara, T.; Ueda, M.; Watanabe, J. *J. Mater. Chem.* **2012**, *22*, 1532.

3. A long time annealing was not necessary because the lack of cross-linkers in the chain ends resulted in no cross-linking reaction from the unchanged DSC thermogram.

4. Sato, K.; Horibe, H.; Shirai, T.; Hotta, Y.;Nakano, H.; Nagai, H.; Mitsuishi, K.; Watari, K. *J. Mater. Chem.* **2010**, *20*, 2749. (f) Li, T.-L.; Hsu, S. L.-C. *J. Phys. Chem. B* **2010**, *114*, 6825.

5. Morikawa, J.; Hashimoto, T. *J.Appl. Phys.* **2009**, *105*, 113506.

6. Hill, R. F.; Supancic, P. H. *J. Am. Ceram. Soc.* **2002**, *85*, 851.

7. Yoshihara, S.; Ezaki, T.; Nakamura, M.; Watanabe, J.; Matsumoto, K. *Macromol. Chem. Phys.* **2012**, *213*, 2213.

8. Morikawa, J.; Hayakawa, E.; Hashimoto, T.; Buividas, R.; Juodkazis, S. *Optics Express*, **2011**, *19*, 20542.

Chapter 6

General Conclusion

Conclusions of each chapter and further prospect for the development of high thermally conductive insulating materials based on liquid crystalline polyimides are summarized in this chapter.

The general introduction regarding the background of this study is described in chapter 1.

In chapter 2, a new series of LC semialiphatic polyimides containing siloxane spacer units were synthesized. The transition temperature with the increasing siloxane spacer units showed lower crystal-LC transition temperatures (203 °C on the cooling processes), compared to polyimides containing alkylene or oxyethylene spacer units. The layered morphologies of LC polyimides with siloxane spacer units were confirmed by the WAXD experiments. A SmA phase was formed in the polyimides derived from PMDA, while the polyimides based on BPDA formed a SmC phase as well as a SmA phase. Moreover, the layer spacings of SmA indicated that the alkylene chains in the flexible spacer take a relatively extended conformation, while the siloxane units are not extended at all from 2θ intensity profiles.

In chapter 3, a new series of laterally substituted LC semialiphatic polyimides

containing siloxane spacer units were synthesized. Among the methyl, chloro, and fluoro substituents, the fluoro substituent apart from the central part of the mesogen was the most effective in stabilizing the liquid crystal phase: it reduces the crystal melting temperature substantially (163 °C on the heating process), maintaining the isotropization temperature of LC. The SmA and SmC phases of the liquid crystals are formed for polyimides, as confirmed by the X-ray patterns taken for the oriented fibrous samples.

In chapter 4, the relationship between the morphology of the cross-linked LC polymide films and their thermal diffusivity has been clarified. The thermal diffusivity in the thickness direction of the cross-linked LC polyimide films increased with the increasing extent of the cross-linking from 0.116 $mm^2 s^{-1}$ to 0.185 $mm^2 s^{-1}$. Moreover, for the results of the WAXD patterns by the beam irradiation parallel to the film surface, the layer reflections on the meridian gradually became strong with the increasing extent of the cross-linking. These results indicated that the smectic layer comparatively formed the vertical alignment of the polymer chains in the thickness direction of the films. The scanning WAXD profiles indicated that the homeotropic alignment of chains near the KBr substrate side was maintained compared to that near the air surface side. This homeotropic alignment of the chains in the thickness direction and the increase in the areas for the aligned chains can be related to the 50% increase in the thermal diffusivity of the cross-linked LC polyimide films.

In chapter 5, the h-BN composite films with the high thermal diffusivity have been developed using the cross-linked LC polyimide aligned in the thickness direction of the film as a matrix. The thermal diffusivity values were enhanced with increasing the amount of h-BN in the anisotropic polyimide matrix, and the 30 vol% h-BN composite

film showed the highest value of 0.679 $mm^2 s^{-1}$, which value was ca. 10 % higher than that of the composite film using the amorphous polyimide matrix. The advantage of the oriented LC polyimide over the amorphous one in the composite system has been demonstrated, showing the effective phonon conduction along the oriented direction.

In this dissertation, the development of high thermally conductive materials is focused on the improvement of the heat transporting properties for the organic polymer matrices based on the LC polyimides, considering the practical screen printing applications. The LC polyimides with siloxane units (chapter 2 and chapter 3) show the solution processability via the poly(amic acid) precursors and the low processing temperatures (<170 °C). The heat transporting property of the cross-linked LC polyimides (chapter 4) aligned in the thickness direction of the films was improved by the simply increasing extent of the cross-linking. Moreover, these alignments play an important role in the effective phonon conduction to enhance the heat transporting property in the obtained h-BN composite films based on the cross-linked LC polyimide (chapter 5), which revealed that the development of the high thermally conductive materials could be accomplished by improving the heat transporting properties of the organic polymer matrices as mentioned above.

The development of the high thermally conductive insulating materials is currently summarized in two approaches, such as the addition of an inorganic filler material and the improvement of the thermal conductivity for the organic polymer matrices. Thus, for the further improvement of the heat transporting properties for the insulating materials, the fusion of these approaches can bring new potential and the development of the high thermally conductive materials to the next stage. That is, the combination of the highly ordered polymers and the proper sized and shaped fillers, which have not been

investigated in detail, might be promising for one of the candidates in many applications.

The author hopes that this study will be helpful for the development of the high thermally conductive materials for the practical use in the near future.

Appendix

List of publications (concerning this dissertation)

(1) "Synthesis of Thermotropic Liquid Crystalline Polyimides with Siloxane Linkages" Shoji, Y.; Higashihara, T.; Watanabe, J.; Ueda, M. *Chem. Lett.* **2009**, *38*, 716.

(2) "Thermotropic Liquid Crystalline Polyimides with Siloxane Linkages: Synthesis, Characterization, and Liquid Crystalline Behavior" Shoji. Y.; Ishige, R.; Higashihara, T.; Watanabe, J.; Ueda, M. *Macromolecules* **2010**, *43*, 805.

(3) "Synthesis and Liquid Crystalline Behavior of Laterally Substituted Polyimides with Siloxane Linkages" Shoji. Y.; Ishige, R.; Higashihara, T.; Kawauchi, S.; Watanabe, J.; Ueda, M. *Macromolecules* **2010**, *43*, 8950.

(4) "Characteristic Smectic Structures of Main-Chain Liquid-Crystalline Polyimides Driven by a Microphase Separation between Aromatic Imide Mesogen and a Siloxane Spacer" Ishige, R.; Shoji, Y.; Higashihara, T.; Ueda, M.; Watanabe, J. *J. Mater. Chem.* **2012**, *22*, 1532.

(5) "Cross-Linked Liquid Crystalline Polyimides with Siloxane Units: Their Morphology and Thermal Diffusivity" Shoji. Y.; Ishige, R.; Higashihara, T.; Morikawa, J.; Hashimoto, T.; Takahara, A.; Watanabe, J.; Ueda, M. *Macromolecules* **2013**, ASAP.

(6) "Thermal Diffusivity of Hexagonal Boron Nitride Composites Based on

Cross-Linked Liquid Crystalline Polyimides" Shoji, Y.; Higashihara, T.; Tokita, M.; Morikawa, J.; Watanabe, J.; Ueda, M. *ACS Appl. Mater. Interfaces* **2013**, Submitted.

List of other publications

(7) "Synthesis of Aramids by Polycondensation of Aromatic Dicarboxylic Acids with Aromatic Diamines Containing Ether Linkages" Shoji, Y.; Mizoguchi, K.; Ueda, M. *Polym. J.* **2008**, 40, 680.

(8) "Synthesis of Poly(*m*-phenyleneisophthalamide) by Solid-state Polycondensation of Isophthalic Acid with *m*-Phenylenediamine" Zhang, C.; Shoji, Y.; Higashihara, T.; Tsukuda, A.; Ochi, T.; Ueda, M. *J. Polym. Sci. Part A: Polym. Chem.* **2011**, *49*, 4725.

(9) "Synthesis of Aramids by Bulk Polycondensation of Aromatic Dicarboxylic Acids with 4,4'-Oxydianiline" Shoji, Y.; Zhang, C.; Higashihara, T.; Ueda, M. *Polym. Chem.* **2012**, *3*, 1978.

List of presentations (Domestic) (○: presenter)

(1) "Synthesis of Aramids by Polycondensation of Aromatic Dicarboxylic Acids with Aromatic Diamines Containing Ether Linkages" ○Shoji, Y.; Mizoguchi, K.; Ueda, M. *57th SPSJ Annual Meeting* Yokohama, May **2008** (poster).

(2) "Synthesis of Liquid Crystalline Polyimides Containing Siloxane Spacer Units" ○Shoji, Y.; Higashihara, T.; Ueda, M. *58th SPSJ Annual Meeting* Kobe, May **2009** (abstract).

(3) "Synthesis of Liquid Crystalline Polyimides Containing Siloxane Spacer Units and Their Thermotropic Liquid Crystalline Behaviors" ○Shoji, Y.; Ishige, R.;

Higashihara, T.; Watanabe, J.; Ueda, M. *58th Symposium on macromolecules* Kumamoto, September **2009** (poster).

(4) "Synthesis and Liquid Crystalline Behavior of Laterally-Substituted Liquid Crystalline Polyimides with Siloxane Linkages" ○Shoji, Y.; Ishige, R.; Higashihara, T.; Kawauchi, S.; Watanabe, J.; Ueda, M. *59th SPSJ Annual Meeting* Yokohama, May **2010** (oral).

(5) "Evaluation of Thermal Diffusivity of Cross-Linked Liquid Crystalline Polyimides" ○Shoji, Y.; Harada, M.; Ishige, R.; Higashihara, T.; Morikawa, J.; Hashimoto, T.; Watanabe, J.; Ueda, M. *61th SPSJ Annual Meeting* Yokohama, May **2012** (poster).

(6) "Vertically Aligned Liquid Crystalline Polyimides Containing Siloxane Units Induced by Cross-linking and Their Thermal Diffusivity" ○Shoji, Y.; Ishige, R.; Harada, M.; Higashihara, T.; Morikawa, J.; Hashimoto, T.; Watanabe, J.; Ueda, M. *61th Symposium on macromolecules* Nagoya, September **2012** (oral).

(7) "Synthesis and Characterization of Polyindenoindene Derivatives by Thermal Transformation via Novel Soluble Precursor Polymers" ○Shoji, Y.; Ueda, M.; Swager, T. M. *61th Symposium on macromolecules* Nagoya, September **2012** (poster).

(8) "Vertically Aligned Liquid Crystalline Polyimides Containing Siloxane Units Induced by Cross-linking and Their Thermal Diffusivity" ○Shoji, Y.; Ishige, R.; Harada, M.; Higashihara, T.; Morikawa, J.; Hashimoto, T.; Watanabe, J.; Ueda, M. *Environment and Energy Materials Thermal Property Symposium* Tokyo, November **2012** (oral).

List of presentations (International)

(9) "Synthesis of Aramids by Polycondensation of Aromatic Dicarboxylic Acids with Aromatic Diamines Containing Ether Linkages" ○Shoji, Y.; Mizoguchi, K.; Ueda, M. *236th ACS National Meeting* Philadelphia (USA), August **2008** (poster).

(10) "Thermotropic Liquid Crystalline Polyimides with Siloxane Linkages: Synthesis, Characterization, and Liquid Crystalline Behavior" ○Shoji, Y.; Ishige, R.; Higashihara, T.; Watanabe, J.; Ueda, M. *Advanced Polymeric Materials and Technology Symposium* Jeju (Korea), January **2010** (poster).

(11) "Thermotropic Liquid Crystalline Polyimides with Siloxane Linkages: Synthesis, Characterization, and Liquid Crystalline Behavior" ○Shoji, Y.; Ishige, R.; Higashihara, T.; Watanabe, J.; Ueda, M. *Polycondensation* Kerkrade (Netherlands), September **2010** (poster).

(12) "Evaluation of Thermal Diffusivity of Cross-Linked Liquid Crystalline Polyimides" ○Shoji, Y.; Harada, M.; Ishige, R.; Higashihara, T.; Morikawa, J.; Hashimoto, T.; Watanabe, J.; Ueda, M. *Tokyo Tech-EPFL Joint Workshop* Hakone (Japan), February **2012** (oral).

(13) "Evaluation of Thermal Diffusivity of Cross-Linked Liquid Crystalline Polyimides" ○Shoji, Y.; Harada, M.; Ishige, R.; Higashihara, T.; Morikawa, J.; Hashimoto, T.; Watanabe, J.; Ueda, M. *244th ACS National Meeting* Philadelphia (USA), August **2012** (oral).

(14) "Morphology of Cross-linked Liquid Crystalline Polyimides Containing Siloxane Units and Their Thermal Diffusivity" ○Shoji, Y.; Ishige, R.; Harada, M.; Higashihara, T.; Morikawa, J.; Hashimoto, T.; Watanabe, J.; Ueda, M. *9th SPSJ International Polymer Conference* Kobe (Japan), December **2012** (poster, Young Scientist Poster Award).

List of other related presentations (Domestic)

(15)"Thermotropic Liquid Crystalline Polyimide as Candidate Materials for Three Dimensional Chip Stack" ○Murase, T.; Aikyou H.; Mizutani, F.; Shoji, Y.; Higashihara, T.; Ueda, M. *19th Micro Electronics Symposium* Fukuoka, September **2009** (oral).

(16)"Direct Synthesis of Poly(*m*-phenyleneisophthalamide) by Solid-Phase Polycondensation" ○Zhang, C.; Shoji, Y.; Higashihara, T.; Ueda, M. *59th SPSJ Annual Meeting* Yokohama, May **2010** (poster).

(17)"Unusual Liquid Crystal Structures Formed by a Novel Liquid Crystalline Polyimide with Siloxane Moiety in the Spacer Group" ○Ishige, R.; Shoji, Y.; Higashihara, T.; Ueda, M.; Watanabe, J. *59th Symposium on macromolecules* Hokkaido, September **2010** (poster).

(18)"Unusual Liquid Crystal Structures Formed by a Novel Liquid Crystalline Polyimide with Siloxane Moiety in the Spacer Group" ○Ishige, R.; Shoji, Y.; Higashihara, T.; Ueda, M.; Watanabe, J. *59th Symposium on macromolecules* Yamagata, September **2010** (oral).

(19)"Synthesis and Probability of Melt spinning of Aramid by Solid-state Polycondensation of Isophthalic Acid with *m*-Phenylendiamine and 3,4'-Oxydianiline" ○Zhang, C.; Tsuskuda, A.; Ochi, T.; Shoji, Y.; Higashihara, T.; Ueda, M. *60th SPSJ Annual Meeting* Osaka, May **2011** (poster).

List of other related presentations (International)

(20)"Thermotropic Liquid Crystalline Polyimides toward High Heat Conducting

Materials for 3D Chip Stack" ○Murase, T.; Aikyou H.; Mizutani, F.; Shoji, Y.; Higashihara, T.; Ueda, M. *19th Micro Electronics Symposium IEEE 3D System Integration Conference* San Francisco (USA), September **2009** (poster).

(21) "Synthesis of Poly(*m*-phenyleneisophthalamide) by Direct Polycondensation of Isophthalic Acid with *m*-Phenylendiamine" ○Zhang, C.; Shoji, Y.; Higashihara, T.; Ueda, M. *240th ACS National Meeting* Boston (USA), August **2010** (poster).

List of patents

(1) "Aromatic Polyamides Substantially Free from Halogen Ions and Having High Degree of Polymerization and Their Manufacture" Ueda, M.; Shoji, Y.; Mizoguchi, K. *Jpn. Kokai Tokkyo Koho* **2009**, (JP2009256610)

(2) "Liquid Crystal Polyimide, Liquid Crystal Resin Composite Containing Same, and Resin Film for Semiconductor Elements" Ueda, M.; Shoji. Y.; Mizutani, F.; Murase, T. *PCT Int. Appl.* **2010**, (WO2010131657).

(3) "Liquid Crystal Polyimide, Liquid Crystal Resin Composite Containing Same, and Resin Film for Semiconductor Element" Ueda, M.; Shoji. Y.; Mizutani, F.; Murase, T. *Jpn. Kokai Tokkyo Koho* **2011**, (JP2011122130).

Acknowledgements

The studies described in this dissertation have been carried out under the direction of Prof. Mitsuru Ueda at Department of Organic and Polymeric Materials, Graduate School of Science and Engineering, Tokyo Institute of Technology during 2010 to 2013. The studies are concerned with the development of high thermally conductive insulating materials based on liquid crystalline polyimides.

The author wishes to express his gratitude to Prof. Mitsuru Ueda for his ardent guidance and invaluable suggestions throughout this work. The author is sincerely grateful to Assistant Prof. Tomoya Higashihara in Tokyo Institute of Technology for their helpful advices, and also expresses his appreciation to Assistant Prof. Ryohei Ishige in Kyushu University, Assistant Prof. Sungmin Kang, Associate Prof. Junko Morikawa, Associate Prof. Masatoshi Tokita, Prof. Shinji Ando, Prof. Toshimasa Hashimoto, Prof. Junji Watanabe in Tokyo Institute of Technology, and all members in Ueda group for their collaboration.

The author is grateful to Prof. Timothy M. Swager in Massachusetts Institute of Technology for giving me an opportunity to collaborate with him for one year and his ardent guidance and help. The author also gives his thanks to all members in Swager group for their kind help.

Finally, the author wishes to express his deep appreciation to his parents, brother, and sister, Takashi Shoji, Shigeko Shoji, Shun Shoji, and Ran Shoji for their constant assistance, and also special thanks to Ms. Yukari Segawa, Mr. Tadanori Kurosawa, Mr. Sotaro Inomata, Mr. Hiroyuki Fujita, and all my friends.

Yu Shoji

March 2013